AALBORG UNIVERSITY

DENMARK

Title:
    Inclusion of Dynamic Inflow
    in Model Predictive Control
    of Wind Turbines

Theme:
    Control Engineering

Project period:
    Control and Automation
    4. semester
    Spring 2014

Project group:
    1031

Group members:
    Anders Overgaard
    Henrik Steffensen
    Martin Ø. Jørgensen

Supervisors:
    Peter Fogh Odgaard
    Torben Knudsen
    Lars Finn Sloth Larsen

Copies: 7

Pages: 152

Appendix: 7

Project finished: 03-06-2014

Synopsis:

This thesis investigates the need for including dynamic inflow in Model Predictive Control (MPC) of wind turbines. The main design drivers are generated power and tower fatigue. The project has been proposed and partly supervised by Vestas Wind Systems A/S in Aarhus, Denmark.

The wind turbine used in this thesis to generate results is the NREL 5 MW wind turbine, which is a 3 bladed onshore upwind HAWT simulated in FAST. An analysis of the system and the problem is made that clarifies, which things that should be addressed in the design of an MPC including dynamic inflow. Furthermore, an initial evaluation is made of the possible improvements from including dynamic inflow. In this analysis the rainflow counting method is also shown as a measurement of fatigue, where a Damage Equivalent Load is found.

A model including aerodynamics, drivetrain, tower dynamics, pitch actuator and generator is established. From here the model is split into two models. One where the aerodynamics is a quasi-steady model and one where the aerodynamics contain a simple dynamic inflow model. These models of the wind turbine are used for two MPCs, which are then compared. The comparison are done as Pareto fronts, as there exist a trade-off between power generation performance and tower fatigue.

The results show significant improvements just above rated wind speed, where dynamic inflow is most outspoken. The MPC with dynamic inflow information is able to improve the fatigue by more than 20%, while also improving the mean absolute error from the reference of the power at about 5%.

AALBORG UNIVERSITY
DENMARK

Titel:
Inklusion af dynamisk inflow
i model prediktiv regulering
af vindmøller

Tema:
Reguleringsteknik

Projektperiode:
Control and Automation
4. semester
Forår 2014

Projektgruppe:
1031

Gruppemedlemmer:
Anders Overgaard
Henrik Steffensen
Martin Ø. Jørgensen

Vejledere:
Peter Fogh Odgaard
Torben Knudsen
Lars Finn Sloth Larsen

Oplag: 7

Sidetal: 152

Bilag: 7

Afsluttet den: 03-06-2014

Synopsis:

Denne afhandling analyserer behovet for inkludering af dynamisk inflow i modelprediktiv regulering af vindmøller. De undersøgte hovedområder er effektproduktion og tårntræthed. Projektet er foreslået og delvist vejledt af Vestas Wind Systems A/S i Aarhus, Danmark.

I denne afhandling anvendes en 5 MW vindmølle fra NREL, som er en 3-vinget landbaseret opvinds, horisontal-akset vindmølle, der simuleres i FAST.

Der er lavet en analyse af systemet og problemet, der klarlægger hvilke ting, der skal med i designet af en modelprediktiv regulator, der inkluderer dynamisk inflow. Derudover er der lavet en evaluering af de mulige forbedringer, som kan vindes ved inkludering af dynamisk inflow. I analysen er metoden rainflow counting undersøgt og anvendt til at udregne tårntræthed, hvor en skadesækvivalent belastning bliver udregnet.

Der opstilles en model, som inkluderer aerodynamik, drivtog, tårndynamik, vingeaktuator og generator. Herfra bliver modellen delt op i to modeller. En der anvender en quasistatisk inflow model og en som anvender en simpel dynamisk inflow model. Modellerne er anvendt i to modelprediktive regulatorer, som er sammenlignet. Denne sammenligning er lavet ved hjælp af Pareto kurver, da der eksisterer en afvejning imellem effektproduktion og tårntræthed.

Sammenligningen viser en markant forbedring lige over rated vindhastighed, hvor dynamisk inflow er mest markant. Den modelprediktive regulator med information om dynamisk inflow er i stand til at forbedre træthedsækvivalentet med mere end 20%, samtidig med en forbedring på 5% i den gennemsnitlige absolutte effektfejl.

Preface

This report is written to document the work, which has been made on the 4. semester on the Master of Science (MSc) in Engineering, Control and Automation. The title of the project is *"Inclusion of Dynamic Inflow in Model Predictive Control of Wind Turbines"*. The project is made in cooperation with the Danish company Vestas that develops and produces wind turbines. The project has been proposed by Peter Fogh Odgaard and Lars Finn Sloth Larsen [Odgaard and Larsen, 2014], who also supervise along with Torben Knudsen.

The main objectives of this semester, related to the project, are as follows [The Faculty of Engineering and Science Aalborg University, 2011]:

- have knowledge, at the highest international level of research, of at least one of the core fields of the education
- have comprehension of implications of research (research ethics)
- are able to reflect on a scientific basis on their knowledge,
- can argue for the relevance of the chosen problem to the education including specifically account for the core of the problem and the technical connections in which it appears
- can account for possible methods to solve the problem statements of the project, describe and assess the applicability of the chosen method including account for the chosen delimitation and the way these will influence on the results of the product
- can analyse and describe the chosen problem applying relevant theories, methods and experimental data
- are able to describe the relevant theories and methods in a way that highlights the characteristics and hereby document knowledge of the applied theories, methods, possibilities and delimitations within the relevant problem area
- have the ability to analyze and assess experimental data, including the effect the assessment method has on the validity of the results.
- are able to communicate scientific problems in writing and orally to specialist and nonspecialist.
- are able to control situations that are complex, unpredictable and which require new solutions,
- are able to independently initiate and to perform collaboration within the discipline and interdisciplinary as well, and to take professional responsibility,
- are able to independently take responsibility for his or her own professional development and specialization.

The documentation of the project is written in English. It documents the chronology, methods, results and conclusions. In each chapter, except for summarizing chapters, tops and tails are made. Tops and tails are text parts written in italic which respectively explains the objective of the chapter and the results gathered from the chapter. A nomenclature is made to explain terms and abbreviations of words, which might be unclear to the reader. References to documentation is made according to the Harvard-method, where a link is made in the text pointing to a specific source in the bibliography. On the CD attached references to electronic documents, references and various other material can be found. The 💿 symbol will tell, when there is material to be found on the cd.

Acknowledgement

The authors of this thesis wish to thank the supervisors Peter Fogh Odgaard and Torben Knudsen for their support, ideas and feedback on the project. Furthermore, the authors would like to thank external supervisor Lars Finn Sloth Larsen from Vestas for his feedback throughout the project.

Authors

Anders Overgaard

Henrik Steffensen

Martin Østergaard Jørgensen

Nomenclature

Abbreviations

AAU	Aalborg University
BEM	Blade Element Momentum
DEL	Damage Equivalent Load
DI	Dynamic Inflow
DOF	Degree Of Freedom
EKF	Extended Kalman Filter
FFT	Fast Fourier Transform
GDW	Generalized Dynamic Wake
IEC	International Electrotechnical Commission
KKT	Karush–Kuhn–Tucker
LKF	Linear Kalman Filter
LQR	Linear Quadratic Regulator
MA	Mean Absolute
MAE	Mean Absolute Error
MMPC	Multiple Model Predictive Control
MPC	Model Predictive Control
NREL	National Renewable Energy Laboratory
ODE	Ordinary Differential Equation
PEM	Prediction Error Method
PI	Proportional-Integral
PID	Proportional-Integral-Derivative
QP	Quadratic Programming
RPM	Rotations Per Minute
TSR	Tip Speed Ratio

Contents

Introduction 1

Wind energy is one of the fastest growing renewable energy sources [GWEC, 2012] and is a rather new area in the energy production. Wind turbines are becoming larger, more complex and operates in many different environments, which gives rise to challenges in controlling and optimizing the power production and reducing the fatigue of the system. As this area of technology is fairly new, there are many techniques and phenomena, which still are to be investigated.

A common used method of control is presented in [Johnson et al., 2006], where the optimal setpoint for optimizing the power production is calculated continuously without knowledge of the wind speed. A classic controller is typically used in combination with this as in [Hwas and Katebi, 2012].

More advanced control methods as optimal, adaptive and nonlinear control has been investigated as well. In [Bossanyi and Hassan, 2003] optimal control is introduced in the form of a LQG controller for individual blade pitch control with the aim of load reduction. Furthermore, good results are obtained in [Friis et al., 2010] using repetitive control combined with MPC, which focus on damping structural vibrations and thereby structural fatigue.
In [Jafarnejadsani et al., 2013] an adaptive control strategy is proposed for maximizing the power production. The adaptive control is combined with a neural network and shows better performance, than an optimized gain-scheduled PI controller.
[Kumar and Stol, 2009] addresses the highly nonlinear behaviours in the system by combining feedback linearization and a LQR to optimize power production and reduce fatigue loads in the drive-train, blades and tower.

These proposals works on static models concerning the wind inflow on the blades. [Henriksen et al., 2012a] shows the significance of including the dynamic states in the modeling and suggests a simplified model of dynamic inflow for model based control. However, not much research has been made combining dynamic inflow and MPC, only reference found is [Henriksen et al., 2012b]. In [Henriksen et al., 2012b] it is found that inclusion of dynamic inflow is beneficial, if the bandwidth of the controller is high enough and the dynamic inflow effect is most influential around rated wind speed. [van Engelen and van der Hooft, 2004] investigates the use of linear filters compensating for dynamic inflow in blade pitch control and shows good results in doing so.

Combining dynamic inflow and MPC is an interesting area to investigate, due to the limited research done in the field. Per request from Lars F. S. Larsen from Vestas, this thesis wishes to investigate this in regard to the trade-offs, between power production and structural fatigue, in the tuning of controllers. In [Henriksen et al., 2012b] promising results were shown, for the inclusion of dynamic inflow. However only two set of controller weights were investigated, where this thesis will show results from a larger set of controllers.

1.1 Objective

This master's thesis wishes to investigate the possibility of including dynamic inflow models in a Model Predictive Control setup for wind turbines, with the aim of reducing structural fatigue. So far quasi-steady aerodynamic models have been used in MPC schemes to estimate free mean wind speed. Quasi-steady aerodynamic models estimate the free mean wind speed in steady state operations, thus non-precise when dynamic changes happen, such as a change of pitch on the blades. Dynamic inflow models offer a method of describing the dynamics, when the operating point of the wind turbine changes. This knowledge of dynamic behaviour can be used in a MPC scheme. The result of this work should clarify, if a MPC with dynamic inflow models is able to improve on power production and/or fatigue levels under dynamic conditions. With regard to fatigue the focus will be on active tower dampening.

Problem statement:
Does adding dynamic inflow to an MPC improve power generation and/or decrease fatigue of the tower?

1.2 Process

This report will not only cover the results, but also some of the process of getting there. This opens up for the reader to better understand, which choices were made leading up to the final results.

The general steps taken into accomplishing the objective:

Analysis

These subjects are to be analysed in an explorative manner giving a knowledge foundation for the further work. This analysis ends in a conclusion of what decisions are made regarding further development.

- Key components of a wind turbine.
- Experience with FAST.
- Classic wind turbine control.
- Fatigue analysis.
- Wind and wind speed estimation.
- Inflow models.
- Frequency analysis of a wind turbine.
- Effect of Dynamic Inflow in Wind Turbine Control.

Modelling

A model suitable for a model predictive control structure has to be developed. Creating a model also has the advantage of increasing the understanding of the system, which will help in the controller design. The modelling will consist of the following general steps.

- A basic nonlinear model including dynamic inflow is derived and parameters are estimated using the NREL 5 MW wind turbine.
- A linear model, which is suitable for MPC, is linearised from the nonlinear model.
- Step 1-2 is repeated without dynamic inflow.
- The different models obtained are compared with the high fidelity model from FAST to analyse any potential improvement.

Design of Model Predictive Control

The main goal is to merge the model understanding of dynamic inflow into a control scheme, improving power generation and/or active damping of the tower deflections. This is done through model predictive control. To represent a real world wind turbine the higher fidelity model simulation tool FAST is used. All the developed control schemes will be tested via this tool. The part objectives of the control design will be as follows.

- Implementing MPC on a gradually more and more complex representation of the system until it works with FAST.
- Tune the MPC to a satisfying performance.

Results

At this point two controllers are designed and tuned: one containing dynamic inflow and one which does not. Now these controllers can be compared in regard to various features. The main results will be a comparison of both power generation and tower fatigue.

Part I
Analysis

Introduction to Analysis 2

This thesis does not only contain results, but also the process leading to these. In the beginning of the project a lot of documentation was read, regarding control of wind turbines in the present and what research has been done in the area. This was done especially in regard to the topics of dynamic inflow and model predictive control. From this work subjects which needed to be covered in an analysis, before a design phase could be undertaken, was established to be:

- Key components of a wind turbine.
  This is to give a general understanding of a wind turbine. This knowledge is used throughout all other subjects.
- Experience with FAST.
  To be able to use FAST for simulations and to understand how FAST simulates wind turbines. This knowledge is needed to test the problem statement that this thesis investigates. Knowledge is also needed of FAST to understand the capabilities of this simulation tool and just as important the deficiencies.
- Classic wind turbine control.
  Get an understanding of what is typically controlled in a wind turbine and how. Knowledge of what is done at the present is needed, to be able to develop new control methods.
- Fatigue analysis.
  Understanding what fatigue is regarding a wind turbine and how it can be measured. Knowledge of fatigue is needed in a controller that wishes to minimize this. Furthermore, a measurement of fatigue is needed to be able to compare methods of control.
- Wind and wind speed estimation.
  Acquiring knowledge of the different wind phenomena. This knowledge is needed, since realistic wind needs to be generated for the simulation to use. Apart from this, it is also basic knowledge that is needed in many aspects, when working with wind turbines.
- Inflow models.
  Since dynamic inflow is the phenomena that is investigated in this thesis, knowledge is needed of this and how it is typically modelled. These learnings are needed to establish what model is going to be used in a control scheme.
- Natural frequencies of a wind turbine.
  When dealing with control in a structure, such as a wind turbine, natural frequencies will be present, so knowledge of these is needed. This knowledge can be used to ensure that the model used in MPC contains information of the relevant natural frequencies.
- Effect of Dynamic Inflow in Wind Turbine Control
  An initial analysis is done to asses the potential improvement of using dynamic inflow in a control scheme.

In this analysis part of the thesis these areas are documented in a cursory manner, such that the reader gets an understanding of the acquired knowledge, which leads to certain decisions throughout the thesis.

Wind Turbine 3

The main components in a wind turbine will be explained in this chapter, to establish atleast a cursory understanding of these. Furthermore the wind turbine which will be tested on throughout this project will be presented. This is done since the wind turbine and simulation tool used to get the results will obviously have an impact.

A wind turbine is a mechanical device, which is able to convert the kinetic energy of the wind into electrical energy. Wind turbines come in varying shapes and sizes. Wind turbines can be divided into either horizontal axis (HAWT) or vertical axis wind turbines (VAWT). This thesis will revolve around the HAWT, as this is the is the most commonly used wind turbine. Other key features that set wind turbines apart are the number of blades and whether the rotor is upwind or downwind. The HAWT type, which will be investigated, is 3 bladed and is an upwind wind turbine. Wind turbines can be placed in varying places. On the sea, wind speeds are often higher, which makes it a desirable area to place wind turbines. This opens up for a new problem, namely the platform structure. Wind turbines with floating structures are made and opens a whole new area of control problems involving balancing the structure while maintaining the power production. However, the focus of this thesis will be on grounded wind turbines, which makes movement of the platform structure negligible.

An illustration naming some of the main components of a HAWT 3 bladed upwind variable speed wind turbine can be seen in Figure 3.1.
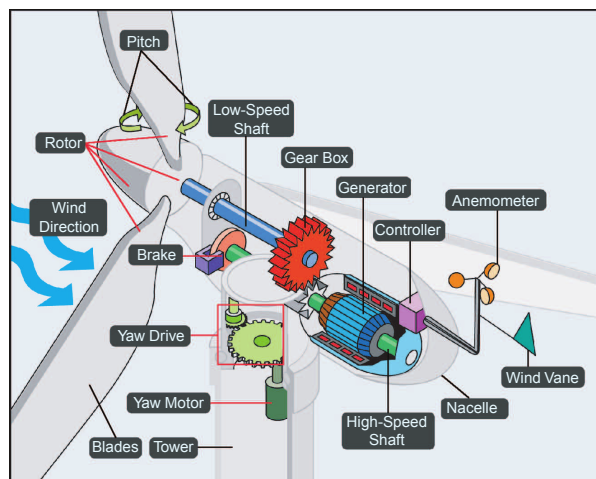

Figure 3.1. Illustration of key components of a windturbine [Johnson et al., 2006].

Functionality of some of these main components will here be explained:

Tower - The tower is the support of the nacelle and the rotors. The nacelle and the rotor are placed on top of the tower with a yaw drive in between, which enables it of active control of the yaw to ensure the rotor is facing the wind. A high tower makes it possible to have longer blades and therefore a larger wind area to harvest energy from. Another advantage of a high tower is that the shear effect of the wind is diminished. Since the tower is affected by a force from the wind, deflections of the tower will occur giving rise to fatigue of the structural material.

Nacelle - The nacelle is the construction containing the components, which converts the kinetic energy from the rotor into electrical energy, such as the generator, shafts and gearbox.

Rotors - The rotor is the combination of the three blades. The kinetic energy of the wind, moving mostly in a translational direction, is transformed into rotational kinetic energy by the wind hitting the blades, making them turn in the rotor plane. The rotor blades can change their rotation angle, called pitch. Changing the pitch affects the efficiency of the wind power extraction. The rotor is connected to the shaft via the hub.

Gearbox - The gearbox changes the lower angular velocity of the rotor connected low-speed shaft (LSS) into the higher angular velocity of the high speed shaft (HSS). This is done to get an angular velocity, which is more suitable for the generator.

Generator - The generator transforms the kinetic power into electrical power. Power control is added to be able to run at variable speed on the generator, while keeping constant power quality on the AC output.

3.1   Simulation

Due to the scope and financials of this project the methods developed will not be implemented on a real wind turbine. Instead the simulation tool FAST is used. FAST has the ability to linearise the nonlinear models that are used and compute these for model dependent control schemes. This feature will not be used for model used in Model Predictive Control, since it is assessed that a better understanding of the system can be gained, by making a model specific for the project fitting the desired MPC structure. FAST will be used to estimate parameters of this model and to validate it. Furthermore, the developed MPC scheme using the developed model will be tested through FAST. FAST has a MATLAB Simulink interface making it very suitable, since especially quadratic programming tools from MATLAB will be used when creating the model predictive controller. More information about FAST can be found in Appendix A on page 122.

3.2 Verification Model

For verification purposes a specific wind turbine model has to be used. A 5 MW 3 bladed onshore and upwind HAWT developed by NREL will be used, since this model has been used in numerous state of the art articles, concerning modern wind turbine control, mentioned in Chapter 1 on page 1. The 5 MW NREL wind turbine has the following key specifications [Jonkman et al., 2009]:

Parameter	Value	Unit
Rated electrical power	5	[MW]
Rotor diameter	126	[m]
Hub height	90	[m]
Hub diameter	3	[m]
Cut-in wind speed	3	[m/s]
Rated wind speed	11.4	[m/s]
Cut-out wind speed	25	[m/s]
Rated rotor speed	12.1	[rpm]
Rated tip speed	80	[m/s]
Rotor mass	110000	[kg]
Nacelle mass	240000	[kg]
Tower mass	347460	[kg]
Rated generator speed	1173.7	[rpm]
Gearbox ratio	97:1	[−]
Number of blades	3	[−]

Table 3.1. Principle data of the test wind turbine NREL 5 MW.

The basics of structural and technical components of a wind turbine has been presented. The wind turbine used for testing is a 5 MW onshore upwind HAWT, which has been developed by NREL. This wind turbine will be used in the simulation software FAST. The control issues associated with this kind of wind turbine are now to be presented.

Classic Control 4

This chapter describes the classic control objectives associated with a 5 MW wind turbine as presented in Chapter 3 on page 6. This is done to determine, which control objectives lies within the scope of this thesis.

The main goal to optimize in a wind turbine is to be profitable. Profitability of a wind turbine can generally be described as:

$$\text{Profit} \;=\; \int_{t_i}^{t_d} Q(t)J(t) - R(t)W(J(t),t) \; dt - C \tag{4.1}$$

Where: t_i is the time of installation of the wind turbine.
t_d is the time of dismantling the wind turbine.
$Q(t)$ is the earnings per energy production (in Denmark [dkk/kWh]).
$J(t)$ is the energy production (typically [kWh]).
$R(t)$ price of maintenance per fatigue.
$W(J(t),t)$ fatigue of the wind turbine.
C contains the one time costs such as construction, installation
and dismantlement the wind turbine.

This is a very simplified profitability analysis, but shows some of variables which can be influenced. Besides lowering the one time costs the goal is to maximize $Q(t)J(t) - W(J(t),t)$. This optimization is very complex, since correlation between $J(t)$ and $W(j(t),t)$ is very high meaning that to produce more energy, the wind turbine needs to be stressed more, increasing the fatigue. The optimization becomes even more complex, since both $Q(t)$ and $R(t)$ are time dependent and hard to mathematically model. From this knowledge the two general objectives of wind turbine control is to maximize power generated and minimize fatigue. These objectives are described more detailed in Section 4.1 on page 12 and Chapter 5 on page 14.

With the introduction of variable speed generators, variable rotor speed was suddenly possible. Since the power gained from the wind is dependent of the wind speed and rotor speed, the power gain can be optimized by changing the speed of the rotor. This new kind of generator meant that a high quality of power, in regard to phase, frequency and amplitude could be maintained, while running at variable speed. Nowadays, variable speed generators are the most common type used.
Power quality is another control objective. Control of power quality is mainly about controlling the voltage and frequency. A wind turbine operated at variable speed works by rectifying the AC generated into DC and then inverting it back into AC delivered on the grid. Power control is typically also an issue, when controlling wind farms of multiple wind turbines, where the supply and demand also need to be matched. Control of the power quality is not within the scope of this project and will not be investigated further in this thesis.

Most variable speed wind turbines has three main actuators, which can be used for control. The first is a yaw actuator, which can be used to turn the nacelle and rotors to be pointing into the

wind. This actuator is usually controlled very slowly to avoid loads stemming from a gyroscopic movement. Next the angle of the blades can be controlled by pitch actuators. These actuators turn the whole or parts of the blade to change the aerodynamic load on the rotor. Pitch can be controlled either collectively or individually. An advantage of individual pitch control is better load compensation with regard to inhomogeneous wind fields. Creating control to compensate for inhomogeneous wind fields is not focus of this thesis, so a collective pitch scheme is used. The last main actuator is generator torque, which can be used to optimize the angular velocity of the rotor. In this thesis, control of the yaw is omitted due to it being a much slower control routine, compared to the two others.

By having the weighing between power generated and fatigue in mind, a classic control strategy is to divide the area of operation into different control regions. These regions are here described and can be seen in Figure 4.1.

Control Regions:

1. In this region the wind turbine is stopped or just starting up due to low wind speeds. Below the cut-in speed the operation cost of the wind turbine is higher, than what can be gained.
2. The objective of this region is to maximize wind power extracted from the wind. Variable speed control is usually used in this region, where pitch is kept constant and torque on the generator is controlled. This region is typically called partial load region due to the wind turbine operating at lower than rated load.
3. The power extracted is limited and kept constant to avoid loads larger, than what the wind turbine is rated to. Constant speed control is often used in this region, where pitch is controlled (either collectively or separately) and generator torque is kept constant. This region is referred to as full load region since the wind turbine is operated at the rated power. The objective of the control in this region is the minimize the variance in power generation. Too little power is less profitable and too much power increases fatigue on the wind turbine.
4. This region starts when hitting wind speed larger, than the cut-out threshold and the wind turbine is brought to a stop. Here the blades are pitched out to minimize the resulting aerodynamic torque and the brakes are enabled to stop movement of the rotor.

Region 1 and 4 which involves start up and shut down of the wind turbine is out of the scope of this project and will not be analysed in this thesis. The focus will be on control at the beginning of region 3, where dynamic inflow has the largest influence.

In Figure 4.1 the different control regions are depicted with an illustration of total energy contained in the wind and extracted power of the wind turbine as a function of the wind speed.
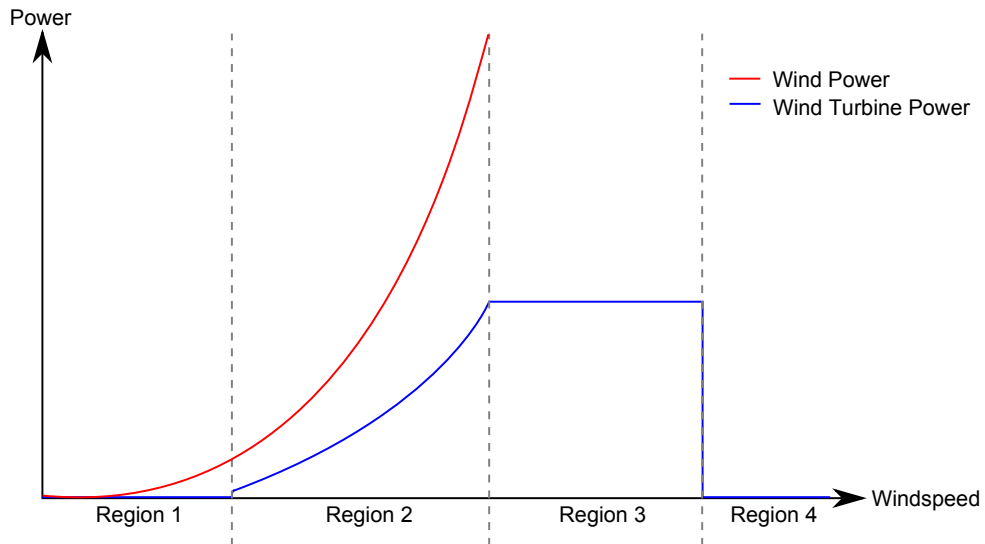
Figure 4.1. Illustration of power generated in the different control regions.

As mentioned a compromise between power extraction and fatigue on the wind turbine has to be implemented. A classical control scheme is to make individual controllers on fatigue and power generation, which can be seen on Figure 4.2.
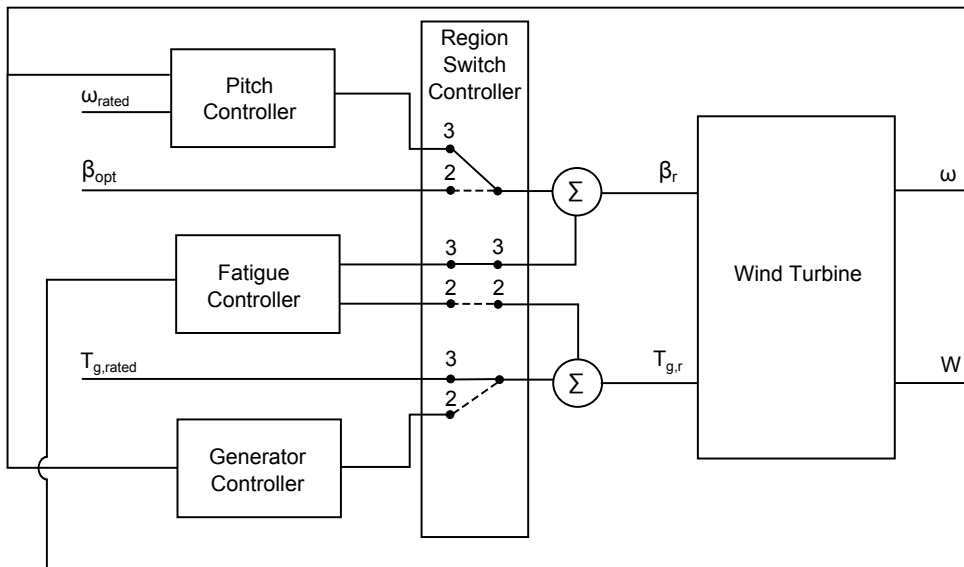

Figure 4.2. Classis control here switched to control in region 3. W is non-specified measurement of fatigue.

This control scheme consist of both region 2 and 3 control. In region 3 the fatigue controller pitches out of the wind, when the stress on the wind turbine gets too large. In region 2 the fatigue controller acts on the generator torque to decrease the stress. A multitude of different control schemes exists dealing with this weighing between fatigue and power generated. Since these control schemes consists of different individual controllers it can be hard to ensure optimality of the control actions. A control scheme combining both the power control and fatigue control is investigated in the project.

4.1 Power Optimizing

There are multiple objectives, when controlling a wind turbine. The first is optimizing the capture of the kinetic energy in the wind. How efficient power is extracted from the wind is described by the power coefficient C_p:

$$C_p(\lambda(t), \beta(t)) \;=\; \frac{P_r(t)}{P_w(t)} \tag{4.2}$$

Where: $C_p(\lambda(t), \beta(t))$ is the power coefficient [-].
           $\lambda(t)$ is the Tip Speed Ratio (TSR) [-].
           $\beta(t)$ is the pitch of the blades [°].
           $P_r(t)$ is the aerodynamic rotor power [W].
           $P_w(t)$ is the wind power [W].

Betz' limit $C_{p,opt}(\lambda(t), \beta(t)) = 59.26\%$ is the highest percentage of energy that can be extracted from an ideal wind stream. Betz' limit can be derived relatively simply from mass flow rate balances as seen in [Ragheb and Ragheb, 2011]. A specific wind turbine has a specific $C_p(\lambda(t), \beta(t))$ function dependent of pitch and TSR. Tip speed ratio is the ratio between the speed at the tip of the blades compared to the wind speed:

$$\lambda(t) \;=\; \frac{\omega_r(t)R}{v_w(t)} \tag{4.3}$$

Where: $\omega_r(t)$ is the angular velocity of the rotor $\left[\frac{\text{rad}}{\text{s}}\right]$.
           R is the radius of the rotor, the blade length [m].
           $v_w(t)$ is the wind speed $\left[\frac{\text{m}}{\text{s}}\right]$.

The characteristics of the power coefficient $C_p(\lambda(t), \beta(t))$ for the NREL 5 MW wind turbine can be seen in Figure 4.3 and 4.4:
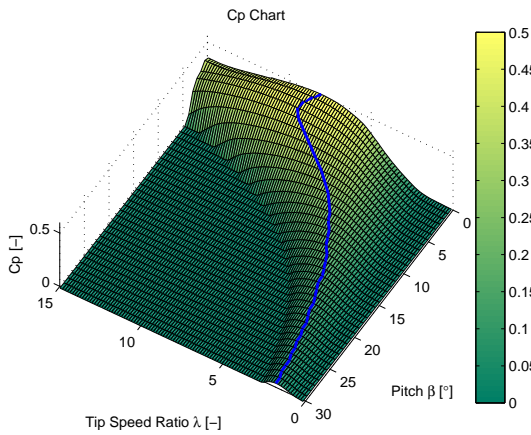

Figure 4.3. Characteristics of $C_p(\lambda(t), \beta(t))$ for the NREL 5 MW wind turbine. The blue line is maximum C_p given at different pitch and negative values have been set to zero.
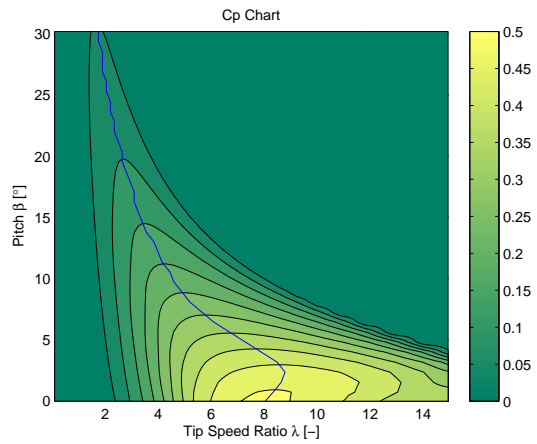
Figure 4.4. Contour plot of $C_p(\lambda(t), \beta(t))$ for the NREL 5 MW wind turbine. The blue line is maximum C_p given at different pitch and negative values have been set to zero.

Control to optimize energy gained from the wind is therefore a question of controlling the wind turbine in such a way that $C_p(\lambda(t), \beta(t))$ is at its maximum. In region 2 this can be done by controlling the torque as a function of the rotor rotational velocity by using a gain determined from the maximum C_p at the given pitch angle and the optimal TSR. This means that wind speed does not need to be known, only the rotor rotational velocity, which is easier to measure. This is described further in Appendix B on page 126.

This chapter explains the classic control objectives in wind turbine control and narrows down the scope of the project to involve: Power and fatigue control using collective blade pitch and generator torque as control inputs. Furthermore, knowledge about the different region of power control a wind turbine goes through, along with learnings of power coefficients, is acquired for use, when moving forward with the project.

Fatigue 5

The loads exerted on a wind turbine wear on the structure, which can cause failure. In the effort of increasing the life time of the structure, an analysis is made to establish a measure for fatigue, which is used in the assessment of a controller.

Wind turbines are exposed to large variations in wind speed, which exerts varying loads to the structure. These loads causes weakening/fatigue of the structure and increases the probability of failure over time. A controller can change the fatigue loading significantly and thereby prolong the lifetime of the wind turbine.

The fatigue increases with bigger loads, which means that it is not always possible to extract maximum power from the wind, as the structural damages might make it non-profitable.
In order to incorporate this in a controller, a measure for fatigue has to be established. Multiple modes of the structure is influenced by the wind, but some of the prominent parts are: Tower deflections, blade deflections and drivetrain torsion. The wind acts on the tower and rotor with a force deflecting the tower, leading to a displacement of the nacelle.
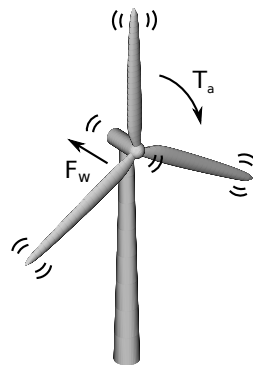

Figure 5.1. The wind acting on the wind turbine causes deflection and oscillations in the tower and blades.

The blades are exposed to a force, which results in deflections of the blades. Furthermore, the drivetrain will have two torques acting on it from the rotor and the generator, which will induce a torsion load. In this thesis only tower tower fore-aft deflections are addressed.

The most common thing to use for fatigue calculations is the torque in bottom of the tower, which makes sense, if the tower is modelled as a mass, spring, damper system and the spring is assumed linear. Then by Hooke's law the distance in steady state will be proportional to the applied force and thereby the torque in the bottom of the tower.

5.1 Measuring Fatigue

There are several methods for measuring the fatigue effect from these cyclic loads. [ASTM International, 2011] describes standard procedures for cycle-counting employed in fatigue measurements. The methods used in these analyses includes level-crossing counting, peak counting, simple-range counting, range-pair counting and rainflow counting. Other approaches as Dirliks method has been investigated e.g. in [Ragan and Manuel, 2007], where it is compared to a rainflow counting approach. It shows good performance for some particular loads. However, rainflow counting is a well known and accepted way of determining the number of cycles, thus used in this thesis as well (see Appendix C on page 129). MCrunch is a set tools delivering

methods for fatigue analysis and will be used in this thesis. It performs a rainflow count of the time series data and calculates a fatigue measure from it.

5.2   Fatigue Calculation

The cycles, which are counted by the rainflow count algorithm, indicates how often the system is exposed to a range of amplitudes and at which mean. With increasing amplitude, the fatigue increases as well. Often a damage equivalent load (DEL) is used, when evaluating the damage. The DEL is a measure of a constant-amplitude fatigue load, which comes at fixed load-mean and frequency [Hayman, 2012b]. This results in an equivalent damage to a varying frequency and amplitude of the loads. This means that the varying cycles are converted into equivalents.

The DEL is given by [Hayman, 2012b]:

$$DEL = \left(\frac{\sum_i \left(n_i \left(L_i^{\mathrm{RF}} \right)^m \right)}{n^{\mathrm{STeq}}} \right)^{1/m} \tag{5.1}$$

Where: n_i is the damage count for cycle i.
n^{STeq} is the equivalent cycle counts.
L_i^{RF} denotes the Goodman-corrected load range about a fixed-mean for cycle i.
m denotes the Wöhler constant.

The Goodman-correction is given by (5.2) and ensures that the fatigue cycle load ranges are represented as if they occured around a fixed mean load.

$$L_i^{\mathrm{RF}} = L_i^{\mathrm{R}} \left(\frac{L^{\mathrm{Ult}} - |L^{\mathrm{MF}}|}{L^{\mathrm{Ult}} - |L_i^{\mathrm{M}}|} \right)^m \tag{5.2}$$

Where: L_i^{R} denotes the load range for cycle i.
L_i^{M} is the mean load of cycle i.
L^{Ult} is the ultimate load.
L^{MF} denotes the mean load.

Further elaboration on the calculations can be found in Appendix D on page 131.

5.3 Simulations

A simulation in FAST with open loop has been made with at mean wind speed of about 12 m/s. The time series data is shown in Figure 5.2. Here it is easily seen that there is a correlation between the tower displacement and torque at the bottom of the tower. MCrunch fatigue analysis is used on this torque, which produces a cycle count on the tower deflections as seen in Figure 5.4.
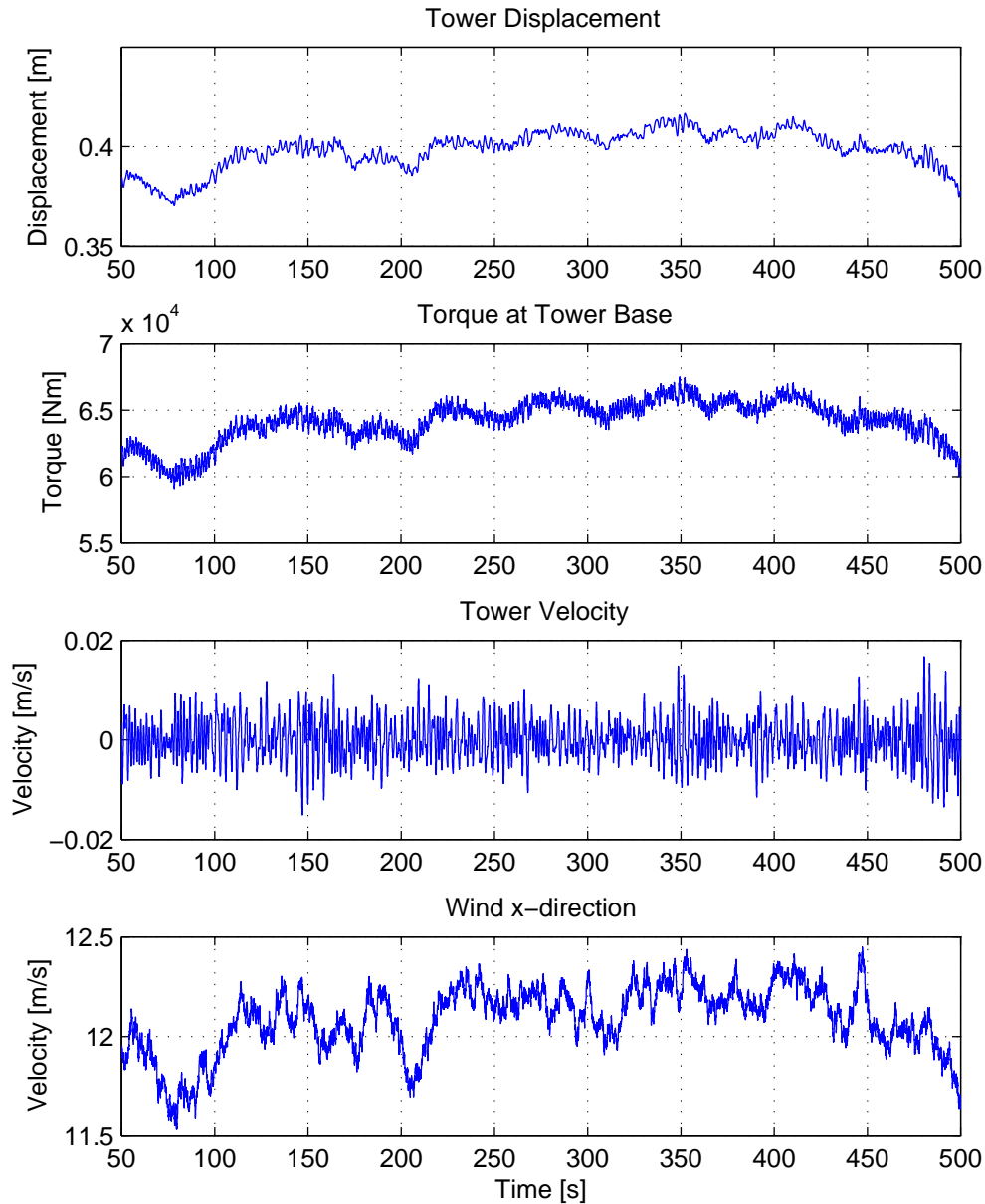

Figure 5.2. Time series data from FAST simulation with a mean wind speed of about 12 m/s. The start up is omitted as the focus is in running condition. It is easily seen that there is a correlation between the displacement and the torque at the bottom of the tower.
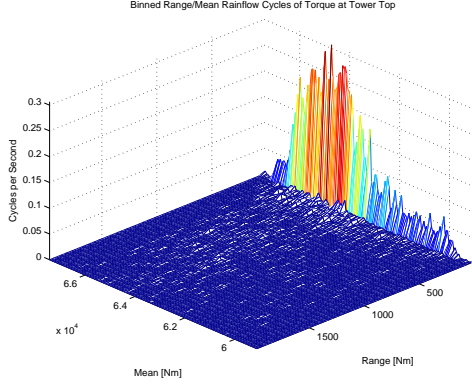
Figure 5.3. Rainflow cycles of tower deflections. If the range information is omitted, the cycles at same range are summarised, which results in Figure 5.4.
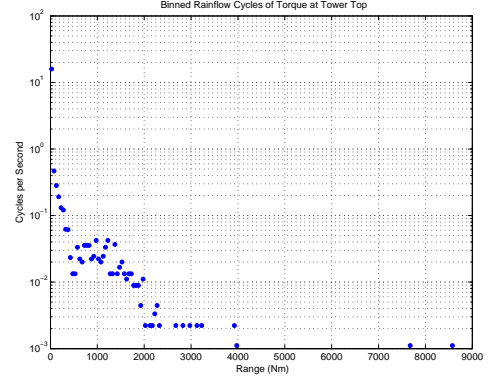
Figure 5.4. Rainflow cycles of tower deflections, where the cycles at same range are summarised.

Figure 5.3 shows how the most significant cycles are distributed regarding mean and range. The majority of cycles is according to Figure 5.4 less than 2 kNm. When calculating the damage-equivalent loads, MCrunch use Equation (5.1). In this thesis the fatigue calculations are only used for comparison of two or more controllers. The mean load L^{MF} is found experimentally by looking at data with common controllers. The ultimate load L^{Ult} where the tower fails was not able to be found. However, MCrunch comes with scenarios, where L^{Ult} consequently is set 10 times higher than L^{MF}. As no better values have been found, this is done as well. The Wöhler constant is a material constant. The tower is made of steel of which the Wöhler constant is in the interval 3-5 [Danish Standards, 2007], which is why it is set to 4. This value is used in [Hammerum, 2006] as well.

L^{Ult} [Nm]	L^{MF} [Nm]	m [-]
525600	52560	4

Table 5.1. Constants used in MCrunch fatigue analysis.

The DEL is here calculated to 1923000 Nm.

This measure is used in order to compare controllers developed in Part III and IV. It is not used directly in the MPC, as it is a tools to apply for longer time series. Therefore another measure for minimising tower fatigue has to be found. The DEL measure relies on a cycle count correlated to the deflections. Thus the cycles can be seen as changes in deflection, which in turn corresponds to velocity. This means that the DEL must be correlated to the tower velocity, which will be used in the MPC. Reducing the tower velocity reduces the tower fatigue.

The force from the wind affects the structural integrity and increases the fatigue, which with time leads to failure. This chapter presents a method of calculating fatigue in order to compare fatigue results from different controllers. The chosen method is rainflow counting in a combination with damage calculations from [Hayman, 2012b], which are implemented in MCrunch [Hayman, 2012a]. This implementation is used in the further work.

Wind 6

This chapter will introduce how wind is generated and some of the special wind phenomena, which needs to be considered when designing wind turbines. A lot of the wind phenomena is not within the specific scope of this project, which is the effect of dynamic inflow, so these are only explained here in low detail to get an initial understanding of effects of the wind.

Wind is generated as certain areas of the globe get more sunlight than others, which causes the air pressure to increase. The sunlight is most intense around equator and as the earth spins around its axis, the zone with hot air is constantly moving [Burton et al., 2001, P. 12]. This means that high and low pressure zones are generated. When the pressure tries to equalize, air will be moving from the high pressure to the low pressure zone.

An estimate of the average wind speed, at a height of 100 m in the northern part of Denmark, can be seen in Figure 6.1.
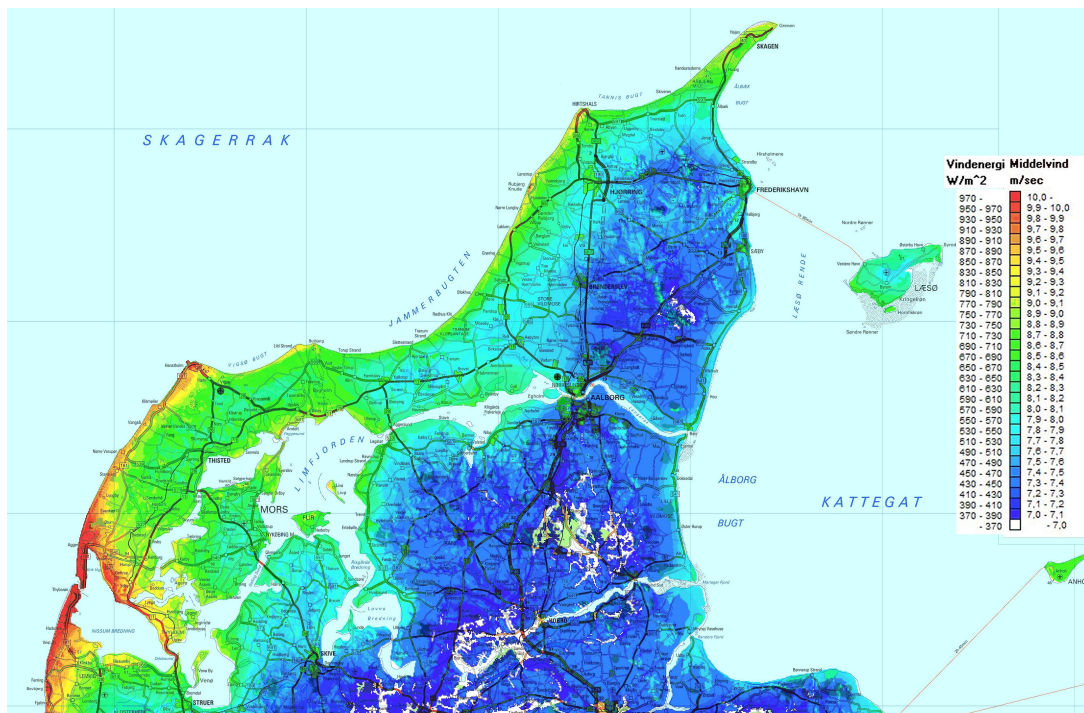

Figure 6.1. An estimate of the average wind speed in northern part of Denmark at 100 m height. Modified version of [RISØ and og Miljødata, 1999].

As seen in the figure, the average wind speed varies in different locations. This knowledge of average wind speed is taken into account, when choosing a wind turbine for a specific location. Taking the northern part of Denmark as an example a wind turbine running at higher rated wind speeds should be chosen for the west coast. When exploring a spot for a wind turbine a wind model for the mean wind of that spot is made. These models are often a Weibull probability distribution.

In 1957 Van der Hoven constructed a wind spectrum plot for Brookhaven, to show how the energy distribution for the frequencies in the wind. Figure 6.2 illustrates the wind spectrum plot.
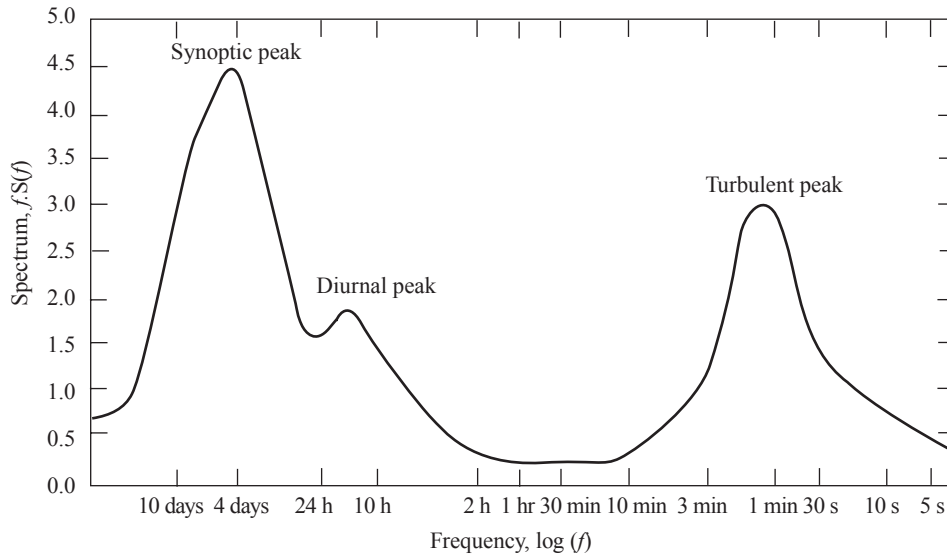
Figure 6.2. Wind Spectrum at Brookhaven, New York [Burton et al., 2001, P. 12]. Original work by Van der Hoven (1957). The synoptic contribution resembles passage of weather systems and the diurnal contribution resembles time of day variations in the wind.

From Figure 6.2 it can be seen that changes in wind can be described as three parts. Synoptic changes which are caused by the different weather systems passing around on earth. Diurnal changes is the daily routine of the weather, e.g. in average there is only sunlight 12 hours each day. In the 1 hour range and higher frequencies, the all dominating energy is in the turbulence.

6.1 Wind Shear

The wind experienced on the surface of the earth is different from the one that is experienced a hundred meters up into the air. This is mainly due to the friction, which the earth creates for the air, but also because of obstacles like mountains, forests or houses. The difference in wind speed from the surface of the earth and vertically up is known as the speed shear effect. There are three types of wind shear effects. Directional, speed and a combination of the two, as illustrated in Figure 6.3.
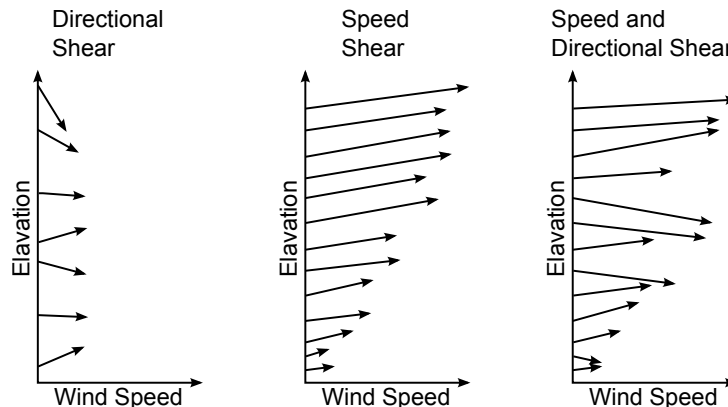The shear effects gives a different load on the blade, when it is pointing down compared to when its pointing up.

Figure 6.3. Types of wind shear [WeatherQuestions, 2010].

The fast variations in the wind speed from the shear effects can put an extra stress on the rotor blades and thereby also cause extra fatigue [Bayne and Giesselmann, 2000]. The variations can also give oscillating power output from the wind turbine, if the variations are faster or larger than what the control system can compensate for.

There are different mathematical models to describe the wind shear effect. One of these are the Prandtl logarithm law [Bianchi et al., 2007, P. 10]:

$$\frac{V_m(z)}{V_m(z_{ref})} \;=\; \frac{ln\left(\frac{z}{z_0}\right)}{ln\left(\frac{z_{ref}}{z_0}\right)} \tag{6.1}$$

Where: z is the height above ground [m].
z_0 is the roughness length [m].
z_{ref} is the reference height [m].

An illustration of the effect of the roughness parameter can be seen in Figure 6.4. The bigger the roughness parameter is, the faster the wind speed will decrease at a lower height, compared to the wind speed at the reference height.
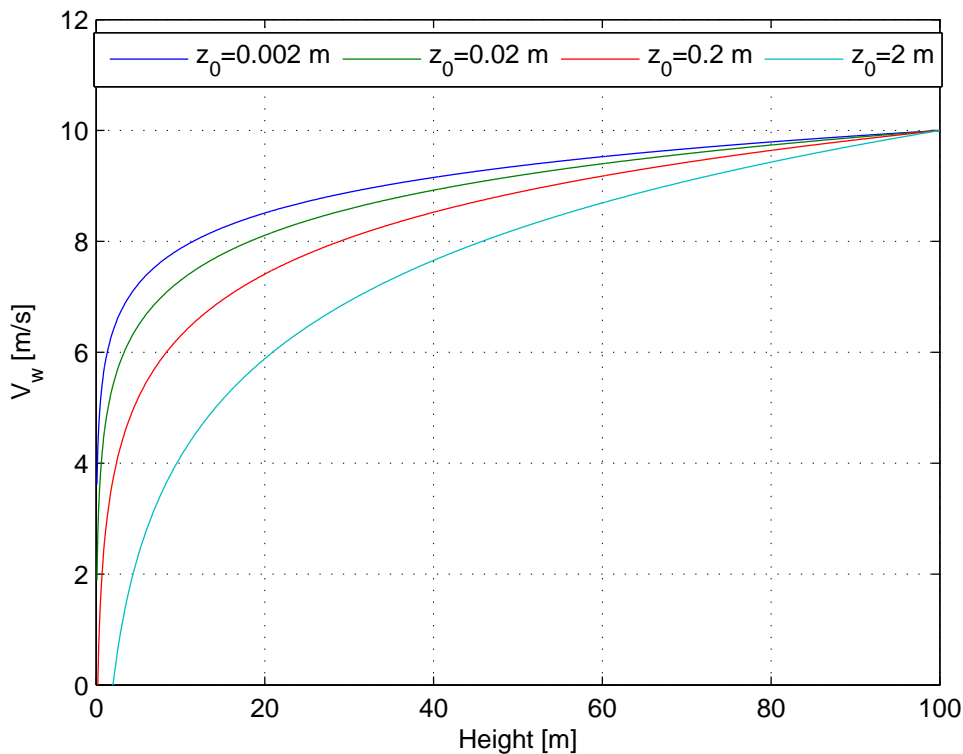

Figure 6.4. The effect of different roughness lengths. The reference height is set to 100 meters with a wind speed of 10 m/s.

6.2 Turbulence

In fluid dynamics turbulence is used to describe a chaotic nature of e.g. wind. Talking about turbulence in wind speed refers to relatively fast fluctuations in the wind speed often less than 10 min on a time scale [Burton et al., 2001, P. 17]. A stochastic approach to describing turbulence is often used, because a mathematical model of the wind turbulence would become very complex, Furthermore small deviations in the initial conditions could make a large difference in the predictions after a short time [Burton et al., 2001, P. 17].

Turbulence is primary caused by two components. The first component is friction from the earth surface, where e.g. hills and mountains are creating flow disturbances, by forcing the wind in certain directions. The second component is thermal effects, where temperature variations can cause e.g. vertical air flow. Turbulence can have a large influence on the energy output from wind turbines and cause increased stress on the structural loads.

Measured wind speeds are often collected in intervals of 10 min and a Gaussian approximation can then be made of that interval. From this approximation the turbulence intensity factor can be defined as [Burton et al., 2001, P. 17]:

$$I = \frac{\sigma}{\bar{U}} \tag{6.2}$$

Where: I is the turbulence intensity factor $[-]$.
σ is the standard deviation in the time interval $\left[\frac{m}{s}\right]$.
$\bar{U}$ is the mean wind speed in the time interval $\left[\frac{m}{s}\right]$.

The size of the intensity factor depends on multiple features, such as surface roughness, obstacles or local thermal alterations. Since the interaction with the earth's surface is a large contribution to intensity factor, this decreases at higher altitudes.

Different ways of describing the spectrum of turbulence has been developed, some of these can be seen in Figure 6.5.
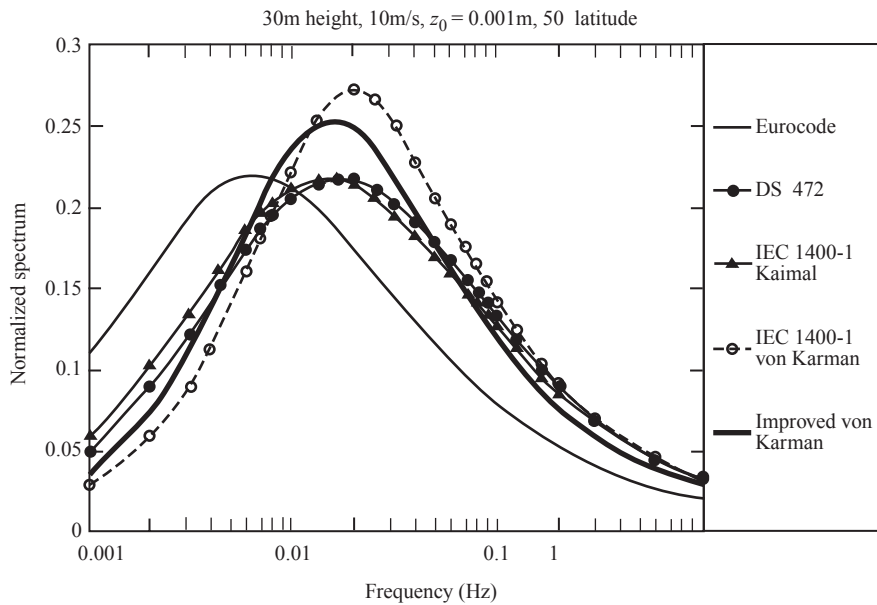

Figure 6.5. Proposed spectrums for turbulence at 30 m height, 10 $^m/_s$ mean speed and a roughness of 0.001 m [Burton et al., 2001, P. 25].

Apart from the eurocode spectrum, which is shifted a little in frequency, the frequency containing most energy in all the models lies around 0.02 Hz.

Wind used for testing in this project is made with TurbSim from NREL. In TurbSim a multitude of spectrum models for the turbulence can be used. It is chosen to use the IEC Kaimal model when generating wind files. By generating such a wind file and doing a Fast Fourier Transform (FFT) of the wind the following result is found:
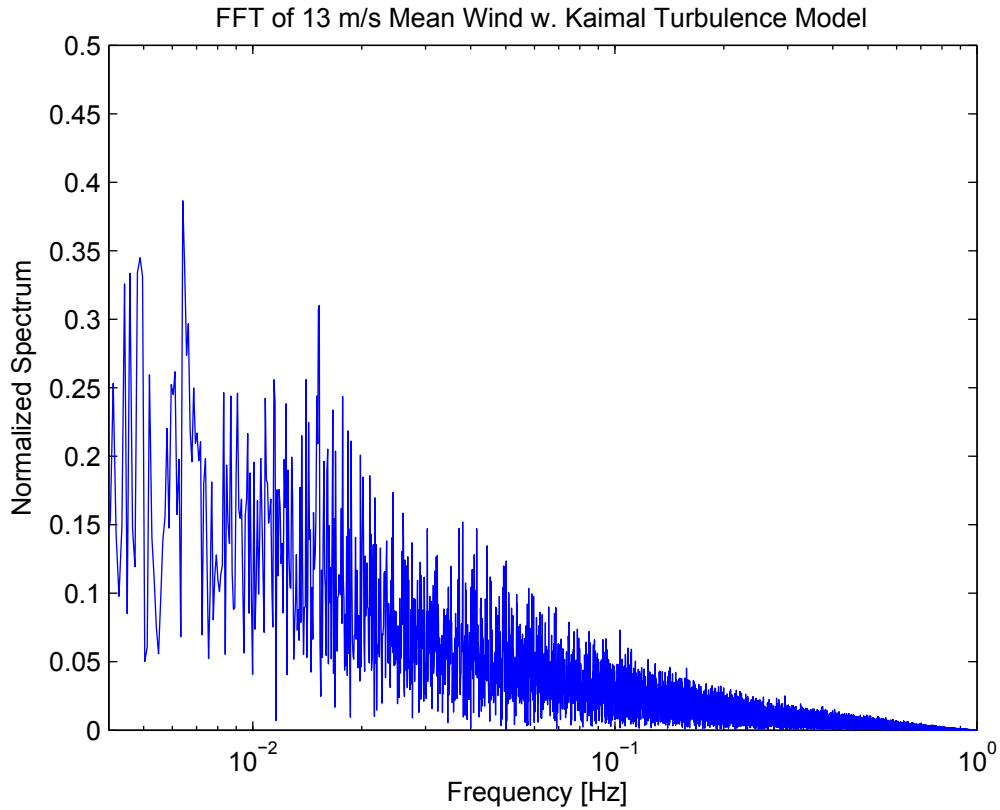

Figure 6.6. FFT of wind file generated through TurbSim.

The area containing the most energy is centred around 0.006 Hz, with contribution into the range of 0.1 Hz. This changes a bit in regard to randomisation depending on seeding in the wind generation. A specific seeding is decided on for later test to ensure repeatability.

6.3   Wake Effect

The wake effect in wind turbines origins in the wind "escaping" a running wind turbine. When the wind has passed a wind turbine, it will have a reduced wind speed and an increase turbulence level [Burton et al., 2001, P. 35]. This means it will create an irregular load on any wind turbine placed behind it, which can become a problem in wind farms. Wakes will give reduced power output and increase structural load on wind turbines operating downstream from the wake creating turbine [Burton et al., 2001, P. 35].

An illustration of the wake effect in a wind farm can be seen in Figure 6.7. The figure illustrates an extreme example of the wake effect, but it is easily seen that all the wind turbines down wind are affected.

Figure 6.7. The wake effect at Horns Rev 1 [Aeolus, 2014]. Photo by Christian Steiness.

Here a strong downwind wake is being generated in the direction of the subsequent wind turbines, affecting the performance of these.

6.4 Tower Shadow

The energy transfer from wind to rotor in a wind turbine is also affected by the tower, which supports the nacelle and blades. This happens because the wind speed at the tower will be slowed down, compared to the rest of the rotor disk. The effect is called tower shadow and its effect on a three blade wind turbine can be illustrated as seen in Figure 6.8.
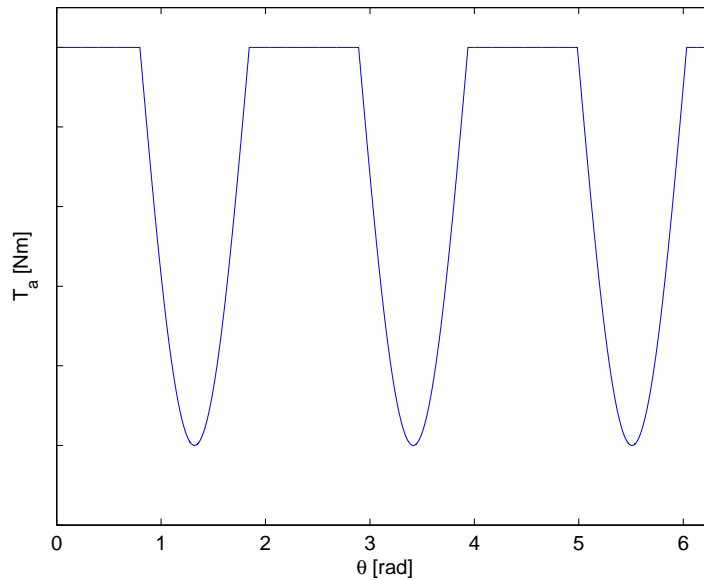

Figure 6.8. A sketch of the tower shadow effect on the aerodynamic torque [Bianchi et al., 2007, P. 27].

This is a simplified model, because while the wind speed in front of the tower is slowed, wind speed at both edges of the tower increases. The tower shadow is a repetitive disturbance and as such repetitive control can be used to minimize the effect of such disturbance. This was done in [Friis et al., 2010], to reduce structural vibrations from tower shadow.

The origin of wind and its characteristics regarding wind turbines has been explained. The scope of this project is the dynamic inflow phenomena, so tower shadow, wind shear and wakes will not be considered in the further work. The spectrum of the turbulence used in the further work was chosen to be IEC 1400-1 Kaimal.

Estimation 7

When creating an MPC input, output and state information is needed. The scope of this project is not to develop means of acquiring this information, but since the information is used, ways of deriving this information are here shown.

Information about input (disturbances), output and states can be measured by using sensors. If the desired information is not directly available through measurements, or the measurements are noisy, an observer or estimator can be used. Throughout this project it is assumed that all the states and outputs are available. This is normally not the case for wind turbines, as e.g. the velocity and position of the tower is not available. Wind turbines is normally only fitted with an accelerometer, to measure how the forces affect the acceleration of the tower.

An example of this is information about wind speed in front of the wind turbine. The wind speed is normally measured after it has passed the wind turbine, via an anemometer on top of the nacelle. The measurement from the anemometer cannot be used directly as free wind speed, since it is not located in the rotor plane. Besides this the blades passes in front of the anemometer at a 3P frequency. This measurement is therefore converted into an estimate of the free wind speed as described in [Smith et al., 2002].

Free wind speed estimation techniques that does not use an anemometer has also been developed. [Østergaard et al., 2007] has created an estimation procedure, where the estimation process is done in two steps. Given a system model of the wind turbine, it is possible to create an observer, which can estimate the resulting aerodynamic torque, originating from the wind. Given this torque estimate, another estimator can be used to estimate the wind speed hitting the rotors. The structure of the first estimation process can be seen in Figure 7.1.
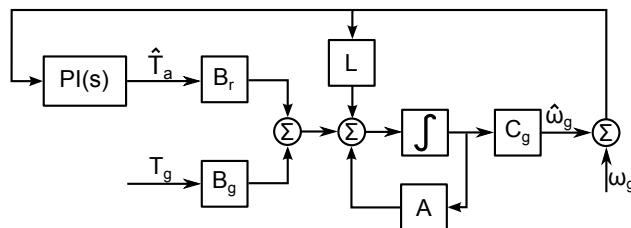

Figure 7.1. The observer structure for estimation of aerodynamic torque [Østergaard et al., 2007].

The error between the estimated angular velocity of the generator and the measured angular velocity is fed into a PI-controller, which then regulates the aerodynamic torque estimate, so there is no estimation error on the angular velocity. The observer can also be looked at as a Kalman estimator, where the gain L is the Kalman gain.

The second estimator is generated from the function describing the aerodynamic torque. By using the definition for the torque in (B.5) and rearranging the equation, the estimator can be formulated as [Østergaard et al., 2007]:

$$\frac{2T_a(t)}{\rho\pi R^5 \omega_r^2(t)} = \frac{C_p(\lambda(t),\beta(t))}{\lambda^3(t)} \qquad (7.1)$$

From (7.1) it is possible to find the TSR that satisfy the relation, given the current pitch angle β. Knowing the TSR, R and ω_r the wind speed can be found. The result of the estimation can be precompiled as a look-up table, such that it has a similar structure to C_p and C_t. A requirement on (7.1) is that no two equal values of the TSR λ can be created from a specific value of $\frac{C_p(\lambda(t),\beta(t))}{\lambda^3(t)}$.

As described here a Kalman filter is used for wind estimation. In this project full state information is assumed available, which would be acquired by using a Kalman filter on sensor data. Kalman estimation is further described in Appendix F.

Inclusion of dynamic inflow in an estimation scheme is also desirable to get a better estimation of the free wind speed, while the wind turbine is in a transient movement. This has been investigated in [Henriksen et al., 2012a] and has been shown to improved the estimate.

The Kalman filter technique for acquiring state information and specific methods for finding the free wind speed was introduced. These methods will not be implemented, but has been shown here to justify that full output, input and state information is available.

Inflow Models 8

Aerodynamical models are here described to give an initial understanding on how the wind interacts with the rotor. Particularly an understanding of where dynamic inflow models diverge from the normal quasi-steady approach is in focus.

Blade Element Momentum (BEM) theory is the aerodynamical model, which calculates the forces on the blades, as a result of the wind. In this approach the blade is divided into a finite number of elements along the blade. The forces are calculated for each of these elements and then integrated to give the full force acting on the rotor.

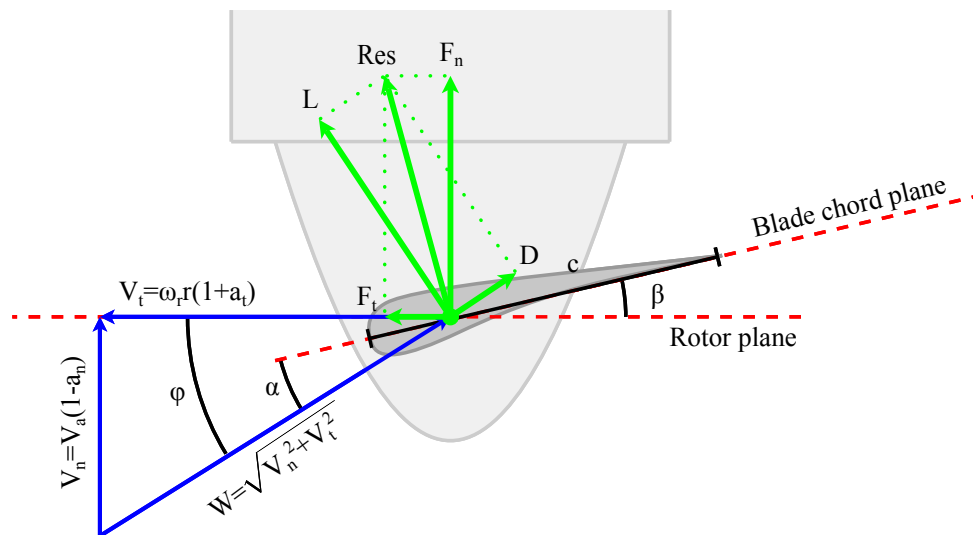How the wind acts on the blade can be seen in Figure 8.1.

Figure 8.1. Rotor with cross section of a blade. The blade is pointing out of the figure (Modified version of figure from [Henriksen et al., 2012a]).

The wind velocity experienced at the blade is a combination of the free wind and the movement of the blade. The free wind gives rise to a velocity component in the nominal direction, depending on a induction factor. The speed of the blade in the rotor plane contributes with a velocity in the tangential direction, depending on a induction factor. This gives rise to the equations [Henriksen et al., 2012a]:

$$V_n = V_a(1 - a_n) \tag{8.1}$$
$$V_t = \omega_r r(1 + a_t) \tag{8.2}$$

Where: V_a is the ambient wind speed.

V_n is the speed of the nominal velocity component.

V_t is the speed of the tangential velocity component.

a_n is the induction factor in the nominal direction.

a_t is the induction factor in the tangential direction.

An element situated at the radius r has the absolute value (speed):

$$W = \sqrt{V_n^2 + V_t^2} \qquad (8.3)$$

Where: W is the absolute speed of the wind experienced.

Since the nominal and the tangential components are perpendicular, the angle of the inflow can be calculated as:

$$\phi = \arctan\left(\frac{V_n}{V_t}\right) \qquad (8.4)$$

Where: ϕ is the angle of inflow [rad].

Another angle is the angle of attack, which is the angle of the inflow compared to the pitch:

$$\alpha = \phi - \beta \qquad (8.5)$$

Where: α angle of attack [rad].
β is the pitch of the blade [rad].

From the lift and drag coefficients of the blade element, the lift and drag can be found as:

$$L = \frac{1}{2}\rho W^2 C_L(\alpha) c \qquad (8.6)$$

$$D = \frac{1}{2}\rho W^2 C_D(\alpha) c \qquad (8.7)$$

Where: L is the lift [N].
D is the drag [N].
C_L is the lift coefficient [−].
C_D is the drag coefficient [−].
c is blade chord length [m].

The lift and drag coefficients vary with the angle of attack. Typical data for these coefficients, retrieved from the airfoil data of one of the elements from the blades of the NREL 5 MW wind turbine, can be seen in Figure 8.2.
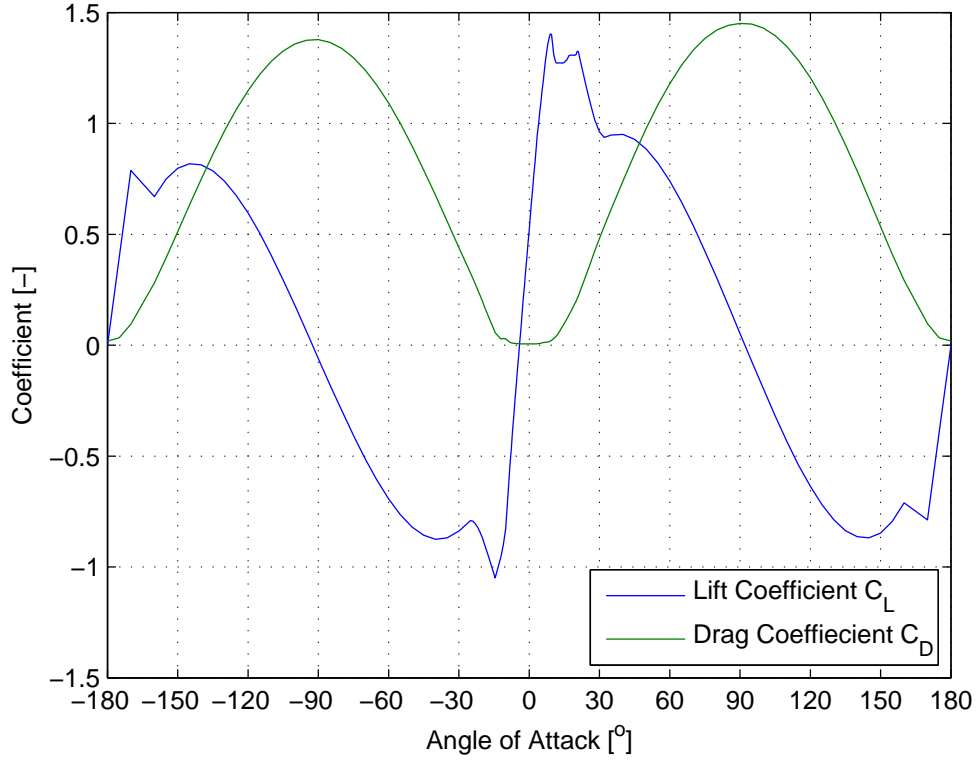
Figure 8.2. Typical airfoil data taken from a blade element of the NREL 5 MW wind turbine.

Lift and drag together results in the resultant force. The resultant force can be divided into force components normal and tangential to the rotor plane:

$$F_n(r) = L\cos(\phi) + D\sin(\phi) \tag{8.8}$$

$$F_t(r) = L\sin(\phi) - D\cos(\phi) \tag{8.9}$$

Where: $F_n(r)$ is the force component normal to the rotor plane [N].

$F_t(r)$ is the force component tangential to the rotor plane [N].

The combined aerodynamic torque and thrust on can be calculated, by integrating over the whole wing and combining all the blades:

$$T_a = n_b \int_0^R r F_t(r) dr \tag{8.10}$$

$$F_{thrust} = n_b \int_0^R F_n(r) dr \tag{8.11}$$

Where: T_a is the aerodynamic torque [Nm].

F_{thrust} is the thrust force on the rotor [N].

n_b is the number of blades [−].

R is the radius of the blade [m].

r is the radius at the element [m].

By using quasi-steady values for the induction factors a_n and a_t the rotor torque and thrust can be calculated using tables of the power coefficient C_p and thrust coefficient C_t. These

29

calculations are only true in steady state as the quasi-steady induction factors was used. This means that for varying rotor speed, wind speed or pitch the dynamics are not captured.

8.1 Dynamic Inflow

To capture these dynamics a model of dynamic inflow is introduced. When changing the operating point of the aerodynamics the wake takes time to settle before the aerodynamical forces are in steady state. Several models have been suggested for modelling this behaviour. An approach is to model the behaviour with a first order dynamic model [Øye, 1986]. The model affects the induced velocities, which for the quasi-steady BEM model were:

$$v_n^{qs}(r) = V_a a_n^{qs}(\lambda, \theta, r) \tag{8.12}$$

$$v_t^{qs}(r) = \omega_r r a_t^{qs}(\lambda, \theta, r) \tag{8.13}$$

Where: v_n and v_t are the induced velocities in the normal and tangential direction.
$a_n^{qs}(\lambda, \theta, r)$ and $a_t^{qs}(\lambda, \theta, r)$ are the quasi-steady induction factors in the normal and tangential direction.
V_a is the ambient wind.
ω_r is the angular velocity of the rotor.
r is the radius which the calculation is done at.

The induced velocities are the changes to the free wind speed in the respective directions after the wind has touched the blade element.

In the model proposed by [Øye, 1986] the quasi steady induced velocities are first computed, then changed according to a first order dynamic of the wake to create intermediate values. These intermediate values are then used again in radius dependent dynamic model which ensures that the tip elements reacts faster than the root. So the effect is gained by using two first order filters in succession, the first which is alike across the whole rotor and one which is radial dependent.

The inclusion of the first order dynamics of the wake gives rise to the state equations for the induced velocities:

$$\dot{v}_{n,int}(r) = \frac{1}{\tau_1}(v_n^{qs}(r) + k\tau_1 \dot{v}_n^{qs}(r) - v_{n,int}(r)) \tag{8.14}$$

$$\dot{v}_{t,int}(r) = \frac{1}{\tau_1}(v_t^{qs}(r) + k\tau_1 \dot{v}_t^{qs}(r) - v_{t,int}(r)) \tag{8.15}$$

Where: $k = 0.6$

From this intermediate value the radius dependent dynamics are computed to give the final difference equations for the induced velocities:

$$\dot{v}_n(r) = \frac{1}{\tau_2}(v_{n,int}(r) - v_n(r)) \tag{8.16}$$

$$\dot{v}_t(r) = \frac{1}{\tau_2}(v_{t,int}(r) - v_t(r)) \tag{8.17}$$

The time constants are calculated as:

$$\tau_1 = \frac{1.1}{1 - 1.3a}\frac{R}{V_a} \tag{8.18}$$

$$\tau_2 = \left(0.39 - 0.26\left(\frac{r}{R}\right)^2\right)\tau_1 \tag{8.19}$$

These calculations have to be done for every blade element on all the blades to compute the resultant rotor torque and thrust having this dynamic behaviour. This makes the model complex and numerically heavy. A simpler model for dynamic inflow have been made, which are better suited for modern control scheme. This will be investigated in the Section 8.3 on page 34.

AeroDyn can be set to use different inflow models. First option is BEM with quasi steady calculations. The next option is calculating inflow using another model than BEM called Generalized Dynamic Wake. GDW is a model, which describes the pressure distribution across the rotor plane. If FAST is set to use the GDW model it only uses it to calculate the norminal induced velocites, while BEM is still used to calculate the tangential induced velocities. For more information about GDW read [Moriarty and Hansen, 2005]. The GDW model developed for FAST was tested on data from a three-bladed 2 MW experimental wind turbine at Tjæreborg, Denmark [Suzuki, 2000]. Different test cases of data was used to test the model performance of the GDW model. One of the results can be seen in Figure 8.3.
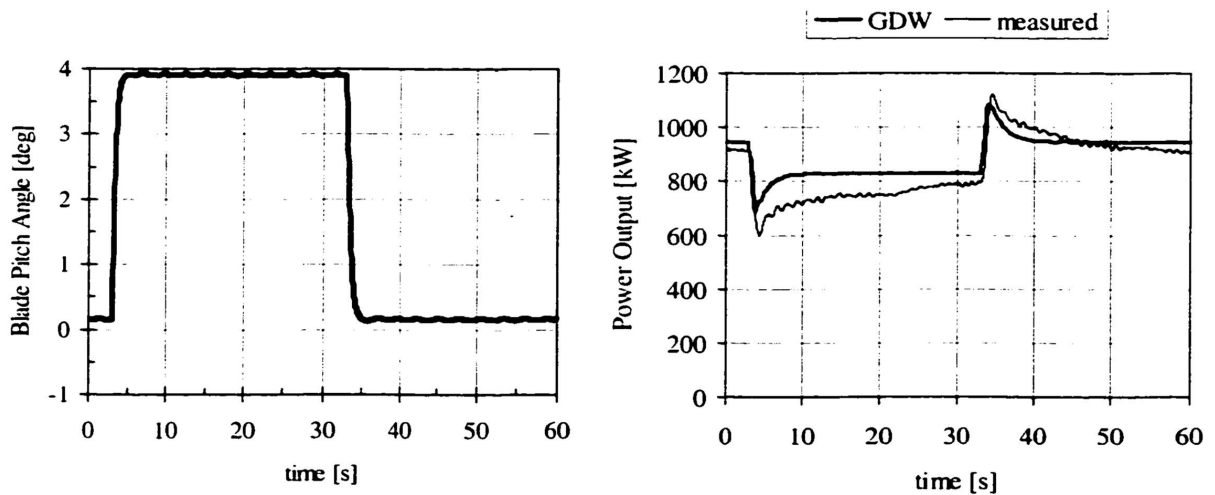

Figure 8.3. Test case for comparison of the GDW model with data from the three-bladed 2 MW experimental wind turbine at Tjæreborg. Averaged hub height wind speed was 10.5 $^m/_s$ at the time of data gathering [Suzuki, 2000, P. 47 and 64].

Here the result show that the GDW does model some of the "overshoot" from the quasi steady case. Only one of the results is here shown, but it should be noted that there are still differences between the measurement data from the Tjæreborg wind turbine and the GDW model. Since no wind turbine can be tested on in this project, GDW is the model used to represent a real wind turbine.

In Figure 8.4 the comparison between running FAST with BEM-quasi steady and GDW, when a change of operating point is performed.
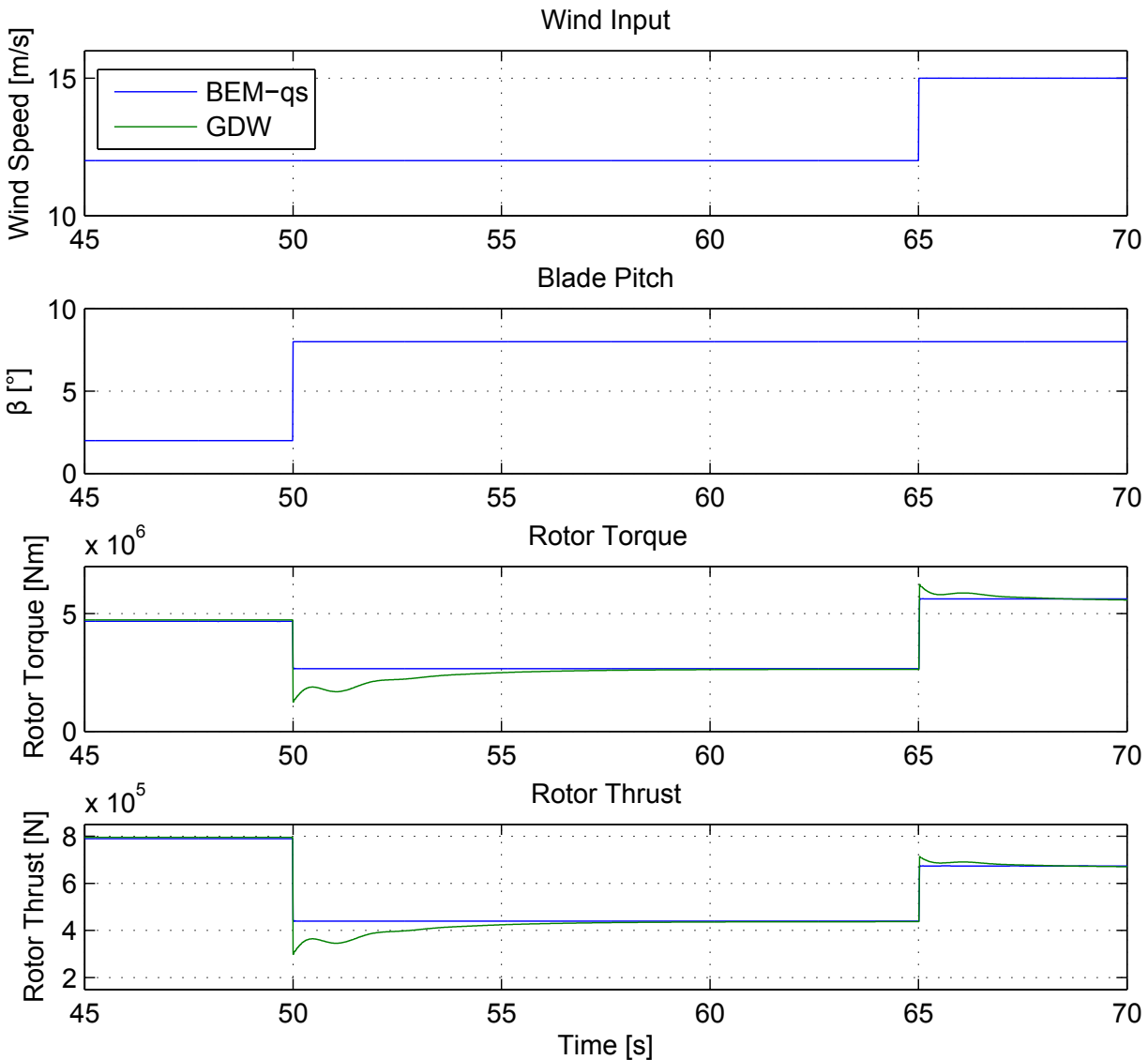

Figure 8.4. Comparison of AeroDyn equilibrium and dynamical model for inflow resulting in rotor torque and rotor thrust induced by changes in pitch and wind speed.

Here it is seen that one of the differences between GDW and quasi steady BEM calculations is the overshoot of the rotor torque and thrust before returning slowly to the steady state value. All though hard to see on Figure 8.4, there is a difference also in steady state values of the torque and thrust between the two models. This difference becomes more pronounced at lower pitch angles. This difference will be taken into account when using a simple dynamic inflow model.

8.2   Dynamic Stall

Dynamic Stall occurs on an airfoil, when a motion that takes the angle of attack above the critical angle of attack [Holierhoek et al., 2013]. In such a motion the aerodynamics experienced differ from the quasi-steady stall situation. The critical angle of attack is where the lift starts to decrease. An example of the critical angle can be seen on Figure 8.2 on page 29 around 9°,

where the lift reaches a maximum. When dynamic stall occurs a vortex is generated on the leading edge of the airfoil. This vortex which consist of fast moving air induces a brief increase of lift. As the vortex travels down the upper edge of the airfoil past the trailing edge, the lift decreases rapidly and the airfoil reaches steady state stall.

FAST uses the Beddoes–Leishman method to model this behaviour. Read [Beddoes, 1983] for more information on how this model works. A comparison of FAST responses with and without dynamic stall can be seen in Figure 8.5.
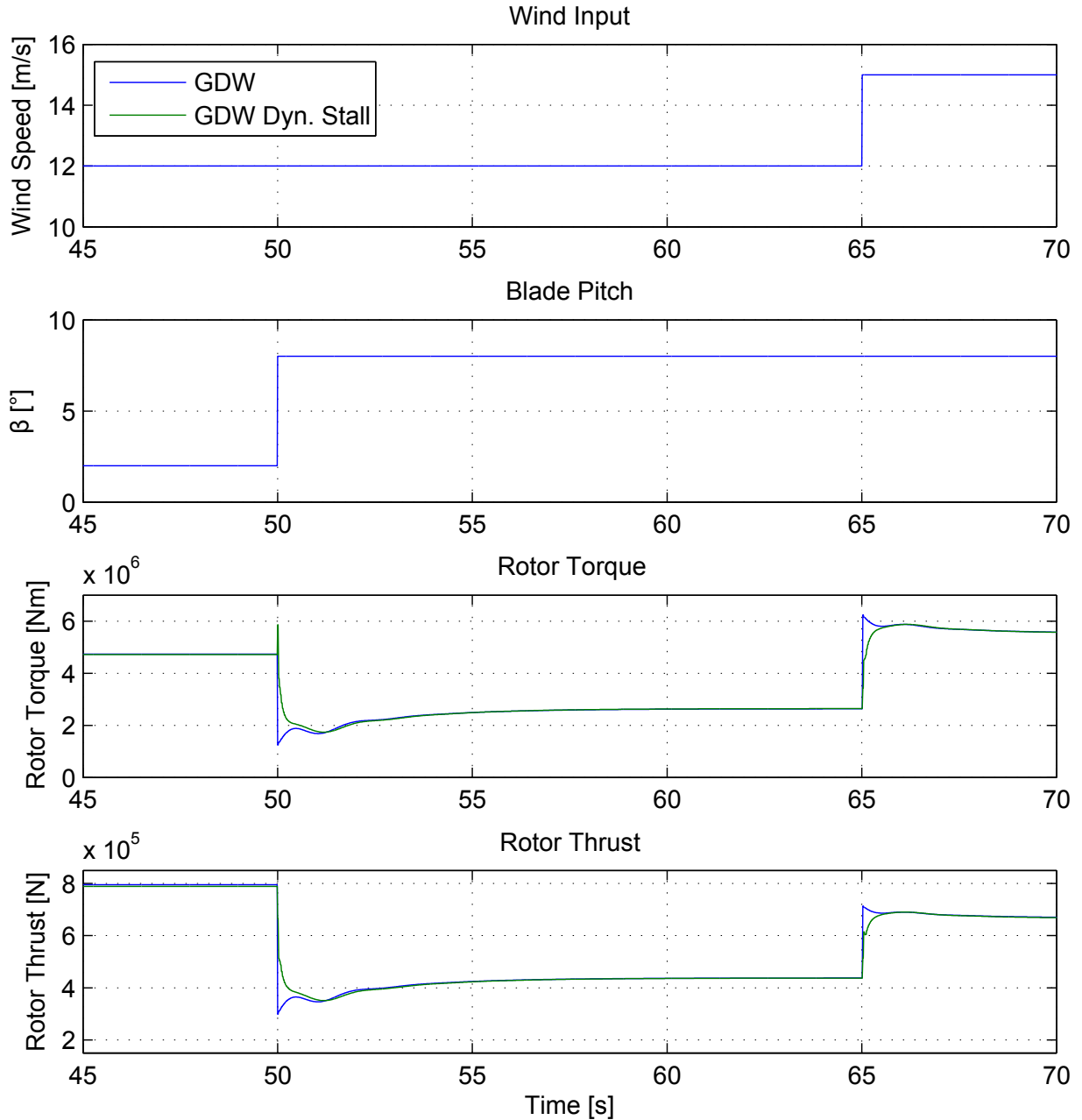

Figure 8.5. Comparison of AeroDyn steady and Beddoes model for stall resulting in rotor torque and rotor thrust induced by changes in pitch and wind speed.

Dynamic stall is not the focus of this project and no further investigation is done to include this phenomenon.

8.3 Simple Dynamic Inflow Model

The simple dynamic inflow model shown here is the one presented in [Knudsen and Bak, 2013]. The dynamic inflow model described earlier involved calculating the forces on every element spanning the blade leading to a numerically heavy approach. This simple model combines all the elements into one resulting in one induction factor. This induction factor is then extended with first order dynamics to capture the behaviour of dynamic inflow.

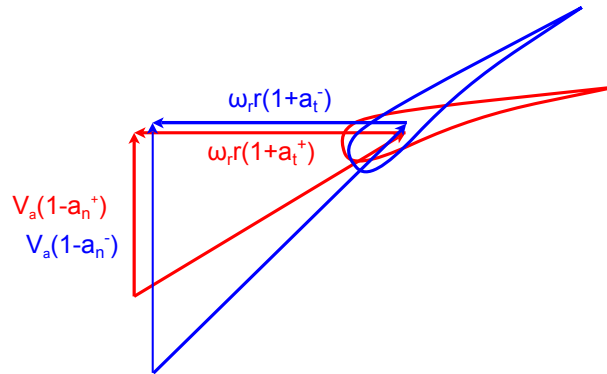The dynamic change of induction factor used in the simple model can be explained with Figure 8.6 as a reference.

Figure 8.6. The stationary speeds before and after a change in pitch here shown on the cross section of a blade. The blue represents the initial position and red the final position.

In the blue case the wind speed is steady and the aerodynamics are in a quasi steady state. Then the pitch is changed instantaneously to the red position. Now the aerodynamics will slowly change from the blue towards the red case, until it fully reaches the steady red case. This transition is done by introducing a fictive ambient wind speed:

$$V_f = V_a \frac{1 - a_a^-}{1 - a_a^+} \tag{8.20}$$

Only the change in the axial induction is used since it is assessed that the change in tangential induction factor is less important. The change in axial induction factor is modelled as a first order system:

$$\dot{a}_a^- = \frac{1}{\tau_s}(a_a^+ - a_a^-) \tag{8.21}$$

The time constant is approximated as:

$$\tau_s = \frac{3D_r}{2V_a} \tag{8.22}$$

Where: D_r is the rotor diameter.

To find the axial induction for the new steady state a_a^+ the following approximation is made from the C_t table:

$$C_t = 4a_a^+(1 - a_a^+) \quad \wedge \quad 0 \le a_a^+ \le \frac{1}{2} \tag{8.23}$$

$$\Updownarrow$$

$$a_a^+ = \frac{1}{2}\left(1 - \sqrt{1 - C_t}\right) \tag{8.24}$$

Where: $C_t(\lambda(t), \beta(t))$ is the thrust coefficient $[-]$.

From the fictive ambient wind speed the rotor force and rotor torque can now be calculated as:

$$T_a(t) = \frac{1}{2\omega_r(t)}\rho V_f^3(t) A C_p(\lambda(t), \beta(t)) \tag{8.25}$$

$$F_t(t) = \frac{1}{2}\rho V_f^2(t) A C_t(\lambda(t), \beta(t)) \tag{8.26}$$

This simple model is implemented and compared to the GDW model of FAST. Step responses of pitch changes at rated wind speed can be seen in Figure 8.7. Only the responses for rotor torque and not thrust is shown as the show same behaviour in regard to comparison between the simple dynamic inflow model and GDW.
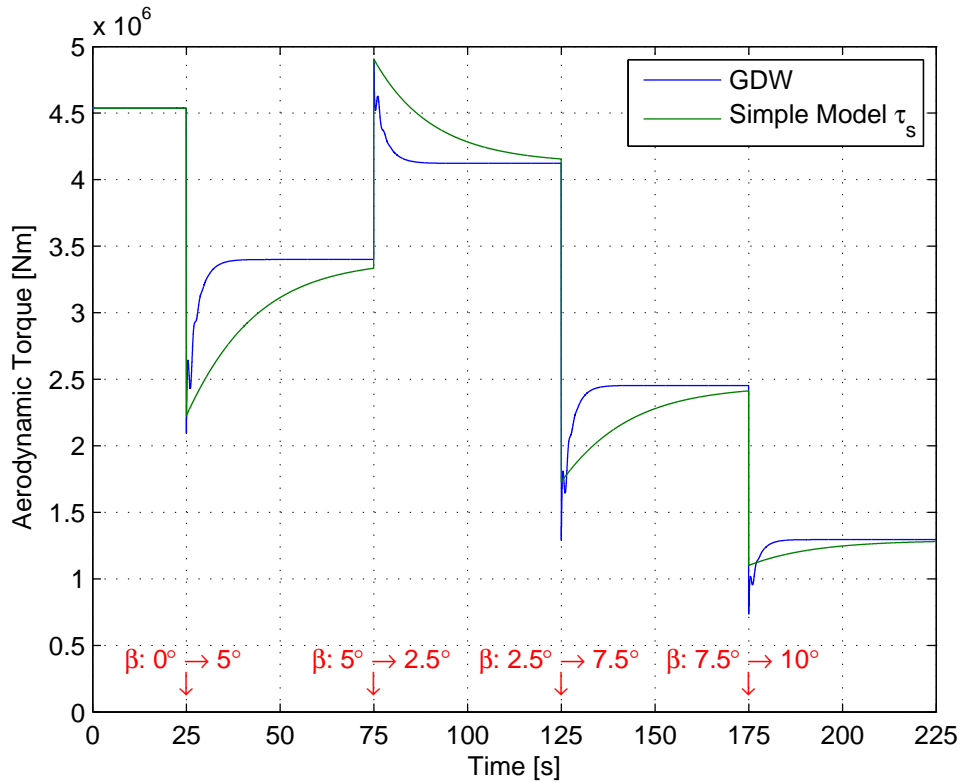

Figure 8.7. Comparison of GDW with simple dynamic inflow model.

There are two main differences - firstly the dynamics of GDW are nonlinear and is not a neat first order response. That said, a first order response seems to model the overall influence on the torque decently. The next difference is that the time constant is too long. A parameter estimation has been done on the time constant changing it from $\tau_s = (3 \cdot 136\ m)\ (2 \cdot 11.4\ ^m/s) = 16.58\ s$ to the revised time constant $\tau_{sr} = 2.89\ s$ at rated wind speed. This gives the following result:
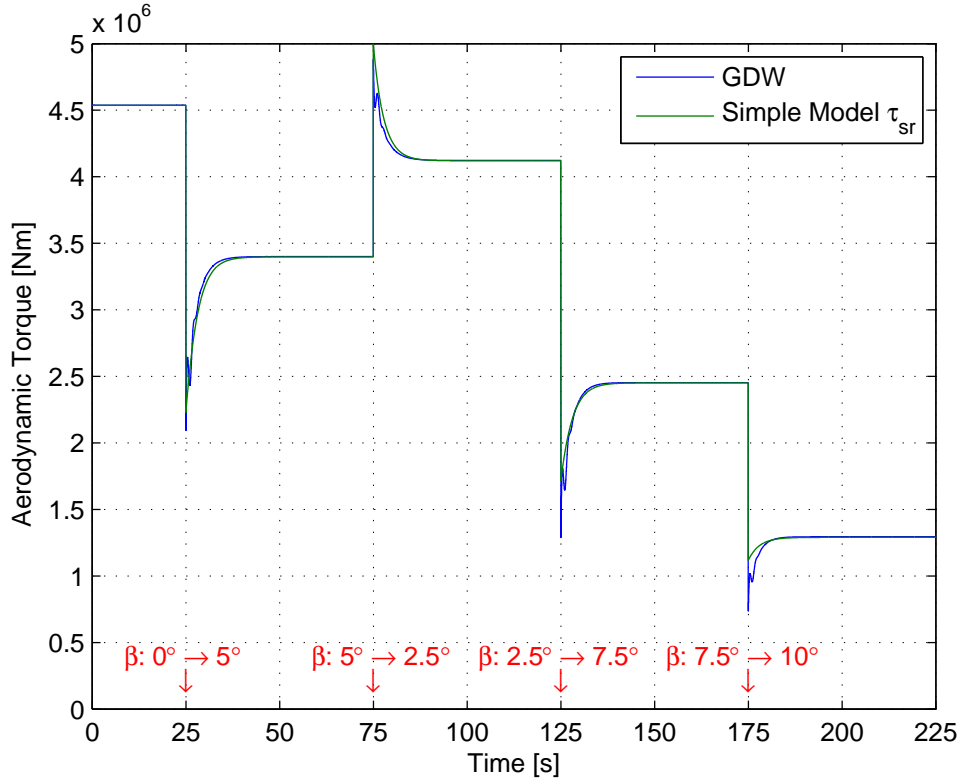

Figure 8.8. Comparison of GDW with simple dynamic inflow model at changes in pitch with a revised time constant.

This time constant gives the best fit, both in regard to changes in pitch and changes in wind speed. The simple dynamic inflow model with a revised time constant results in a good fit for changes in pitch, though less precise at higher pitch angles. The simple dynamic inflow model however does not provide the same results as GDW when changing wind speeds. This is most pronounced at changing wind speed at lower constant pitch angle. On Figure 8.9 step responses to change in wind at a constant pitch of 2° is seen.
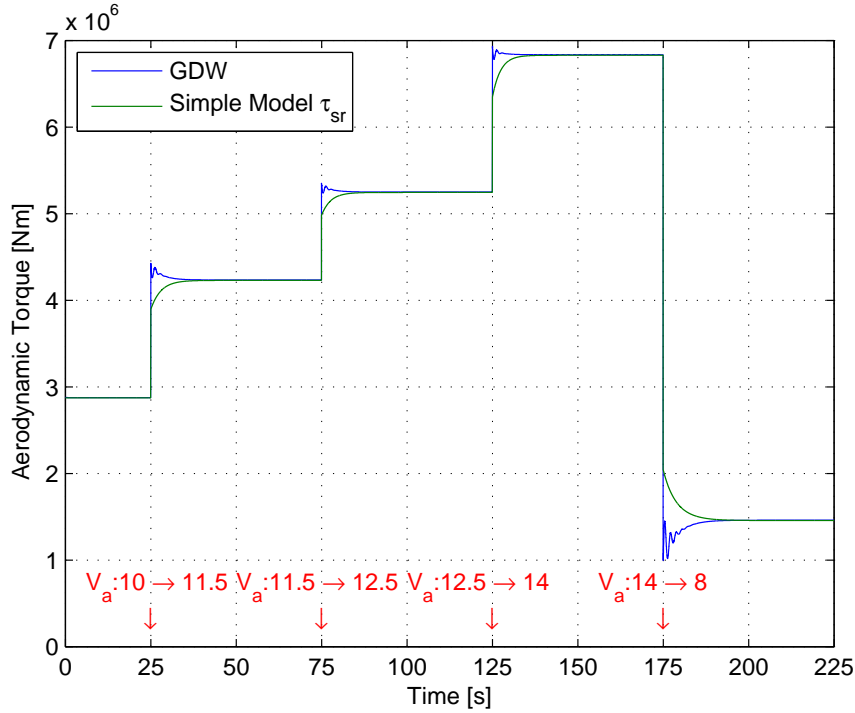
Figure 8.9. Comparison of GDW with simple dynamic inflow model at changes in wind speed with a revised time constant.

This discrepancy is not as important when used in the controller since no prediction model of changing wind is implemented in the controller. In other words, the controller will calculate the control inputs considering the wind to be constant in the future, so a model describing changes in the wind will have no effect.

Since the time constant of the simple dynamic inflow model was lower than expected as per [Knudsen and Bak, 2013] it was tested on another wind turbine in FAST, the 1.5 MW Windpact wind turbine. This showed similar result of a faster time constant fitting the smaller length of the blades. By also comparing to the time constants of simple dynamic inflow model described in another work [Henriksen et al., 2012a], where the 5 MW NREL wind turbine was tested via HAWC2 instead of FAST, the reduced time constant found here is deemed fitting. It is hard to say, if the data gained by these simulations for dynamic inflow would fit that of a real wind turbine, without having access to a wind turbine for test. Since the model for the 5 MW NREL wind turbine have been used in various peer-reviewed articles and the dynamic inflow phenomenon for the wind turbine have been tested through both HAWC2 and FAST, they are deemed fit to describe the reality of dynamic inflow on a wind turbine.

Dynamic inflow has the largest contribution at lower pitch as seen in Figure 8.8. This means the operating area that is of most interest in this thesis is in the start of region 3, where the pitch is low but changed often to reject disturbances in the wind. The operating point which the controller is designed for is at 12 m/s, which is in the lower part of region 3. The rated wind speed for the 5 MW NREL wind turbine is 11.4 m/s.

A quasi steady, dynamic and a simple dynamic inflow model was presented and compared. The simple dynamic inflow model with a decreased time constant was concluded to be precise enough to be used in the control scheme. An operating point is established to be at 12 m/s. which is close to rated speed, but still allows for fluctuation around this without going below rated wind.

37

Structural Natural Frequencies 9

The wind turbine has structural natural frequencies. If resonance increases the energy of oscillations at these frequencies, it can lead to damage of the structure. To minimize structural damage an analysis is made, such that it is ensured that knowledge of the relevant modes is used in the controller.

In every mechanical system the components have natural frequencies at which there will be unforced oscillations, when no damping factor is present. When forced oscillations occur at these frequencies, the amplitude of the oscillations will increase, which is known as resonance. Oscillations in a wind turbine can be critical, as oscillations with large amplitude in particular causes fatigue, which eventually leads to failure (see Chapter 5 on page 14).

FAST has the ability to compute linearised models. This is used to get an initial understanding of the system in the frequency domain. Unfortunately FAST can only compute these models when using quasi steady BEM models for the aerodynamical forces. The difference between a linearised dynamic inflow model and a quasi steady BEM model has been shown in Figure 10.1 on page 43.

A bode plot of the linearised model going from pitch as input to tower fore-aft 1. mode deflection in output, gained from FAST, can be seen in Figure 9.1:
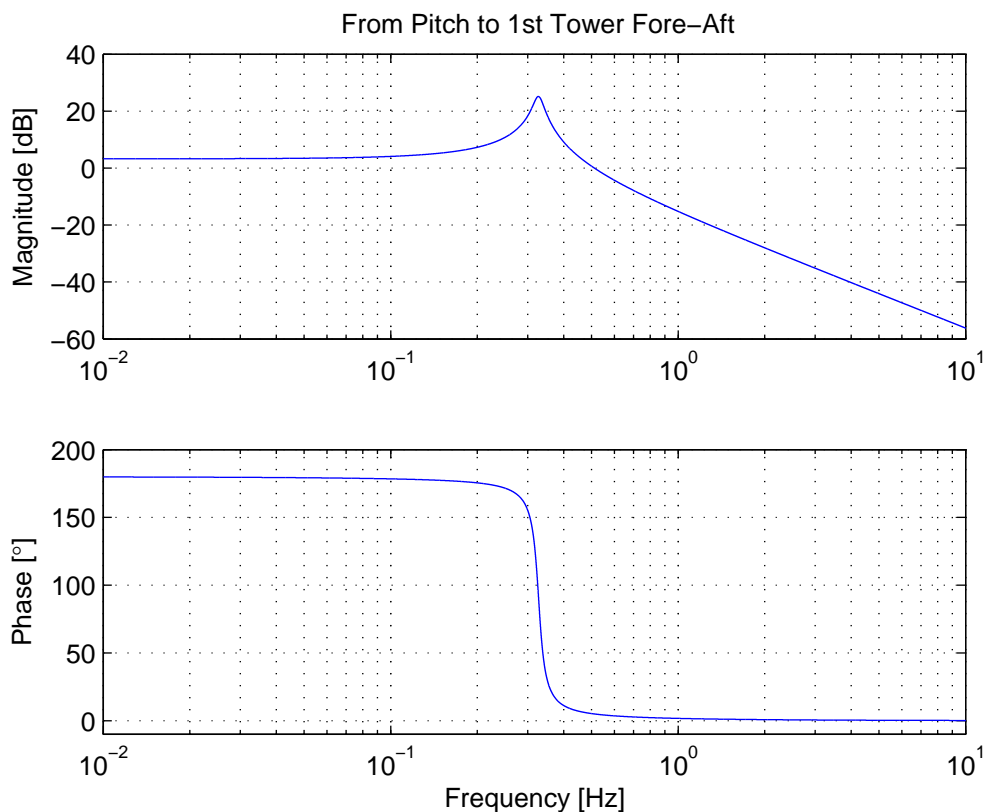

Figure 9.1. Bode plot of the linearised model describing the relation between blade pitch and tower fore-aft 1. mode deflection.

Here it can be seen that the natural frequency appears at 0.324 Hz. Depending on the bandwidth of the control loop, this frequency may or may not be of interest. By comparing this to information of necessary bandwidth of the control system gained in Chapter 10 the natural frequency of the 1. mode deflection of the tower is deemed to be of importance.

It is important that the model used for MPC contains these natural frequencies, which appear below the control bandwidth, such that the controller can take them into account, when calculating the optimal control action. On the basis of the fatigue analysis, minimizing fatigue leads to active damping of tower deflections, which means that this mode is crucial to represent in the models.

By going through the wind turbine making linear models for the structures movement the following natural frequencies is found:

Mode	Description	Frequency [Hz]
1	1st Tower Fore-Aft	0.3240
2	1st Tower Side-to-Side	0.3120
3	1st Drive train Torsion	2.222
4	1st Blade Asymmetric Flapwise Yaw	0.6664
5	1st Blade Asymmetric Flapwise Pitch	0.6675
6	1st Blade Collective Flap	0.6993
7	1st Blade Asymmetric Edgewise Pitch	1.079
8	1st Blade Asymmetric Edgewise Yaw	1.090
9	2nd Blade Asymmetric Flapwise Yaw	1.934
10	2nd Blade Asymmetric Flapwise Pitch	1.922
11	2nd Blade Collective Flap	2.021
12	2nd Tower Fore-Aft	2.900
13	2nd Tower Side-to-Side	2.936

Table 9.1. Full-System Natural Frequencies [Jonkman et al., 2009].

The linear model shown was the relation between blade pitch and tower fore-aft deflection. Obviously the frequencies from the other moving parts can resonate to these natural frequencies. When deciding on the rated speed of the rotor, natural frequencies also has to be taken into account. This can be done by using a Campbell diagram. Normally in a Campbell diagram the eigenvalues change as a function of rotational speed, but in this, generated from the retrieved linear data, the eigenvalues will be constant. The Campbell diagram of the rotor speed shown in Figure 9.2 gives an overview of how to choose an appropriate rotor speed.
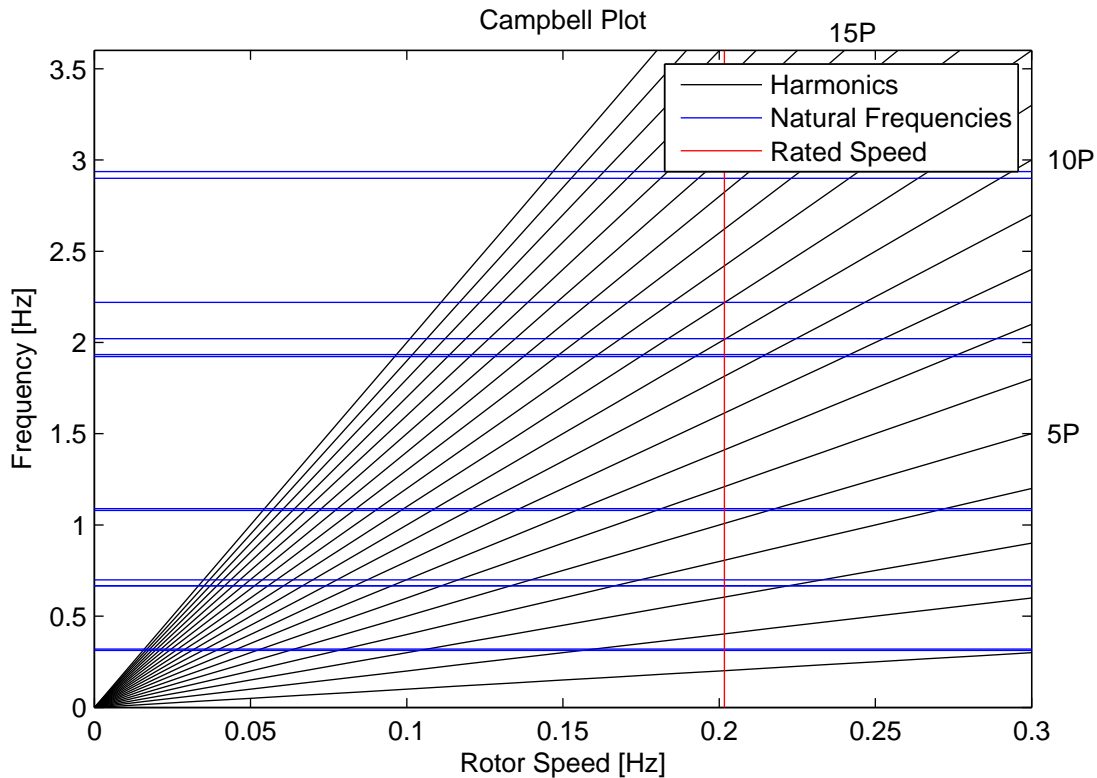
Figure 9.2. Campbell diagram of rotor speed. The diagram shows natural frequencies of the structure (blue) and the harmonics (black). Resonance occurs, where the blue and black lines crosses depending on the energy in the given harmonic. The rated rotor speed is in this wind turbine set to 12.1 rpm = 0.202 Hz (red).

The first harmonic (1P) carries alot of energy and is of greatest importance in regard of hitting the natural frequencies. Which other harmonics that carry energy depends on the design. In a three bladed wind turbine the 3P, 6P, 9P and 12P harmonics can for instance also contain a lot of energy. Since the rated rotor speed is already designed for the chosen wind turbine at 12.1 rpm = 0.202 Hz this can be checked, as seen in Figure 9.2, against the natural frequencies. It is seen that the 10P harmonic 2. mode blade collective flap and 11P harmonic of the drivetrain torsion are very close to the rated speed of the rotor. However, these are deemed insignificant, due to the high order harmonic frequency. In Figure 9.2 the natural frequencies of the different modes are considered constant in regard to rotational speed. The is not completely true since the structures are affected by the operation, such that the natural frequencies changes slightly as a function of rotational speed. A more in depth analysis of the changing natural frequencies as a function of wind speed can be found in [Bir and Jonkman, 2007]. As an example the tower 1. mode fore-aft natural frequency changing at different rotational speeds of the rotor can be seen in Figure 9.3 - extracted from FAST.
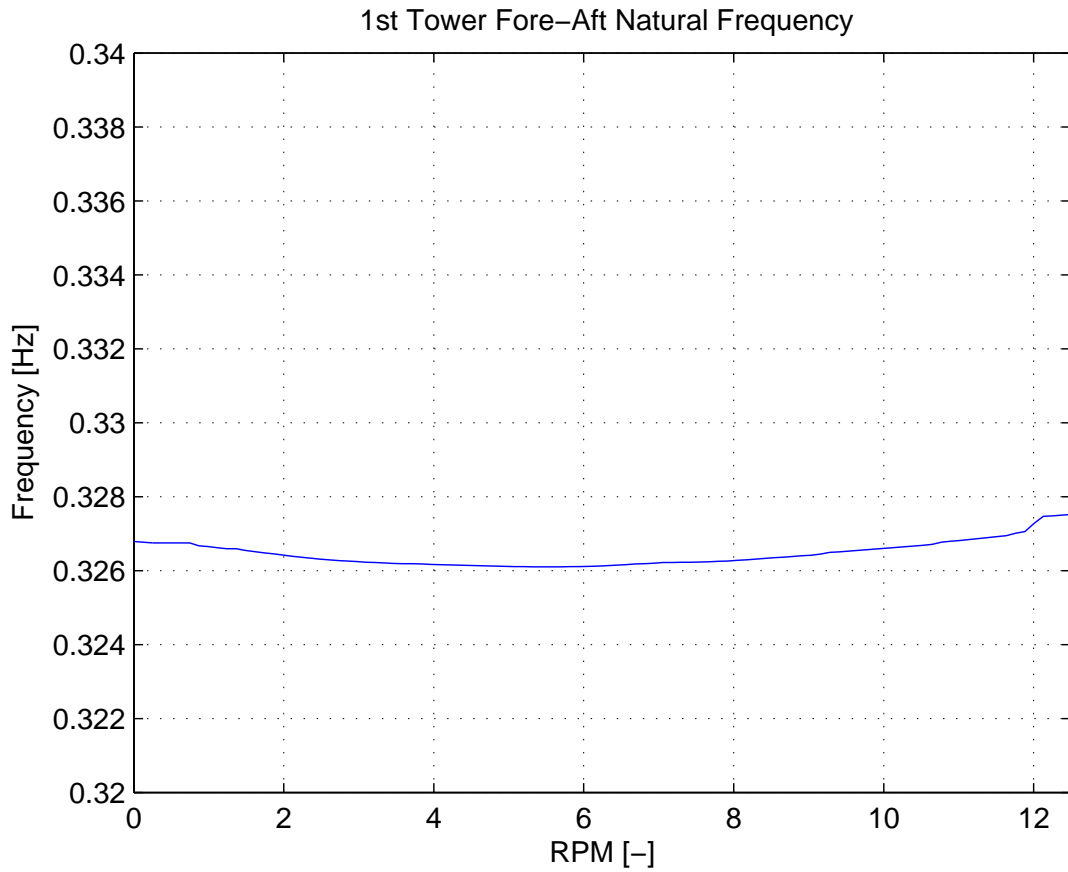
Figure 9.3. 1. mode tower fore-aft natural frequency changing slightly at different rotational speeds of the rotor for the 5 MW NREL wind turbine.

I can be seen that the natural frequency changes only slightly as a function of rpm of the rotor.

The natural frequencies of the 5 MW NREL wind turbine has been found. Depending on the desired bandwidth of the controller, more or less of these should be taken into account when designing the control scheme. The drivetrain torsion and 2. mode blade collective flap natural frequencies are located close to the rated speed of the rotor, but are deemed insignificant, due to the high order harmonic frequency and are furthermore not in the scope of this project.

Effect of Dynamic Inflow in Wind Turbine Control 10

An initial analysis of the relevance of including dynamic inflow in the control scheme is here presented. One of the important questions is, if the bandwidth of the control system is comparable to the dynamic inflow phenomenon, since only then does it make sense to include knowledge of dynamic inflow in the control scheme. First the effect of dynamic inflow on the rotor torque and thrust, later it is analysed how this effect propagates through the rest of the wind turbine and alters the angular velocity of the rotor and the movement of the tower.

10.1   Actuator Influence

By having a high bandwidth better disturbance rejection can be achieved. The main disturbance on the control loop is changes in the wind. The bandwidth of the wind determines how fast the control system has to be to properly reject this disturbance. The spectrum of turbulence can be seen in Section 6.2 on page 21. The spectrum shows that the main energy is centred around 0.02 Hz and flattens out around 10 Hz. Considering this the bandwidth of the control system needs to be in the vicinity or higher than this for proper disturbance rejection. A limiting factor on the bandwidth of the control system is the pitch actuator control loop. This will limit how fast the control loop can be and thus how much of the wind disturbances that can be rejected. The resultant achievable bandwidth will determine if dynamic inflow is relevant. At what bandwidth dynamic inflow is relevant is estimated in the dynamic inflow section of this chapter.

A linear model representing the relation between a pitch reference and torque on the rotor including dynamic inflow and a first order model for the actuator system is made. This linear model is made by linearising the simple dynamic inflow model as described in Chapter 15. It is important to notice that at this point no model of the rest of the wind turbine is used, only the aerodynamical parts. This means that the rotation speed is kept constant. This is a simplification since by changing pitch, rotation speed of the rotor naturally changes, which in turn changes the aerodynamical torque. This simplification is done to give an initial estimate, without going into too great detail of the model, whether it makes sense to include dynamic inflow. The inclusion of the rest of the wind turbine is done later in the chapter.

By neglecting the pitch actuator dynamics ($\beta(t) = \beta_{ref}(t)$) and only looking at the dynamics of dynamic inflow the bode plot from pitch to rotor torque can be drawn as seen on Figure 10.1. The line plotted in the magnitude plot is an illustration of the BEM quasi steady model, which has a magnitude, but infinite bandwidth.
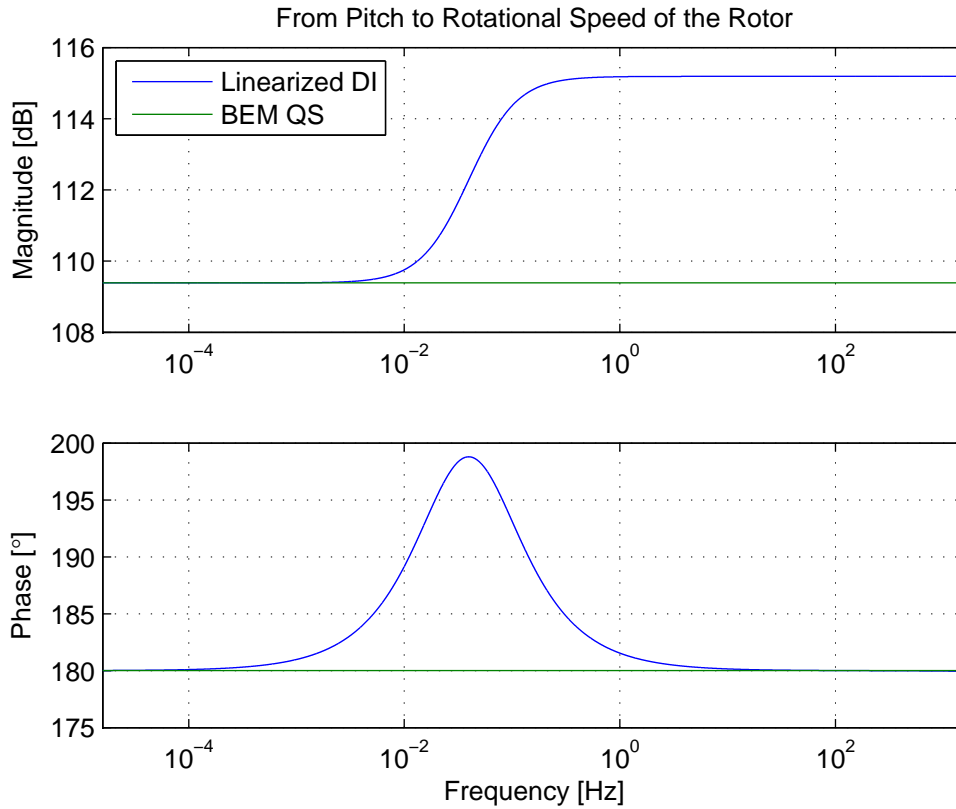
Figure 10.1. Difference between linearised dynamic inflow model and the quasi steady BEM model (has infinite bandwidth) on rotor torque.

At higher frequencies it can be seen that the magnitude of the torque varies 6 dB between the two models, which is a significant impact and is the reason dynamic inflow has to be incorporated in the control, when operating at a high enough bandwidth. The point where the two models differ is the critical frequency, which the actuator control system has to exceed in bandwidth for inclusion of dynamic inflow in the model to start to have an effect. This critical frequency is at 0.003 Hz. At 1 Hz the full 6 dB difference occur. Since the main energy in the turbulence spectrum was at 0.02 Hz, and there is still a contribution from higher bandwidths, dynamic inflow needs to be included in a system which seeks to reject the disturbance from turbulence.

The actuator system puts a limit on how fast a bandwidth of the control system that can be achieved. An illustration of how faster or slower actuator systems respectively makes information about dynamic inflow relevant and irrelevant can be seen in Figure 10.2.
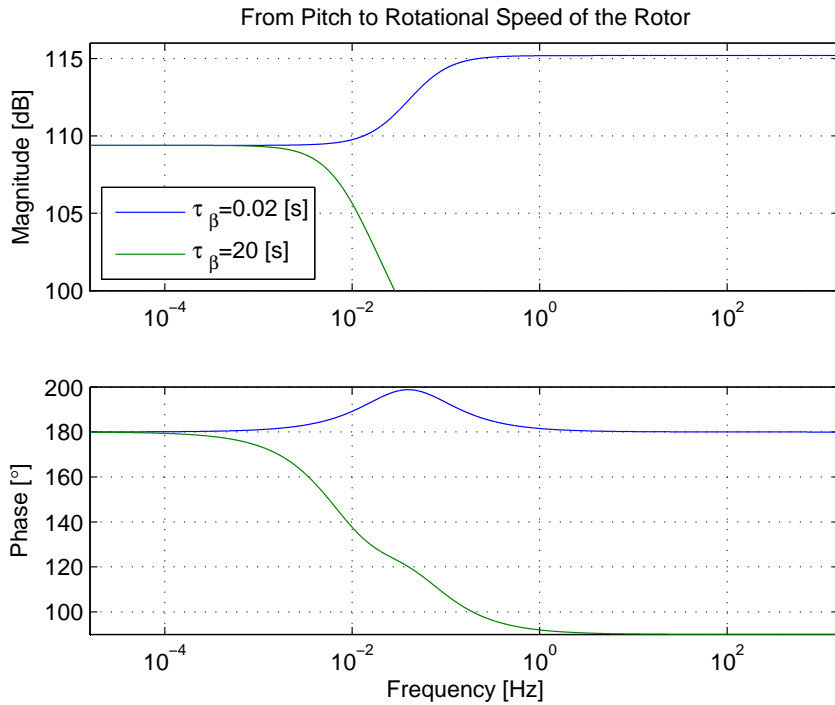

Figure 10.2. System including dynamic inflow and first order pitch actuator with different time constants.

With the slow time constant on the pitch actuator control system, the dynamic inflow is irrelevant with regard to control, where a faster time constant means that dynamic inflow is relevant.

Another way of illustrating this is by making the rotor torque controller, which finds the optimal pitch control inputs that minimizes the tracking error and seeing the effects of inclusion of dynamic inflow. The controller used is a MPC - more information about MPC can be found in Chapter 18 on page 82. Two controllers are made. One which takes dynamic inflow into consideration in the optimizing of the trajectory and one which does not. Both of these are applied to the linearised dynamic inflow system, see Figure 10.3.
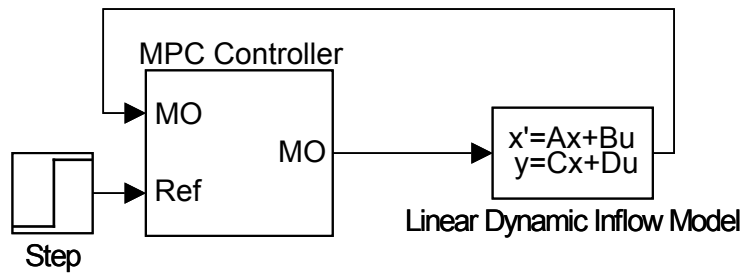

Figure 10.3. The setup for the MPC test on the linearised dynamic inflow model.

With a fast time constant on the pitch actuator control system, it can be seen that the controller, which takes dynamic inflow into account, performs best, see Figure 10.4. With a slow time constant both controllers perform equally, as expected, since the additional knowledge of dynamic inflow can only be used at higher bandwidth.
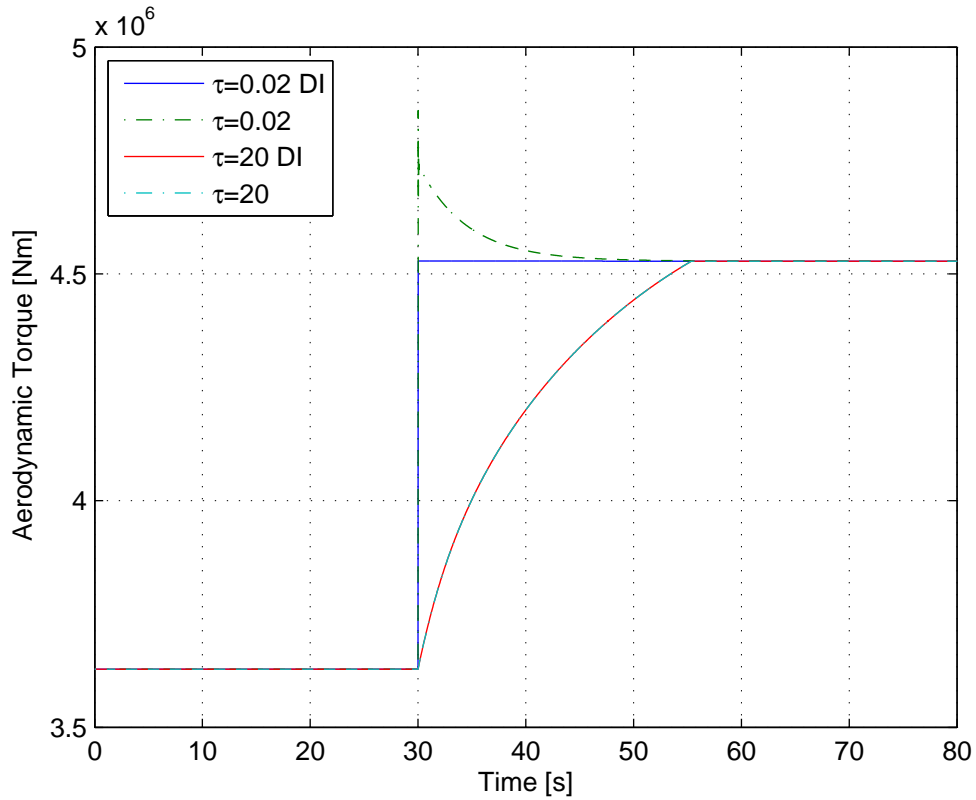

Figure 10.4. Comparison of controllers with and without inclusion of dynamic inflow knowledge acting on a system with dynamic inflow first with a fast time constant on the actuator and then with a slower one.

This simple MPC can also be used to test, if dynamic inflow is relevant, while using a specific actuator with constraints such as slew rate and saturation. As an example the difference between including and not including dynamic inflow in the control, when the actuator has a time constant of 1 s and a slew rate of 10 °/s can be seen on Figure 10.5.
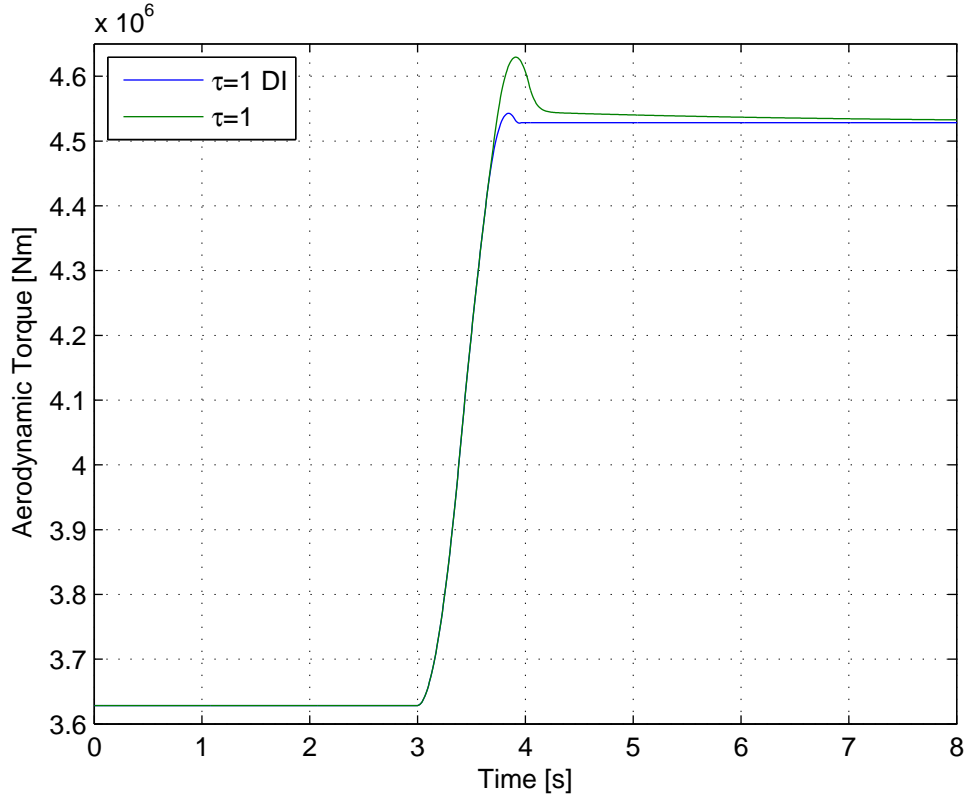

Figure 10.5. Comparison of controllers with and without inclusion of dynamic inflow knowledge acting on a system with dynamic inflow and a pitch actuator with a time constant of 1 s and slew rate of 10 °/s.

With this actuator the controller with dynamic inflow knowledge can suppress the overshoot by some, but not completely because of the limitations of the actuator system. No specific actuator parameters are chosen for the test of the later MPC, since these parameters will be altered in different test to see the implications of changing these.

Now a comparison of wind turbulence, dynamic inflow and actuator system has been carried out with regard to the rotor torque and thrust (only torque shown here, since thrust was almost identical). The center frequency of wind turbulence lies at 0.02 Hz, with contribution ranging into 10 Hz. Contribution from dynamic inflow starts from 0.003 Hz and continues to have influence upwards. No specific dynamic parameters was chosen for the actuator system, but impact by using a slow and faster system was shown.

10.2 Dynamic Inflow in Power and Tower Movement

Now it is analysed how rotor torque and thrust propagates through the rest of the wind turbine and alters respectively the angular velocity of the rotor and the movement of the tower. Where before the effects were shown using only models for aerodynamics, the next is shown using models from FAST. By using models in FAST containing the tower and the power system, consisting of drivetrain and generator, the effects of dynamic inflow on rotor - and tower velocity can be shown. When keeping the generator torque constant, these two states represent the two main outputs that later will be controlled: power and tower velocity.

The models used from FAST are without any effect of a pitch actuator system. The bode plots shown are taken from linearised models of there system, whereas the transient responses are from the FAST model which is non-linear.

First the effect of adding dynamic inflow to the fast model from pitch to rotor speed is investigated in the frequency domain:
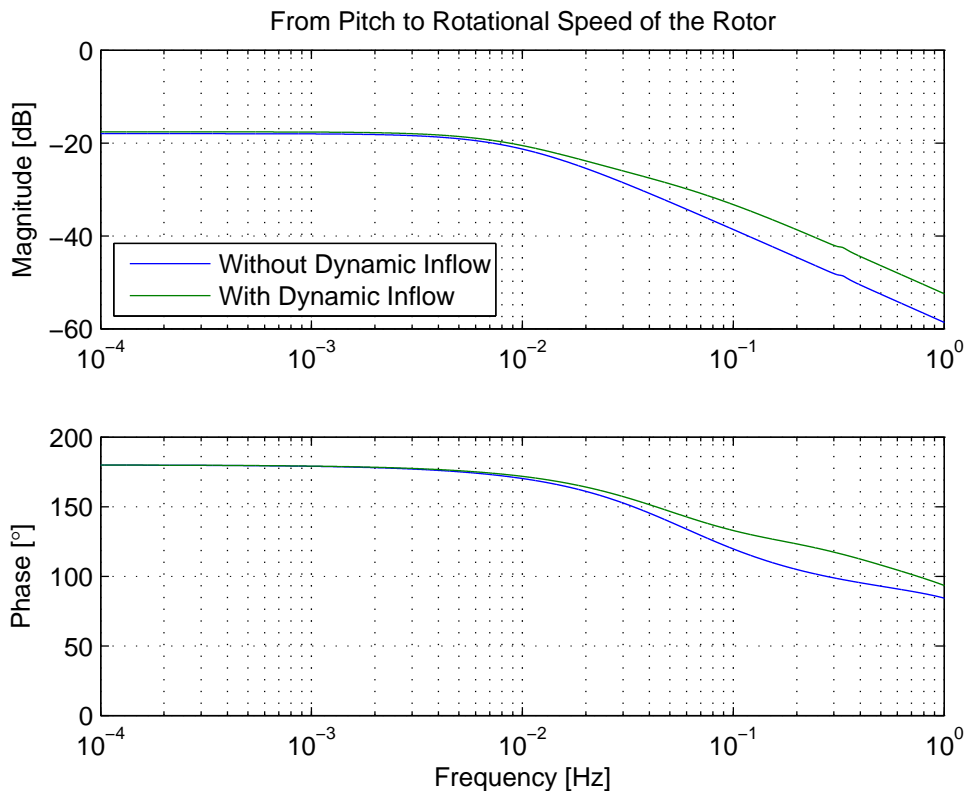

Figure 10.6. Bode plot from pitch to rotor speed with and without dynamic inflow.

Here it is seen that the frequency where the change from dynamic inflow appear at a higher frequency than the cut off frequency of the rotor speed rotational dynamics. This leads to the conclusion that dynamic inflow will not have any relevant impact on they dynamics of the rotational system and therefore the power system on this wind turbine. This could be different on another wind turbine, where the dynamics of the rotational system is faster due to e.g. lower inertia.

In Figure 10.7 the rotor speed with and without dynamic inflow can be seen in the time domain. The rotor speed is changed by applying a step in pitch from 4° to 2°.
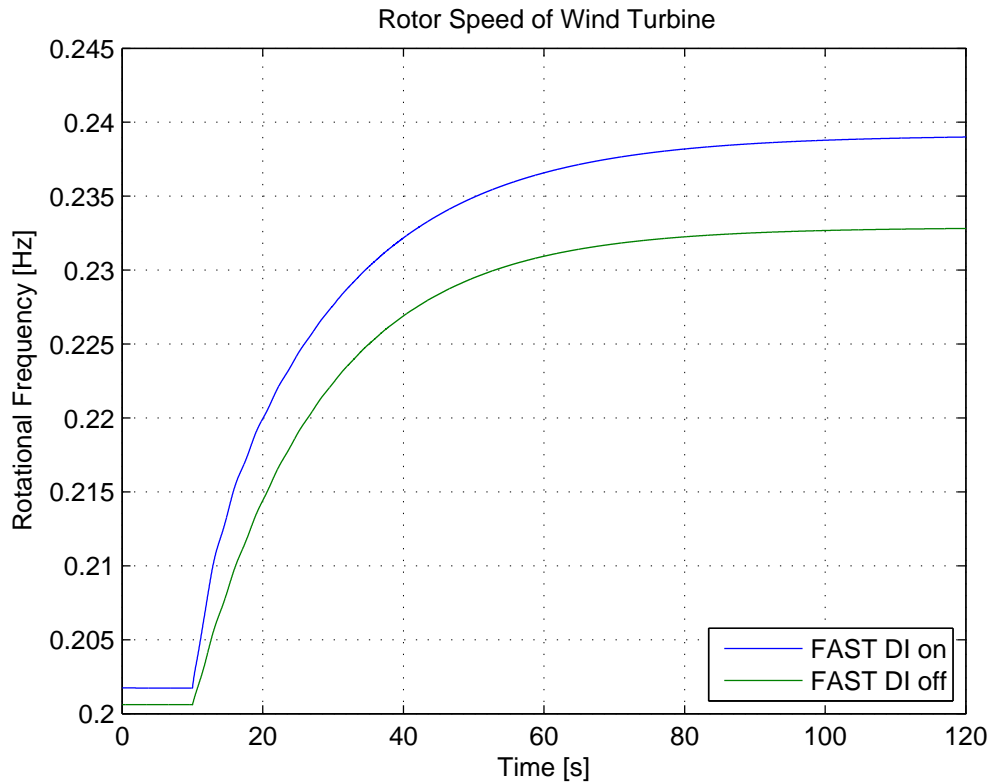

Figure 10.7. Rotor speed response to a step in pitch using FAST with and without dynamic inflow.

As explained in Chapter 8 on page 27, there is a steady state difference in the two models FAST use. This steady state difference is the only difference suggesting that dynamic inflow does not have any noticeable effect on the dynamics of the power system, as determined from looking at the frequency domain. This is due to friction and inertia of the drivetrain and the generator. The extra torque added from dynamic inflow right after the change of pitch does not contain enough energy to cause any significant difference. This suggest that no improvement of the control of power generation on this wind turbine can be made by adding knowledge of dynamic inflow to the control.

Now the same analysis process is made on tower deflections, to get an initial understanding of the impact of dynamic inflow. In Figure 10.8 the frequency response of tower deflections from changes in pitch can be seen.
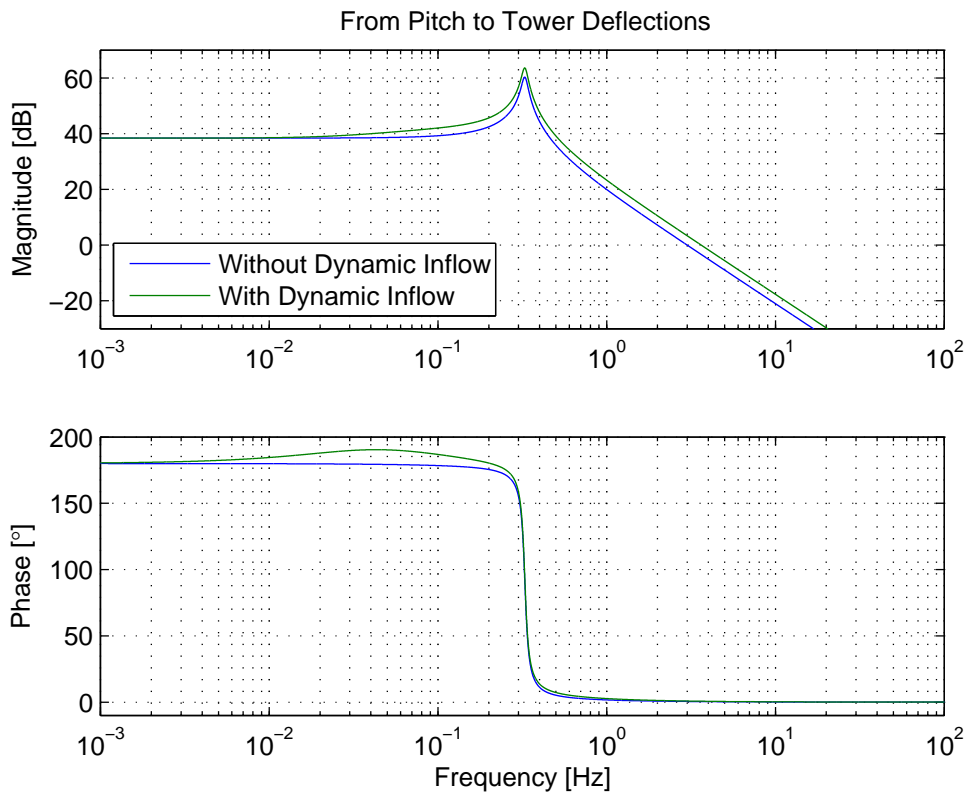

Figure 10.8. Bode plot from pitch to tower deflections with and without dynamic inflow.

Here the dynamics of the tower deflections are fast enough that the changes from dynamic inflow influences both the amplitude and the phase within the bandwidth. To further investigate the changes, which dynamic inflow imposes on the velocity of the tower deflections, a step is done on the pitch in time domain. This tower velocity occurring from this step can be seen in Figure 10.9 on the next page.
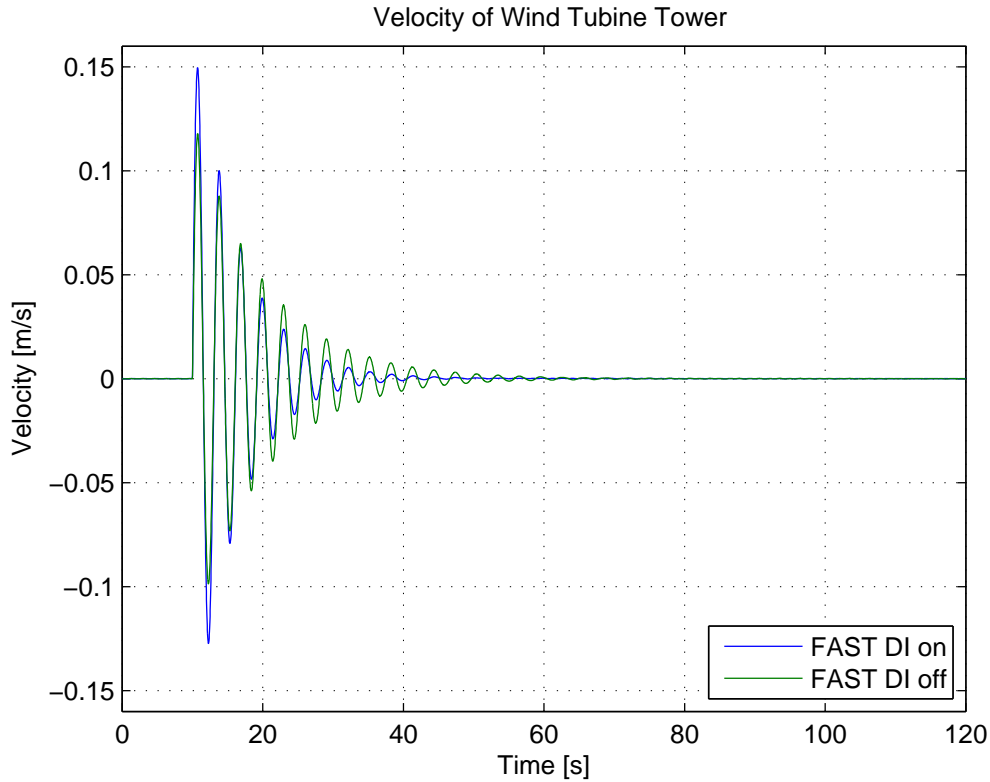
Figure 10.9. Tower velocity response to a step in pitch using FAST with and with dynamic inflow.

Here it can be seen that the added force at that dynamic inflow adds right after the step increasing the first fluctuations of the tower velocity. After that the fluctuations decreases faster than the system without dynamic inflow. This difference suggest that using a controller with knowledge of dynamic inflow can improve active tower damping. Exploring this possibility further is the objective of this thesis.

At first it was shown how dynamic inflow, wind and control bandwidth determine what effect dynamic inflow has on rotor torque and thrust. The effect of having faster or slower pitch actuator in the loop also determines if having dynamic inflow information is necessary. Here it was shown that rate constraints and generally slow dynamic of the actuator can lead to the control system becoming slower than the point where dynamic inflow matters. Dynamic inflows effect on rotor speed and tower velocity was also shown. Only tower velocity was noticeable effected where a difference in the oscillations can be noticed. When developing a model it is important that these effects are covered.

Summary of Analysis 11

Throughout the analysis the system has been described and issues concerning control has been addressed. These topics will in here be summarized.

The scope of this project is to investigate the possibility of using MPC with dynamic inflow models and following implementing the concept. The system used in the project is a simulation of a 5 MW onshore upwind HAWT, which has been developed by NREL. The simulation of the 5 MW NREL wind turbine is done through the simulation software FAST.

There are several control objectives in wind turbines, which can be addressed. In Chapter 4 on page 9 the common types of control are presented. The power production is typically divided into 4 regions depending on wind speed. The region of interest in this project is the third, where minimisation of fatigue, while producing rated power is the objective. These control objectives are to be implemented in an MPC scheme, which will find the optimal control input based on the model. It will be implemented with collective blade pitch and generator torque as control inputs.

The fatigue aspect is addressed in Chapter 5 on page 14, where it is explained how a rainflow count on the deflection will be used to calculate a measure for fatigue. This number will be used, when comparing the fatigue-wise performance of the developed controllers.

The interaction between the wind and the wind turbine is analysed in Chapter 6 on page 18 in order to identify the correct phenomena to include in the project. Tower shadow, wind shear and wakes are investigated, but are found negligible to the scope of the project. This way only dynamic inflow models are the focus. A quasi steady, dynamic and a simple dynamic inflow model was presented and compared. The simple dynamic inflow model with a decreased time constant was concluded to be precise enough to be used in the control scheme.

In order to ensure the relevance of including dynamic inflow in a control scheme, it is investigated if the bandwidth of the system is comparable to the bandwidth of the dynamic inflow phenomenon. This investigation shows that it indeed is favourable to include dynamic inflow, if the dynamics of the actuator is fast enough.

The foundation of an understanding of the system has been made and knowledge of necessary modelling has been found. In addition to modelling the dynamic inflow, it has been chosen to model the 1st tower fore-aft movement. The following part will address the modelling in detail, which in turn is used in the construction part, when developing the MPC.

Part II

Modelling

Introduction to Modelling 12

In order to get an understanding of the wind turbine system and make a basis for the control of it, a model has to be established. The model should describe how the wind affect the states and how the control signals, pitch of the blades and generator torque, influence the system.

Creating a model, which can be used in a Model Predictive Control scheme is done through the following steps:

1. Model description - A nonlinear model describing the relevant modes is developed.
2. Parameter estimation - Parameters of the nonlinear model are found by comparing with results from the higher fidelity models from FAST.
3. Linearisation - A linear model is needed for the Model Predictive Control scheme.
4. Validation - A validation of the developed models.
5. Comparison - Comparison of the linear models with and without dynamic inflow.
6. Enabling all DOF - Comparison of the FAST model, where all modes are used with the developed models.

It is important to keep in mind that the intent of the developed model is not to contain all DOF and the complexity of the full FAST model with all modes activated, but only to the degree and complexity relevant to the desired control scheme.

12.1 FAST

As explained in Appendix A on page 122, FAST is a high fidelity simulation tool, which in this thesis represents the reality and is used to verify results. The model described in this chapter will be a simplified edition of the full FAST model, both in regard to included modes, but also in regard to complexity of the included modes. Since FAST can be set up to include more or less degrees of freedom, the parameter estimation is done by comparing the developed model against FAST, with only the same modes activated.

The verification of the model will also be done against FAST, where only the modes described in the developed model are activated. This is done to make sure that these modes, which are of interest in the control scheme, are properly described. Another comparison is done afterwards to see the effect of the neglected modes.

<div align="right">

Model 13

</div>

The components of interest in regard to the control scheme are here modelled. The model is divided into subsystems, which will be combined to form the entire model. The model is later completed with parameter estimation in Chapter 14 and verified in Chapter 16.

To establish a model, the wind turbine will be divided into a set of subsystems that will be modelled. The subsystem models are then combined to create a model of the entire wind turbine. The chosen subsystem represent a certain amount of fidelity for the model. What to include and what not to include in the model is based an assessment based on knowledge of controller objectives and frequency bandwidth of the control system. The chosen model structure can be seen in Figure 13.1, which divides the system into natural subsystems of mechanical nature.
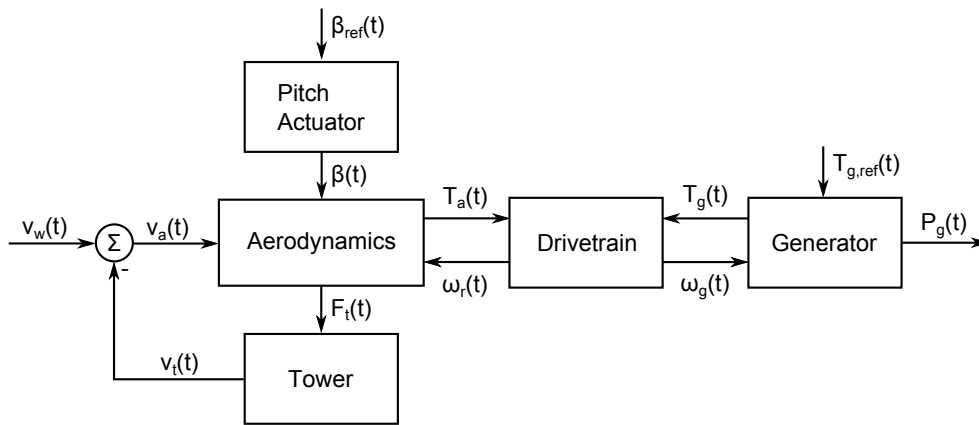
Figure 13.1. Overview of the model structure. The input signals are $v_w(t)$, $T_g(t)$ and β_{ref}, where only the last two are controllable.

13.1   Aerodynamics

The power available in the wind can be expressed as [Bianchi et al., 2007, P. 19]:

$$P_w(t) \;=\; \frac{1}{2}\rho A v_w^3(t) \tag{13.1}$$

The wind speed experienced at the rotor v_a is dependent of the tower fore-aft movements:

$$v_a(t) \;=\; v_w(t) - v_t(t) \tag{13.2}$$

The power transfered to the rotor is dependent on the power coefficient factor and is described as:

$$P_r(t) \;=\; P_w(t)C_p(\lambda(t), \beta(t)) \tag{13.3}$$

The C_p function for the NREL 5 MW wind turbine can be seen in Figure 4.3 and 4.4 on page 12.

The aerodynamic torque acting on the rotor can be expressed by power and angular velocity [Johnson et al., 2006]:

$$T_a(t) = \frac{P_r(t)}{\omega_r(t)} \tag{13.4}$$

Using the torque definition in (13.4), it is possible to combine (13.1) and (13.3), to express the torque as:

$$T_a(t) = \frac{1}{2\omega_r(t)} \rho A v_a^3(t) C_p(\lambda(t), \beta(t)) \tag{13.5}$$

The wind also creates a force acting on the tower through the blades. The force with which the wind is acting on the tower is [Bianchi et al., 2007, P. 19]:

$$F_w(t) = \frac{1}{2} \rho A v_a^2(t) C_t(\lambda(t), \beta(t)) \tag{13.6}$$

Where: $F_w(t)$ is the force acting on the tower [N].

$C_t(\lambda(t), \beta(t))$ is the thrust coefficient [−].

The characteristics of the C_t coefficient for the NREL 5 MW wind turbine can be seen in Figure 13.2 and 13.3.
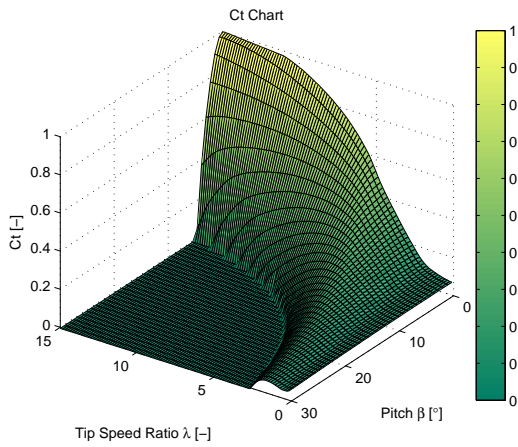

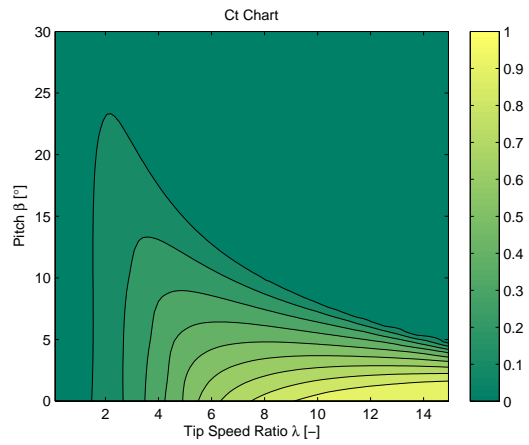**Figure 13.2.** C_t characteristics of the NREL 5 MW wind turbine. Negative values have been set to zero.

Figure 13.3. C_t characteristics of the NREL 5 MW wind turbine. Negative values have been set to zero.

Figures illustrating the C_p table can be seen in Figure 4.3 and 4.4 on page 12. The equations used here to calculate rotor torque and tower force are derived from quasi steady blade element theory, which is better explained in Chapter 8 on page 27.

Dynamic Inflow

The simple dynamic inflow model used here was introduced in Chapter 8 on page 27. From here the induction factors a_a^- and a_a^+ will be known as a_f and a_s respectively. This model uses an ambient fictive wind, which contains the dynamic inflow behaviour. The equations for calculating rotor torque and tower force are:

$$\lambda = \frac{\omega_r R}{v_a} \tag{13.7}$$

$$a_s = \frac{1}{2}\left(1 - \sqrt{1 - C_t}\right) \tag{13.8}$$

$$\dot{a}_f = \frac{1}{\tau_{DI}}(a_s - a_f) \tag{13.9}$$

$$v_f = v_a \frac{1 - a_f}{1 - a_s} \tag{13.10}$$

$$T_a(t) = \frac{1}{2\omega_r(t)}\rho A v_f^3(t) C_p(\lambda(t), \beta(t)) \tag{13.11}$$

$$F_w(t) = \frac{1}{2}\rho A v_f^2(t) C_t(\lambda(t), \beta(t)) \tag{13.12}$$

13.2 Drivetrain

The drivetrain will be modelled as a simple one mass system, without any friction, drivetrain torsion and with an ideal gear to transfer the rotational energy. By assuming there is no loss of energy in the gear and omitting drivetrain torsion, all the inertias in the system can be lumped into one inertia. The dynamics of the drivetrain can thereby be described as:

$$\dot{\omega}_r(t) = \frac{T_a(t) - N T_g(t)}{J} \tag{13.13}$$

Where: $T_g(t)$ is the torque applied by the generator [Nm].
J is the inertia of the lumped components $[\text{kgm}^2]$.
N is the gear ratio.

The lumped inertia is the inertia of the rotor, gearbox, low- and high-speed shaft. The inertia can be found in [Jonkman et al., 2009], but to allow the model a potential better fit, it is assumed unknown. The parameters will be estimated in Chapter 14 on page 60.

From $\omega_r(t)$ the generator angular velocity is found as:

$$\omega_g(t) = N \omega_r(t) \tag{13.14}$$

Where: $\omega_g(t)$ angular velocity of the generator $[\frac{\text{rad}}{\text{s}}]$.

13.3 Tower Dynamics

The tower is affected by the force the wind exerts on the rotor and tower. This causes the tower to bend, which in turn increases the fatigue of the system. In order to be able to minimise the fatigue, a model is made describing the deflection of the tower. The wind turbine can be seen as an arm with a force acting in the top, it could be modelled as an inertia, spring damper system. As the deflections are assumed small, the deflections are instead modelled as a mass spring damper system, neglecting the change in height.
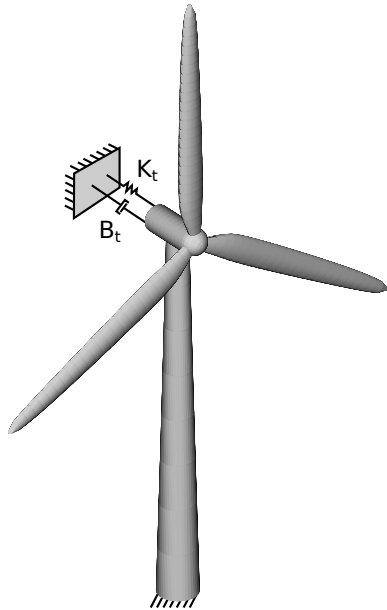

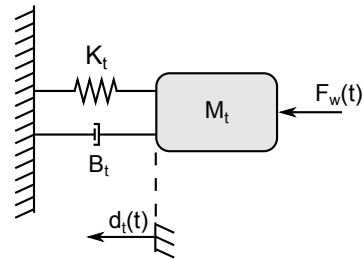**Figure 13.4.** The deflection of the tower is modelled as a mass, spring, damper system.

Figure 13.5. Tower deflection modelled as a mass, spring, damper system.

The system is modelled from the disturbance input namely the wind to the deflection of the tower. The model in Figure 13.4 is simplified to a mass, spring, damper system as seen in Figure 13.5, where M_t covers the lumped mass of the tower, rotor and nacelle. Assuming the oscillations are small, this is considered an acceptable approach for the tower modelling. The forces acting on the mass comes from the damper, spring and the disturbance input from the wind:

$$a_t(t)M_t = -B_t v_t(t) - K_t d_t(t) + F_w(t) \tag{13.15}$$

Where: a_t denotes the acceleration of the lumped mass $\left[\frac{\text{m}}{\text{s}^2}\right]$.

B_t denotes the friction coefficient $\left[\frac{\text{Ns}}{\text{m}}\right]$.

K_t denotes the spring coefficient $\left[\frac{\text{N}}{\text{m}}\right]$.

M_t denotes the mass of the lumped mass [kg].

The total mass of the wind turbine can be found in [Jonkman et al., 2009], but the modelling approach assumes that the mass is collected into one point, instead of being distributed over the entire height and fixed in the bottom. How much of the mass that should be used in the model is therefore unknown and it will be estimated to get the best model fit. The values of B_t

and K_t are also unknown and will also be estimated.

13.4   Pitch Actuator

The pitch actuators on a wind turbine controls the pitch by rotating the blades. The actuators are typically either hydraulic systems or electric servo motors. In this project no specific modelling, going into the physics and mechanics, of the actuator systems will be made. The response of the actuators is modelled as a first order system. Besides this linear representation the nonlinear attributes slew rate and saturation is added to better depict the physical limitations of the pitch actuator system. Pure time delays from communication between the controller and the actuators are omitted, since they are assumed minuscule.

The continues time model therefore becomes:

$$\dot{\beta}(t) \;=\; \frac{1}{\tau_p}\beta_{ref}(t) - \frac{1}{\tau_p}\beta(t) \tag{13.16}$$

$$\beta_{max} \;\geq\; \beta(t) \geq \beta_{min} \tag{13.17}$$

$$\dot{\beta}_{max} \;\geq\; \dot{\beta}(t) \geq \dot{\beta}_{min} \tag{13.18}$$

Where: $\beta(t)$ is the pitch angle [°].
  β_{max} is the maximum pitch angle [°].
  β_{min} is the minimum pitch angle [°].
  $\dot{\beta}_{max}$ is the positive slew rate for the pitch angle [°/s].
  $\dot{\beta}_{min}$ is the negative slew rate for the pitch angle [°/s].
  $\beta_{ref}(t)$ is the reference signal for the pitch angle [°].
  τ_p is the time constant [s].

13.5   Generator

The other control input to the system is the generator torque. The dynamics of the generator torque system is assumed to be much faster, than of the rest of the control system. However to have the have the possibility to change the dynamics of the generator model, a simple first order model is used. The time constant of the model will be set low compared to the rest of the system, to avoid dominating dynamics from the generator model.

The continuous time model of the generator system is:

$$\dot{T}_g(t) \;=\; \frac{1}{\tau_g}T_{g,ref}(t) - \frac{1}{\tau_g}T_g(t) \tag{13.19}$$

Where: $T_g(t)$ is the generator torque. [Nm].
  $T_{g,ref}(t)$ is the reference for the generator torque [Nm].
  τ_g is the time constant [s].

The power output of the generator is described as:

$$P_g(t) = \eta_g T_g(t) \omega_g(t) \tag{13.20}$$

Where: $P_g(t)$ is the generator power [W].

η_g is the efficiency of the generator [−].

13.6 Summary

The models can now be gathered into a nonlinear state space model, which is used for further work. The state equations are shown in (13.21):

$$f(x, u) = \begin{bmatrix} \dot{a_f} \\ \omega_r \\ d_t \\ v_t \\ \beta \\ T_g \end{bmatrix} = \begin{bmatrix} \frac{1}{\tau_{DI}(v_w)}(a_s - a_f) \\ \frac{1}{J}(T_a - NT_g) \\ v_t \\ \frac{1}{M_t}(F_t - K_t d_t - B_t v_t) \\ \frac{1}{\tau_p}(\beta_{ref} - \beta) \\ \frac{1}{\tau_g}(T_{g,ref} - T_g) \end{bmatrix} \tag{13.21}$$

Where: $T_a = \frac{1}{2\omega_r}\rho v_f^3 A C_p(\lambda, \beta)$

$F_t = \frac{1}{2}\rho v_f^2 A C_t(\lambda, \beta)$

The output equations are described by (13.22):

$$h(x, u) = \begin{bmatrix} P_g \\ v_t \\ \omega_r \end{bmatrix} = \begin{bmatrix} N\omega_r T_g \\ v_t \\ \omega_r \end{bmatrix} \tag{13.22}$$

The submodels have been derived and combined into a larger nonlinear model. Some parameters are unknown, which is why these are subject to a parameter estimation in the following chapter. The model is then linearised in Chapter 15 on page 65 for use in the MPC.

Parameter Estimation 14

In this chapter the parameter estimation for the nonlinear model will be done. Four parameters are estimated using the Prediction Error Method.

The lumped inertia and mass of the turbine, spring and friction coefficients are either unknown or assumed unknown and needs to be estimated for the model. From now on, the lumped parameters, inertia and mass of the turbine, will just be referred to as drivetrain inertia and tower mass for simplicity and as this is the way they are modelled.

FAST has no pitch actuator model included, which means the user is free to choose any kind of input dynamic desired. The dynamics of the pitch actuator has previously been described as a first order system. The time constant for the first order system will in this case be user defined and therefore no estimation of that parameter is necessary. The pitch actuator model is not implemented in FAST during this modelling part, in order to simplify the real world. The model is first included in the FAST model, when the MPC is applied.

The estimation will be done in MATLAB, with the PEM function. It is a prediction error method that can handle linear and nonlinear models. Furthermore it is possible to set initial values and constraints for both parameters and states. The estimation will be done using a nonlinear grey box model.
Given a specified input signal, the PEM function will search for the parameter(s), which minimizes the error between a measured output and a predicted output. The PEM function automatically chooses the fastest search algorithm, among the following algorithms:

- Gauss-Newton method
- Adaptive Gauss-Newton method
- A gradient method
- Levenberg-Marquardt search method
- Nonlinear least-squares method

The output of the wind turbine can be written as:

$$\dot{x}(t) = G(t, x(t), u(t)) + w(t) \tag{14.1}$$

$$y(t) = H(t, x(t), u(t)) + e(t) \tag{14.2}$$

Where: $y(t)$ is the output from the wind turbine.
$u(t)$ is the inputs to the wind turbine.
$w(t)$ and $e(t)$ are noise affecting the wind turbine.
G and H are nonlinear dynamics that describe the wind turbine.

In general the PEM finds the parameters that minimizes the sum of squared prediction errors in (14.3) [Mathworks, 2014].

$$V_N(G, H) = \sum_{t=1}^{N} \epsilon(t)^2 \qquad (14.3)$$

Where: $\epsilon(t)$ is the error between the measured and predicted output.

14.1 Operating Area

The control scheme is being implemented in region 3. The operating point for the wind speed is chosen as 12 m/s. This leads to the following operating points:

$$\bar{v}_w = 12 \text{ m/s} \qquad (14.4)$$
$$\bar{\omega}_r = 12.1 \text{ rpm} \qquad (14.5)$$
$$\bar{T}_g = 43093.5 \text{ Nm} \qquad (14.6)$$
$$\bar{\beta} = 4° \qquad (14.7)$$

To avoid going into the transition area between region 2 and region 3 the operating area for the wind is chosen as 11.5-12.5 m/s. This is obviously not the full operational area, but having a small operating area will increase the correctness of especially the linear model. If an MPC can achieve better control by using information about dynamic inflow in a small operating area, it can be expanded to worker over a larger area by using e.g. Multiple Model Predictive Control (MMPC). This leads to the following area:

	Operating point	Operating area
v_w	12 m/s	11.5-12.5 m/s
β	4°	2°-6°

Table 14.1. Operating area for the developed model.

This information will be used when deciding the amplitude of the input signals for parameter estimation and for linearising the model.

14.2 Input Signals

The input signal for the parameter estimation is as seen in Figure 14.1 on the following page. The outputs used to compare the model output will be rotor speed, tower displacement and velocity.

First the pitch and wind speed is changed simultaneous to approximately keep the rated rotor speed. Secondly only the pitch is changed, before only the wind speed is changed. For the parameter estimation the torque is kept constant, as this primarily will cause changes in the rotational speed, whereas pitch both will gives changes in rotor speed and tower position. Later in Chapter 16 on page 67 it will be investigated, how the developed model follow torque changes.
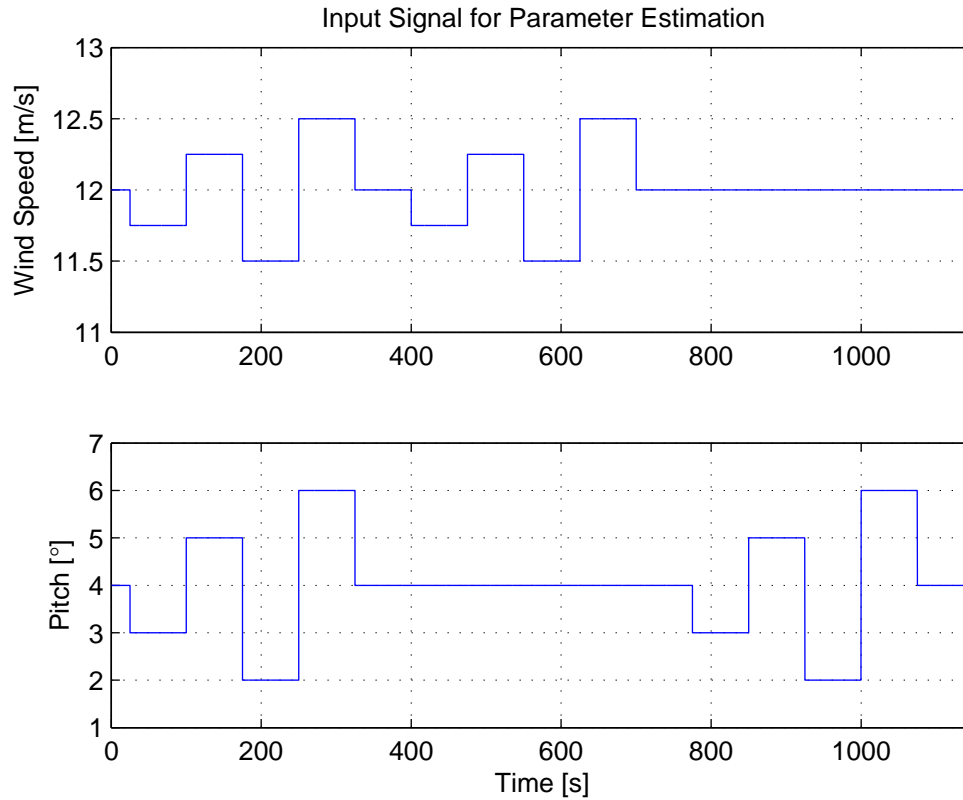
Figure 14.1. The input signal for parameter estimation with PEM.

Applying the PEM function results in the following parameters. The parameters are estimated where all submodels combined, to create the full nonlinear model of the wind turbine.

Estimated Parameter	Value	Unit
Drive train inertia - J	41430600	$\left[\text{kgm}^2\right]$
Tower spring coefficient - K_t	1873530	$\left[\frac{\text{N}}{\text{m}}\right]$
Tower damper coefficient - B_t	65190.4	$\left[\frac{\text{Ns}}{\text{m}}\right]$
Tower mass - M_t	447825	$[\text{kg}]$

Table 14.2. Estimated values for the nonlinear model of the NREL 5 MW wind turbine.

In [Jonkman et al., 2009] the total wind turbine mass is stated to be 697460 kg and the total inertia of the blades, hub, generator and low speed shaft taken around the low speed shaft is 40469564 kgm^2. The inertia is close to the reported number and the estimated mass of the wind turbine is about two thirds of the real value, which is expected as the mass gets more static closer to the ground. The spring and damper values are not stated in [Jonkman et al., 2009] and no comparison can therefore be made with those.

All the estimated parameters are therefore considered to be both valid and realistic for the modelling approach taken.

14.3 Nonlinear Model Fits

The model fits, using the estimated parameters, can be seen in Figure 14.2 and 14.3. The model was estimated based on rotor speed, tower displacement and velocity. For further comparison the generator power is plotted, due to its importance in the final setup. Specific fit percentage will not be given in this chapter, as the model is evaluated later in Chapter 16 on page 67.
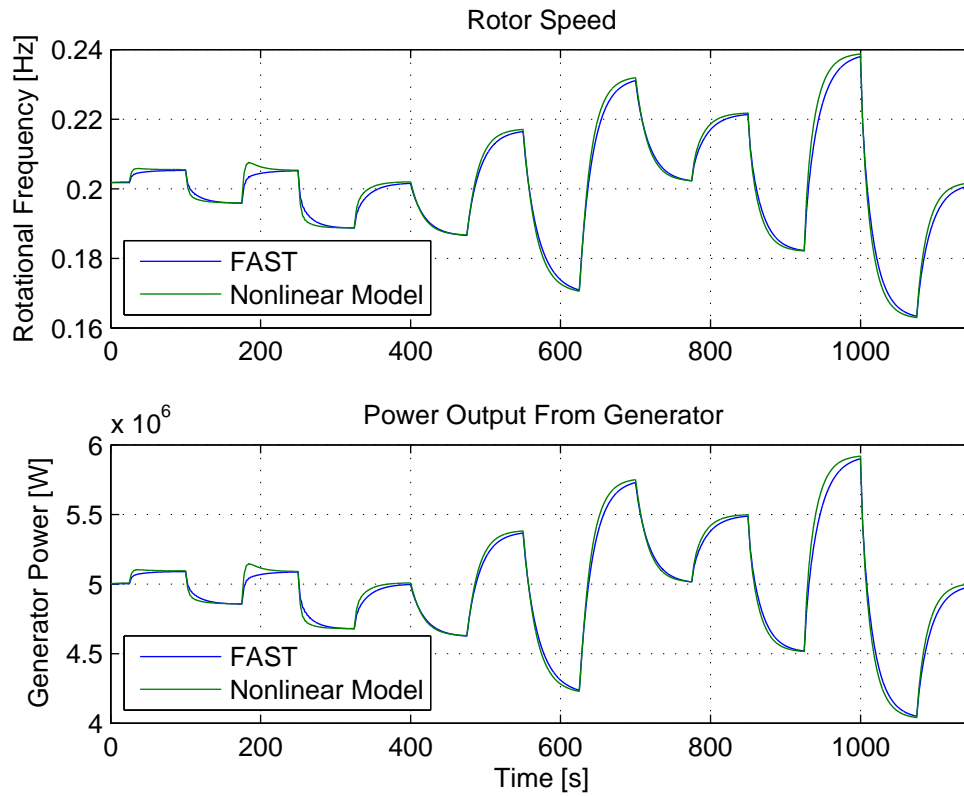

Figure 14.2. A comparison of the rotational frequency of the rotor and generator power between FAST and the nonlinear model.
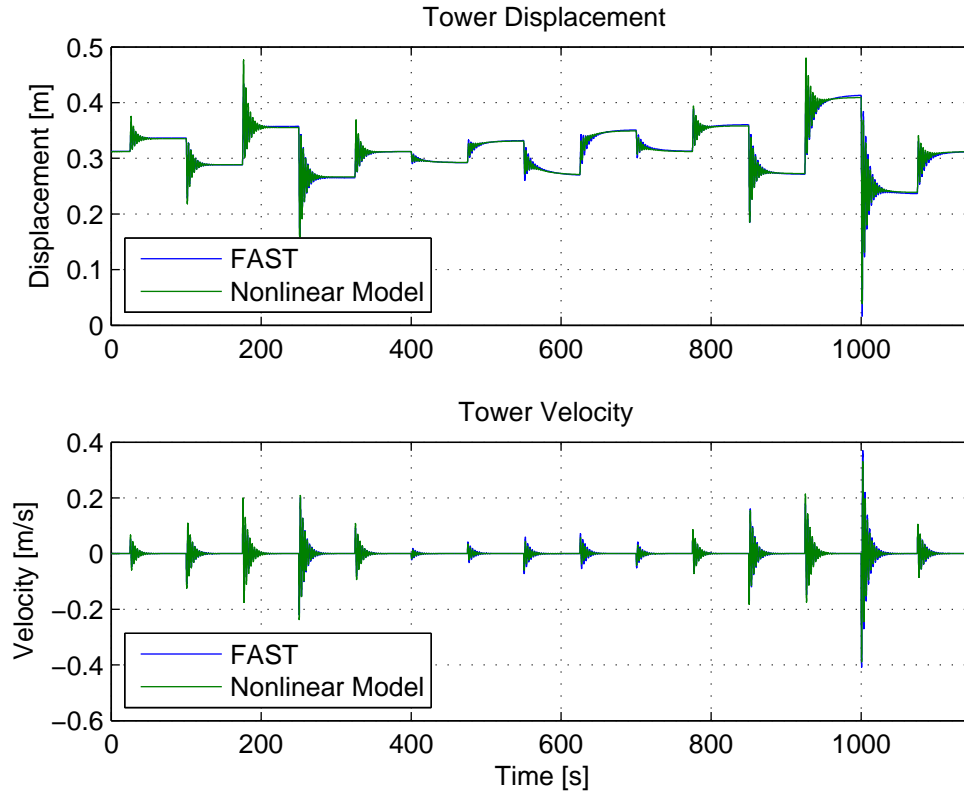
Figure 14.3. A comparison of the displacement and velocity of the tower between FAST and the nonlinear model.

All details of the fit can be hard to see at this range, so a closer visual comparison of the nonlinear model to the FAST output will be done under the validation in Chapter 16 on page 67. How well the nonlinear model fits will be described in the validation chapter.

In this chapter a parameter estimation was made for the nonlinear model derived in Chapter 13. The parameters will be used to generate a linear model in the following chapter, which can be used for an MPC.

Linearisation of Wind Turbine Model 15

In this chapter a linear model with and without dynamic inflow is presented. The linear model with dynamic inflow is linearised from the nonlinear model derived earlier. The model without dynamic inflow is linearised from a simplified nonlinear model without dynamic inflow, before its parameters are estimated again.

In order to have a model, which is usable in a normal MPC setup, the nonlinear model has to be linearised. This is done using a first order Taylor approximation. The equations are linearised around the operating point and the partial derivatives are evaluated at the steady state.

15.1 Linear Model With Dynamic Inflow

The linearisation can be found in Appendix E on page 133 and the result is here shown in a state space representation:

$$
\begin{bmatrix} \dot{a_f^\Delta} \\ \omega_r^\Delta \\ d_t^\Delta \\ v_t^\Delta \\ \beta^\Delta \\ T_g^\Delta \end{bmatrix} =
\begin{bmatrix}
-\frac{1}{\tau_{DI}(v_w)} & \frac{\partial \dot{a}_f}{\partial \omega_r} & 0 & -\frac{\partial \dot{a}_f}{\partial v_w} & \frac{\partial \dot{a}_f}{\partial \beta} & 0 \\
\frac{1}{J}\frac{\partial T_a}{\partial a_f} & \frac{1}{J}\frac{\partial T_a}{\partial \omega_r} & 0 & -\frac{1}{J}\frac{\partial T_a}{\partial v_w} & \frac{1}{J}\frac{\partial T_a}{\partial \beta} & \frac{-N}{J} \\
0 & 0 & 1 & 0 & 0 & 0 \\
\frac{1}{M_t}\frac{\partial F_t}{\partial a_f} & \frac{1}{M_t}\frac{\partial F_t}{\partial \omega_r} & -\frac{K_t}{M_t} & \frac{1}{M_t}\left(-B_t-\frac{\partial F_t}{\partial v_w}\right) & \frac{1}{M_t}\frac{\partial F_t}{\partial \beta} & 0 \\
0 & 0 & 0 & 0 & -\frac{1}{\tau_p} & 0 \\
0 & 0 & 0 & 0 & 0 & -\frac{1}{\tau_g}
\end{bmatrix}
\begin{bmatrix} a_f^\Delta \\ \omega_r^\Delta \\ d_t^\Delta \\ v_t^\Delta \\ \beta^\Delta \\ T_g^\Delta \end{bmatrix}
$$

$$
+ \begin{bmatrix}
0 & 0 & \frac{\partial \dot{a}_f}{\partial v_w} \\
0 & 0 & \frac{1}{J}\frac{\partial T_a}{\partial v_w} \\
0 & 0 & 0 \\
0 & 0 & \frac{1}{M_t}\frac{\partial F_t}{\partial v_w} \\
0 & \frac{1}{\tau_p} & 0 \\
\frac{1}{\tau_g} & 0 & 0
\end{bmatrix}
\begin{bmatrix} T_{g,ref}^\Delta \\ \beta_{ref}^\Delta \\ v_w^\Delta \end{bmatrix}
\tag{15.1a}
$$

$$
\begin{bmatrix} P \\ v_t \\ \omega_r \end{bmatrix} =
\begin{bmatrix} \bar{P} \\ \bar{v}_t \\ \bar{\omega}_r \end{bmatrix} +
\begin{bmatrix}
0 & \frac{\partial P_g}{\partial \omega_r} & 0 & 0 & 0 & \frac{\partial P_g}{\partial T_g} \\
0 & 0 & 0 & 1 & 0 & 0 \\
0 & 1 & 0 & 0 & 0 & 0
\end{bmatrix}
\begin{bmatrix} a_f^\Delta \\ \omega_r^\Delta \\ d_t^\Delta \\ v_t^\Delta \\ \beta^\Delta \\ T_g^\Delta \end{bmatrix}
+ 0 \begin{bmatrix} T_{g,ref}^\Delta \\ \beta_{ref}^\Delta \\ v_w^\Delta \end{bmatrix}
\tag{15.1b}
$$

The partial derivatives are shown in the appendix.

How well the linear model fit will be shown in the validation chapter, see Chapter 16 on page 67.

15.2 Linear Model Without Dynamic Inflow

In order to see if the effect of the inclusion of dynamic inflow models is significant, a linear model without dynamic inflow is made. The model will be made by removing the a_f state and associated equations from the model described previously. Furthermore the partial derivatives are recalculated, as described in Appendix E on page 133. The parameters estimated in Chapter 14 on page 60 are then re-estimated, to allow the best fit. This way the model can attempt to follow as much of the dynamics as possible with the reduced number of states.

The model structure, for the linear model without dynamic inflow, can be seen in (15.2).

$$
\begin{bmatrix} \dot{\omega}_r^\Delta \\ d_t^\Delta \\ v_t^\Delta \\ \beta^\Delta \\ T_g^\Delta \end{bmatrix} =
\begin{bmatrix}
\frac{1}{J}\frac{\partial T_a}{\partial \omega_r} & 0 & -\frac{1}{J}\frac{\partial T_a}{\partial v_w} & \frac{1}{J}\frac{\partial T_a}{\partial \beta} & \frac{-N}{J} \\
0 & 1 & 0 & 0 & 0 \\
\frac{1}{M_t}\frac{\partial F_t}{\partial \omega_r} & -\frac{K_t}{M_t} & \frac{1}{M_t}\left(-B_t-\frac{\partial F_t}{\partial v_w}\right) & \frac{1}{M_t}\frac{\partial F_t}{\partial \beta} & 0 \\
0 & 0 & 0 & -\frac{1}{\tau_p} & 0 \\
0 & 0 & 0 & 0 & -\frac{1}{\tau_g}
\end{bmatrix}
\begin{bmatrix} \omega_r^\Delta \\ d_t^\Delta \\ v_t^\Delta \\ \beta^\Delta \\ T_g^\Delta \end{bmatrix}
$$

$$
+
\begin{bmatrix}
0 & 0 & \frac{1}{J}\frac{\partial T_a}{\partial v_w} \\
0 & 0 & 0 \\
0 & 0 & \frac{1}{M_t}\frac{\partial F_t}{\partial v_w} \\
0 & \frac{1}{\tau_p} & 0 \\
\frac{1}{\tau_g} & 0 & 0
\end{bmatrix}
\begin{bmatrix} T_{g,ref}^\Delta \\ \beta_{ref}^\Delta \\ v_w^\Delta \end{bmatrix} \tag{15.2a}
$$

$$
\begin{bmatrix} P \\ v_t \\ \omega_r \end{bmatrix} =
\begin{bmatrix} \bar{P} \\ \bar{v}_t\bar{\omega}_r \end{bmatrix} +
\begin{bmatrix}
\frac{\partial P_g}{\partial \omega_r} & 0 & 0 & 0 & \frac{\partial P_g}{\partial T_g} \\
0 & 0 & 1 & 0 & 0 \\
1 & 0 & 0 & 0 & 0
\end{bmatrix}
\begin{bmatrix} \omega_r^\Delta \\ d_t^\Delta \\ v_t^\Delta \\ \beta^\Delta \\ T_g^\Delta \end{bmatrix} + 0
\begin{bmatrix} T_{g,ref}^\Delta \\ \beta_{ref}^\Delta \\ v_w^\Delta \end{bmatrix} \tag{15.2b}
$$

The input signal for the parameter estimation is shown in Figure 14.1 on page 62, which is the signal that is used for the nonlinear parameter estimation. The outputs are also the same, namely rotor speed, tower displacement and tower velocity. The PEM function is again given a grey box model to make the parameters estimation on. This time the grey box model can be a linear model, which therefore will be used.

The resulting parameters are:

Estimated Parameter	Value	Unit
Drive train inertia - J	42170000	$\left[\text{kgm}^2\right]$
Tower spring coefficient - K_t	1719000	$\left[\frac{\text{N}}{\text{m}}\right]$
Tower damper coefficient - B_t	9025	$\left[\frac{\text{Ns}}{\text{m}}\right]$
Tower mass - M_t	405400	$\left[\text{kg}\right]$

Table 15.1. Estimated values for the linear model without dynamic inflow.

This linear model without dynamic inflow will be used in Section 16.3 on page 71, where the linear models with and without dynamic inflow are compared.

Two linear models for use in MPC have been derived. They will form the basis for a comparison, where the difference between a model with and without dynamic inflow is investigated. In the following chapter a validation of the nonlinear model and the linear models will be made.

Validation 16

In this chapter a validation of the derived models will be made. This is done to see the effects of the linearisation and how large a difference it makes to include dynamic inflow into a linear model. Furthermore it will be investigated what difference there is, when enabling all the DOF's in FAST.

Validation results of both the nonlinear and the linear models will be shown. The models are validated through how well they fit in terms of generator power, rotor rotational velocity, tower displacement and tower velocity. How well a model fit is done through visual inspection and through computation of the error calculated as following:

$$errn = \frac{\sum\limits_{k=0}^{N} (y_r(k) - y(k))^2}{\sum\limits_{k=0}^{N} (y_r(k) - y_{avg})^2} \cdot 100 \tag{16.1}$$

Where: $errn$ is the normed mean square output error [%].
$y(k)$ is the output from the nonlinear model.
$y_r(k)$ is the output from FAST.
y_{avg} is the average of the output from FAST.

Validation is done by creating a new set of data by applying another input signal, than used for estimation to the FAST model and seeing that the models fit. At first only the nonlinear model and linear model with dynamic inflow is considered. The input is as follows:
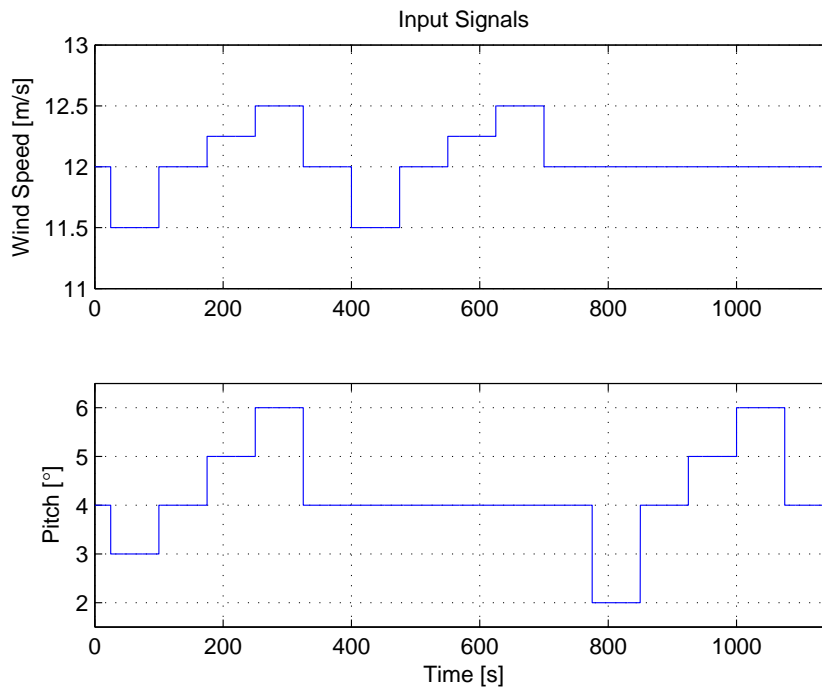

Figure 16.1. Input Signal for model validation.

The input signal consists of parts, where the model is exposed to respectively wind and pitch changes, only pitch changes and then only wind changes. This is done to make sure to cover the full operating area of the models. Initially the torque is kept constant, in order to focus on just wind and pitch changes. Later it is investigated how well the models fit, when there are changes in input torque. The investigated outputs are power, rotor speed, tower displacement and velocity.

Applying the input signal seen in Figure 16.1 produces the following results:
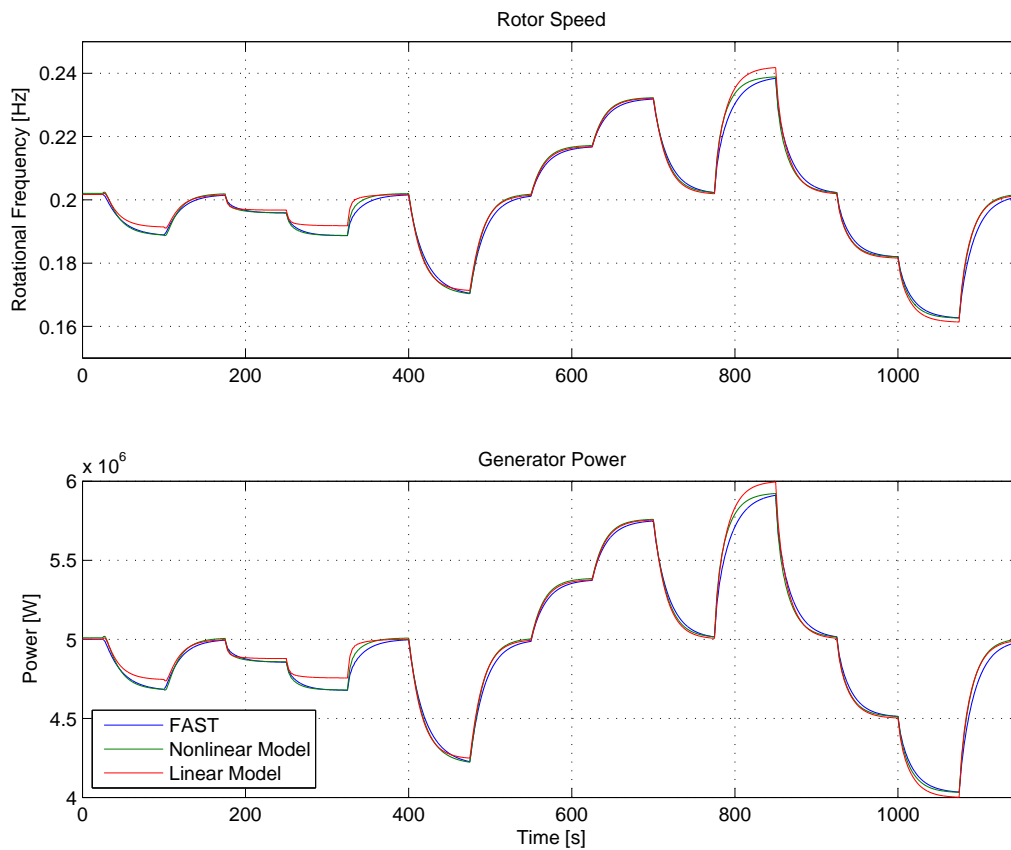
Figure 16.2. Rotational frequency of the rotor and Generator Power from FAST, nonlinear and linear model.

68
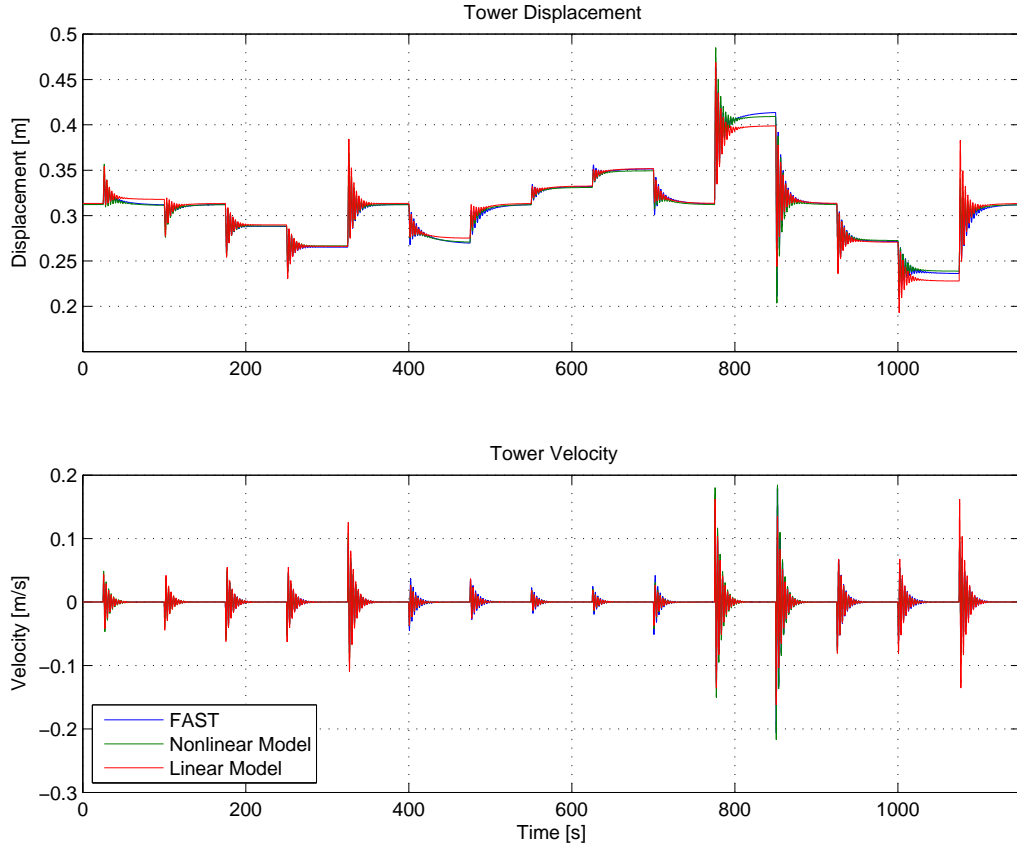
Figure 16.3. Tower deflection and velocity from FAST, nonlinear and linear model.

The calculated errors can be seen in Table 16.1.

Output	Nonlinear Model Error	Linear Model Error
Rotational frequency	0.43%	1.01%
Generator Power	0.43%	1.01%
Tower displacement	0.30%	1.73%
Tower velocity	2.05%	7.40%

Table 16.1. Error from the nonlinear and linear models in the output data shown in Figure 16.2 and 16.3.

The errors are generally small, which indicate a good model fit. As expected the error of the linear model are greater, than those of the nonlinear model. The error made by the models consists of both steady state errors and errors in the dynamic behaviour.

16.1 Steady State

Steady state errors in the linear model occurs due to the linearisation. This is primarily seen in the tower displacement, rotor speed and power. Especially the linearisation of the highly nonlinear C_p and C_t tables causes an error, when moving away from the operating point. This

error can be seen in Figure 16.4 where the gradient plane is plotted against the C_p table along with Figure 16.5 containing a contour plot of the relative error.
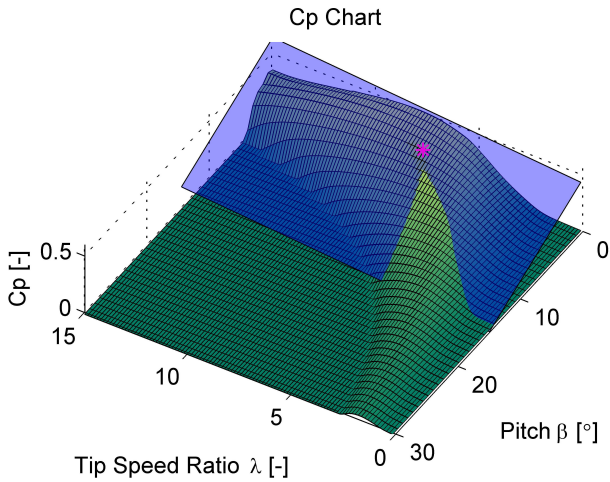

Figure 16.4. C_p table with gradient plane used for linearisation. The magenta mark indicates the operating point.
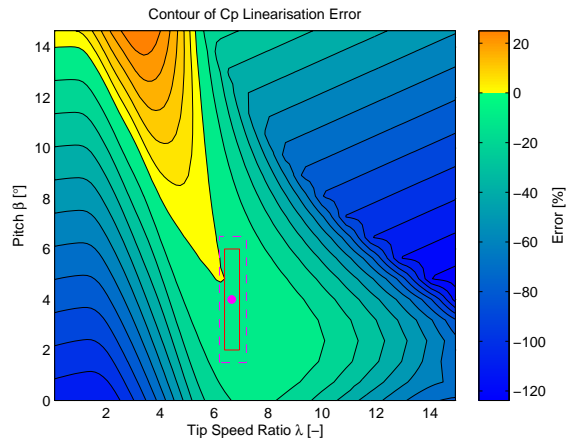
Figure 16.5. Contour plot of the relative error between the C_p and the linearised gradient plane. The red rectangle indicates the operating area and the dashed magenta rectangle is enlarged in Figure 16.6.
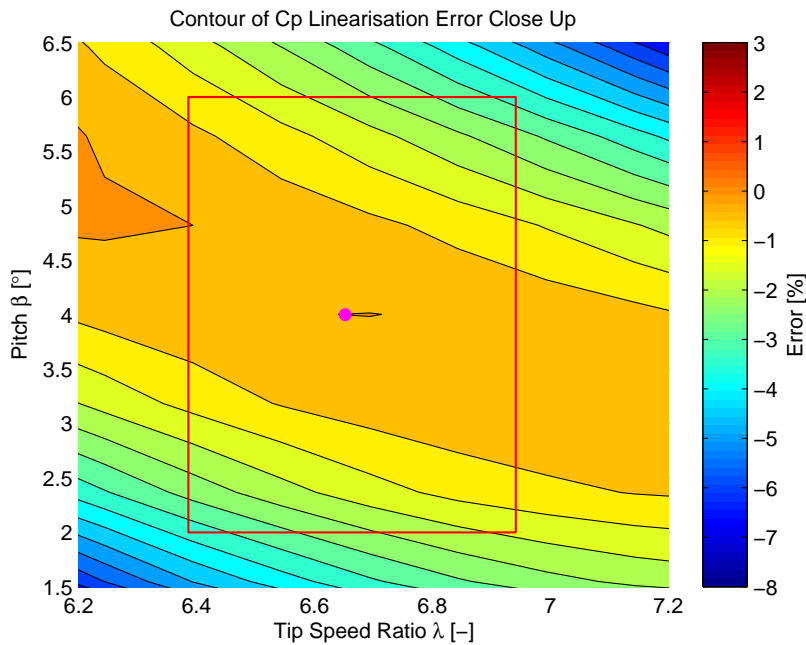

Figure 16.6. A close up of the contour plot, where it is possible to see a more detailed view of the operating area and its associated error. In the middle, there is small area where the error is zero (where the magenta dot is at).

The steady state errors within this operating area are deemed small enough for use in MPC. If this is shown not to be the case a smaller operating area can be used.

16.2 Dynamics

The dynamics of the rotational frequency and the generator power are suitable for both the nonlinear and the linear model.

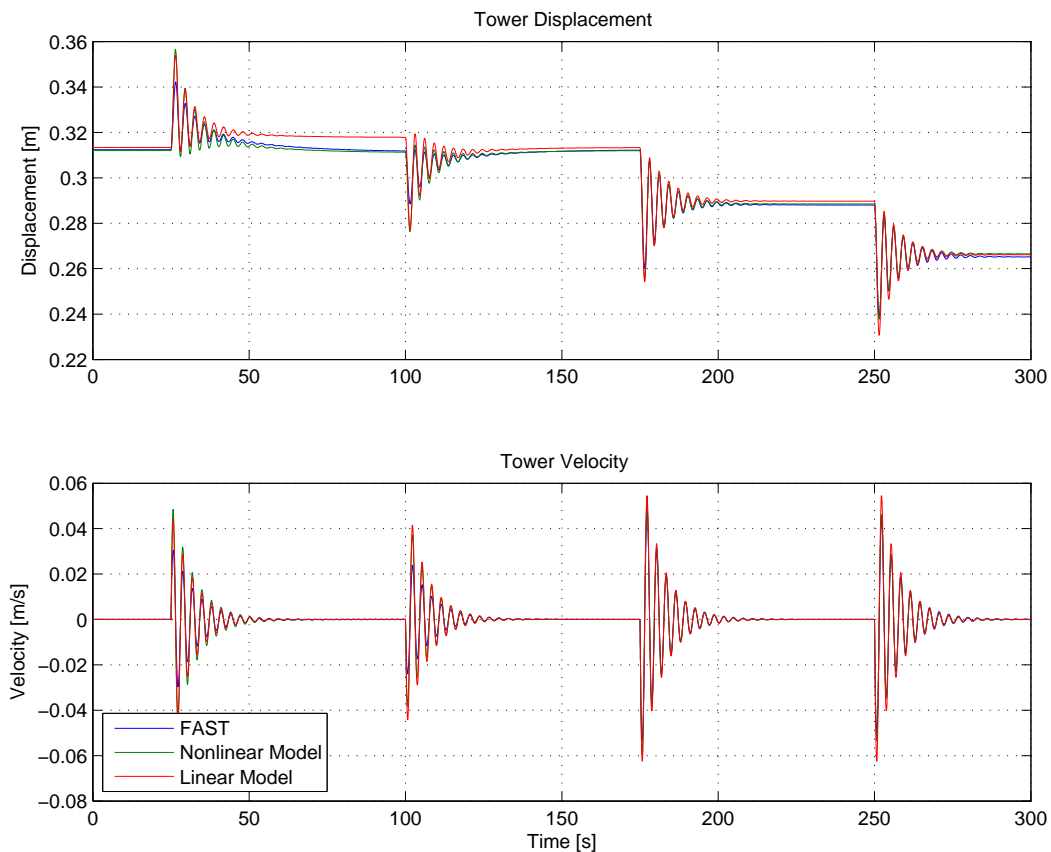To better examine the dynamics of the tower deflections and velocities, a zoom is performed in Figure 16.7:

Figure 16.7. Validation of tower movements in the timerange 0-300 s for easier examination of dynamics.

As seen in Figure 16.7 the tower oscillations are consistent along the three transients. These oscillation are with the tower fore-aft natural frequency (0.324 Hz as seen in Table 9.1 on page 39).

16.3 Linear Models With and Without Dynamic Inflow

In Chapter 10 on page 42 the differences between FAST models with and without dynamic inflow were shown. The major difference is the amplitude of the fluctuations of the tower and the damping of these fluctuations. To get an idea of the developed linear model better resembles these features, than a linear model without dynamic inflow, a linear model without dynamic inflow was made in Section 15.2 on page 66. This model was made by taking the linearised model in Chapter 15 on page 65 and removing the a_f state and all relating partial derivatives.

Then a parameter estimation was done directly on the linear model without dynamic inflow to see if adjustment of the remaining parameters can "help" cover for the missing state. Figure 16.8 shows a close up of the comparison of the models in the fluctuations which are created by respectively wind and pitch change, wind change and pitch change.
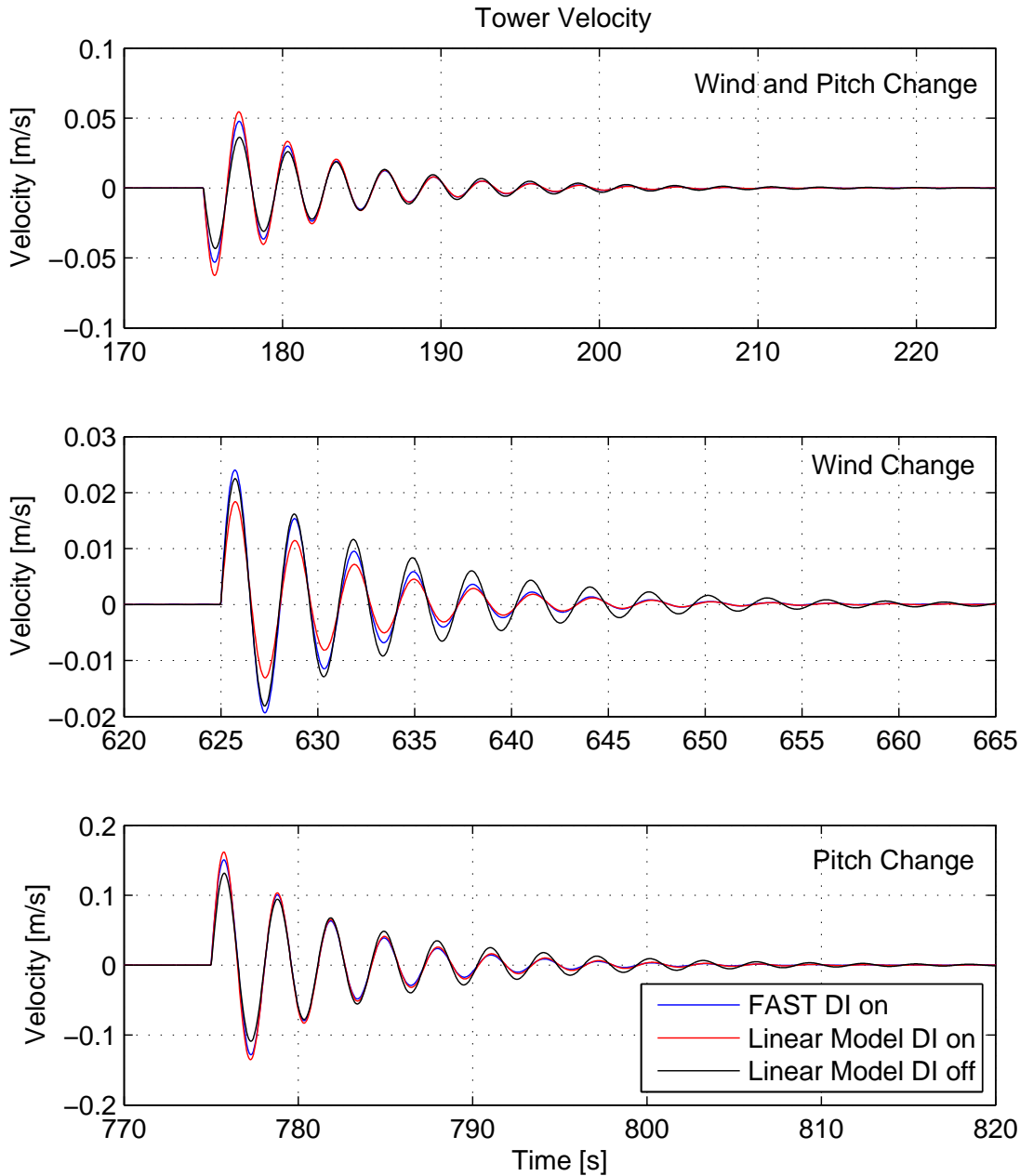

Figure 16.8. Three zooms on the validation data of tower velocity compared against a linear model with and without dynamic inflow. The three different zoom regions are from respectively: wind and pitch step, wind step only, pitch step only.

From this it can be seen that a linear model containing dynamic inflow better reaches the amplitude of the first fluctuations, when exposed to wind and pitch or a pure pitch step. Furthermore the damping is a better match, when including dynamic inflow.

In the scenario where only wind is changed the linear model without dynamic inflow actually

performs better in the first fluctuations, but the dampening in the linear model with dynamic inflow matches better. This specific part, where only wind was changed, does not behave better with dynamic inflow accounted for, as hoped, but since the system will be controlled, a scenario where wind changes without the pitch changing too will not occur. It was already shown in the initial analysis in Chapter 8 on page 27 that the simplified dynamic inflow model, which is used, has some deficiencies, when wind changes are applied. Since the MPC scheme will not have any knowledge of future wind changes the wind will be constant in the horizon, meaning that the deficiency will not have an effect.

When taking all the output data from tower movements and comparing the calculated error, the result is:

Output Error	Linear Model DI On	Linear Model DI Off
Tower displacement	1.73%	2.07%
Tower velocity	7.40%	7.76%

Table 16.2. Error from the linear models with and without dynamic inflow.

Here it is seen that the error is improved a little when using dynamic inflow. As mentioned before the MPC scheme will consider the wind constant within the horizon, so the model only needs to match changes in pitch and torque. By taking only the part of the output data, where pitch was changed alone, the calculated errors become.

Output Error	Linear Model DI On	Linear Model DI Off
Tower displacement	1.82%	2.33%
Tower velocity	5.54%	7.01%

Table 16.3. Error from the linear models with and without dynamic inflow from data with only pitch changes.

Here the improvement from using dynamic inflow is more expressed. This encourages the idea of an MPC, which includes dynamic inflow being able of decreasing tower movements compared to an MPC without dynamic inflow.

The linear model is to be used for Model Predictive Control. The linear model have been shown to contain the desired dynamics of the system. Steady state errors are deemed small enough for control. In case of problems due to errors in steady state in the linear model the operating range can be decreased.

16.4 Torque Changes

So far the validation has been done, without focus on changes in torque. It will now be tested how the nonlinear model and linear model with DI handles a change in input torque. The input signal can be seen in Figure 16.9 on the next page.
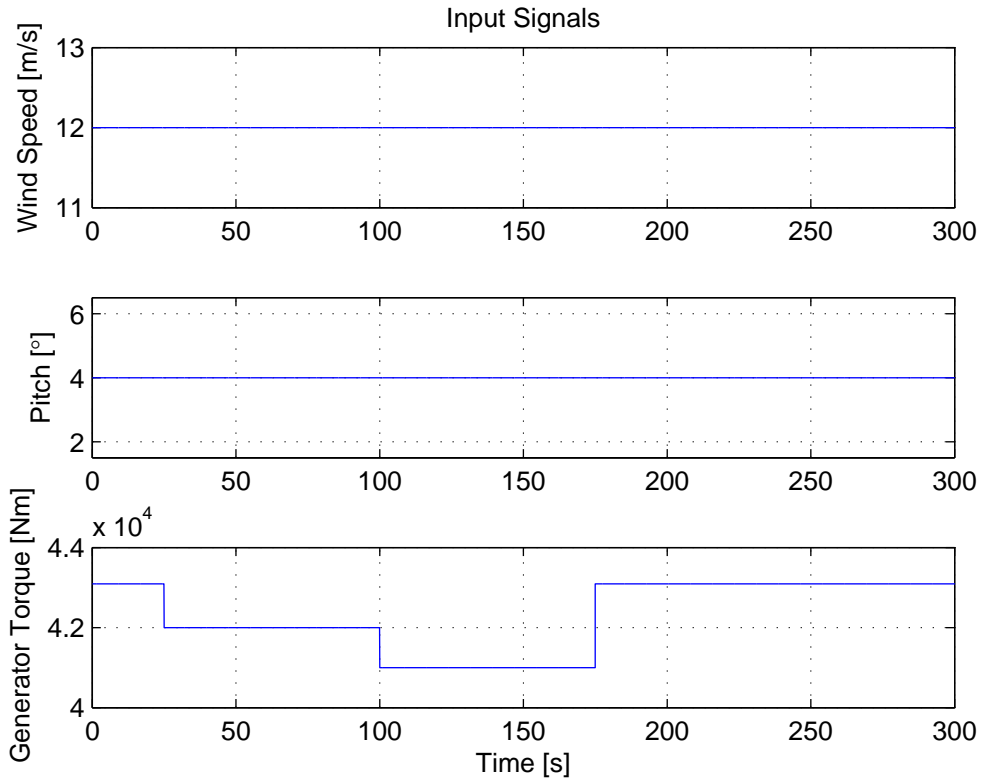
Figure 16.9. The input signal for the torque test.

The torque changes three times stepwise to see how it affects the wind turbine. The result of this stepwise input can be seen in Figure 16.10 and 16.11.
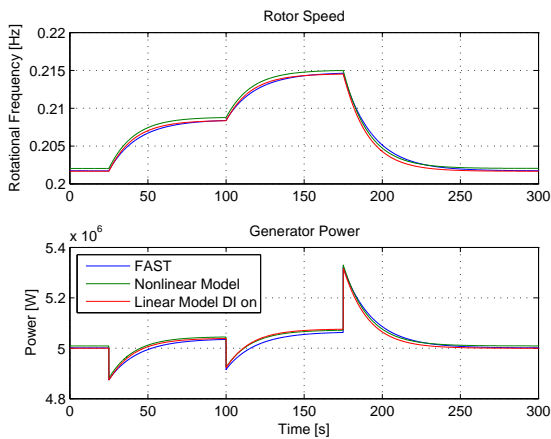

Figure 16.10. Comparison of rotational frequency and power output between FAST, the nonlinear and linear model for the torque test.
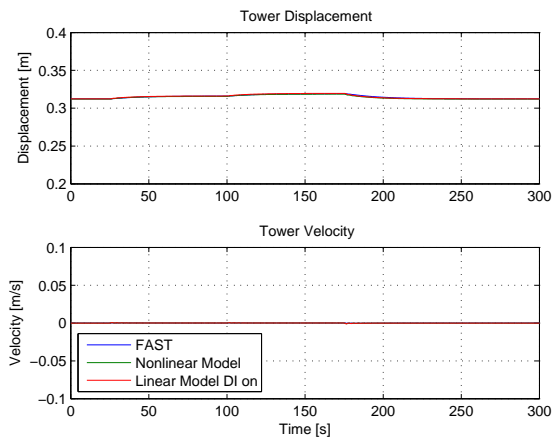
Figure 16.11. Comparison of tower displacement and velocity between FAST, the nonlinear and linear model for the torque test.

From Figure 16.10 and 16.11 it can be seen that both the nonlinear model and linear model is capable of handling these torque changes.

16.5   Enabling All DOF

Since only the modes represented in the model was used in FAST for validating, a comparison is done where all modes are enabled in FAST, see Appendix A on page 122 for a description of all the DOF in FAST. The reason why some modes have been neglected from the model is first of all that the other modes have been deemed negligible, by having a higher natural frequency. In this section the error made by neglecting these mode are visualised. This is done by applying a step in pitch, from 5° to 6°, to the different models and make a comparison in the time domain. By applying a step all frequencies will be tested, meaning that the error might be worse, than what would actually be experienced in a control scheme with lower bandwidth. It is only the effect of the two main outputs used in this project, namely generator power and tower velocity, which will be examined.

By turning on all degrees of freedom in FAST and applying a step in wind and pitch, while comparing to the linear model constructed from fewer DOF, the error can be assessed. First of is the comparison in generator power.
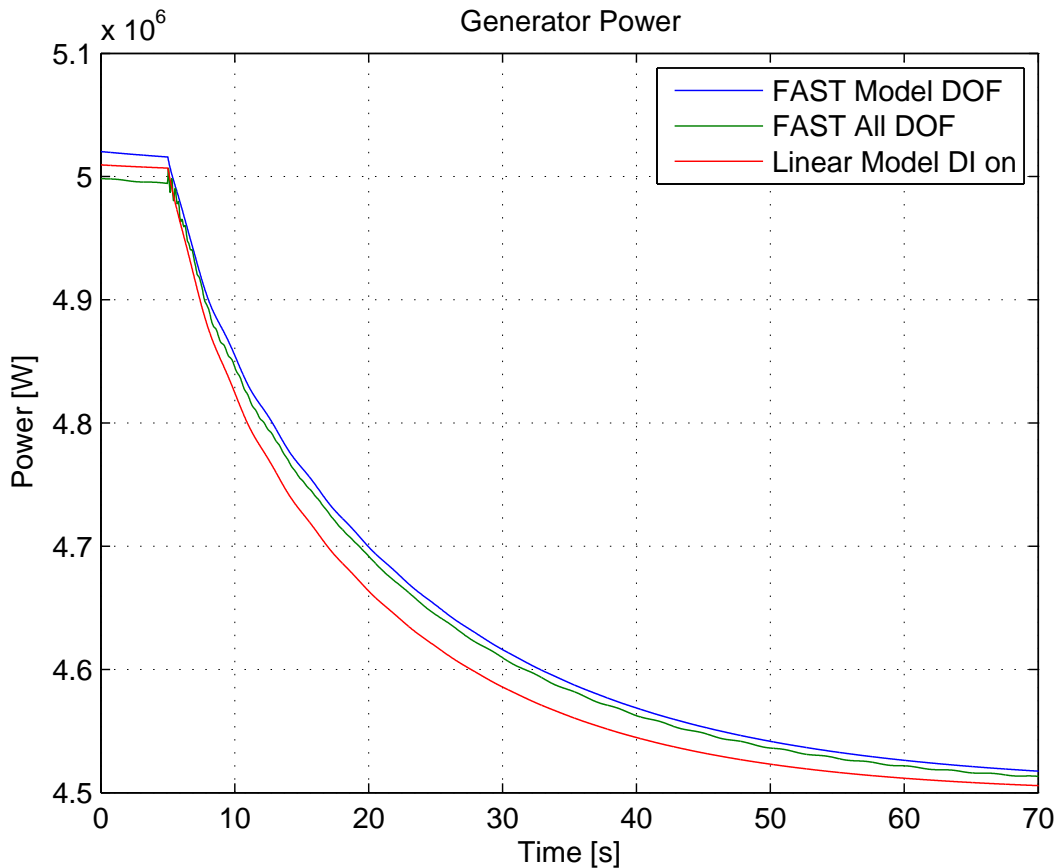

Figure 16.12. Wind and pitch step applied to FAST model with all DOF, FAST with only the DOF used in the model and the linear model comparing generator power.

In regard to generator power a slight constant difference can be experienced. Apart from this, when examining closer as in Figure 16.13, it can be seen that fluctuations happen just after the step stemming from the natural frequencies of the other modes, such as the drivetrain. These minor differences are deemed small enough to neglect in the model. If this shows to not be the case this can be re-evaluated.
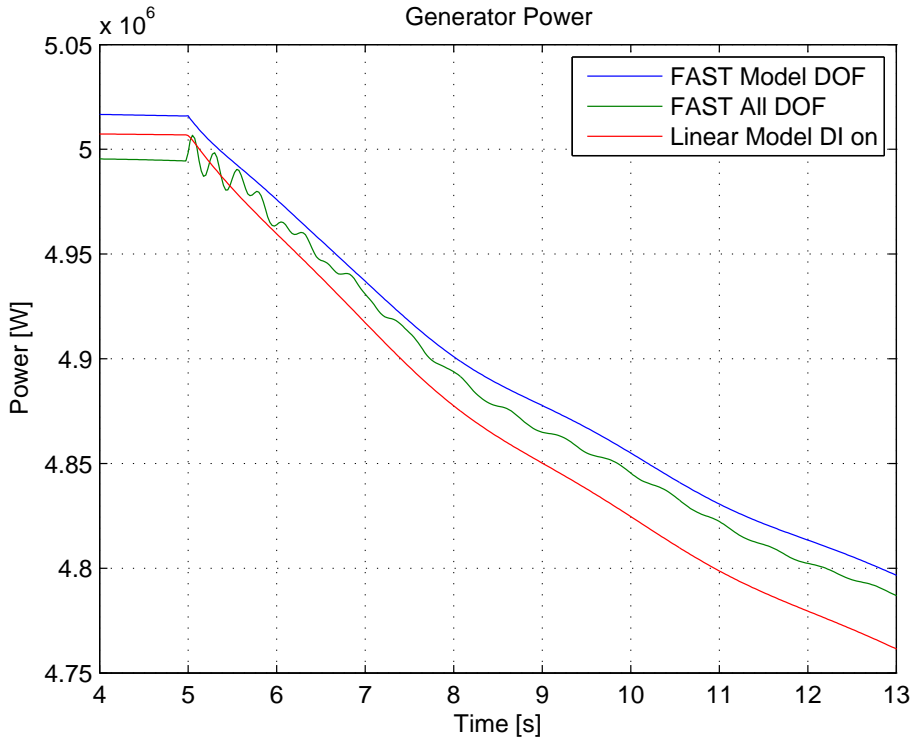
Figure 16.13. Wind and pitch step applied to FAST model with all DOF, FAST with only the DOF used in the model and the linear model comparing generator power. Zoomed in at the start of the response to see fluctuations on the FAST model with all DOF.
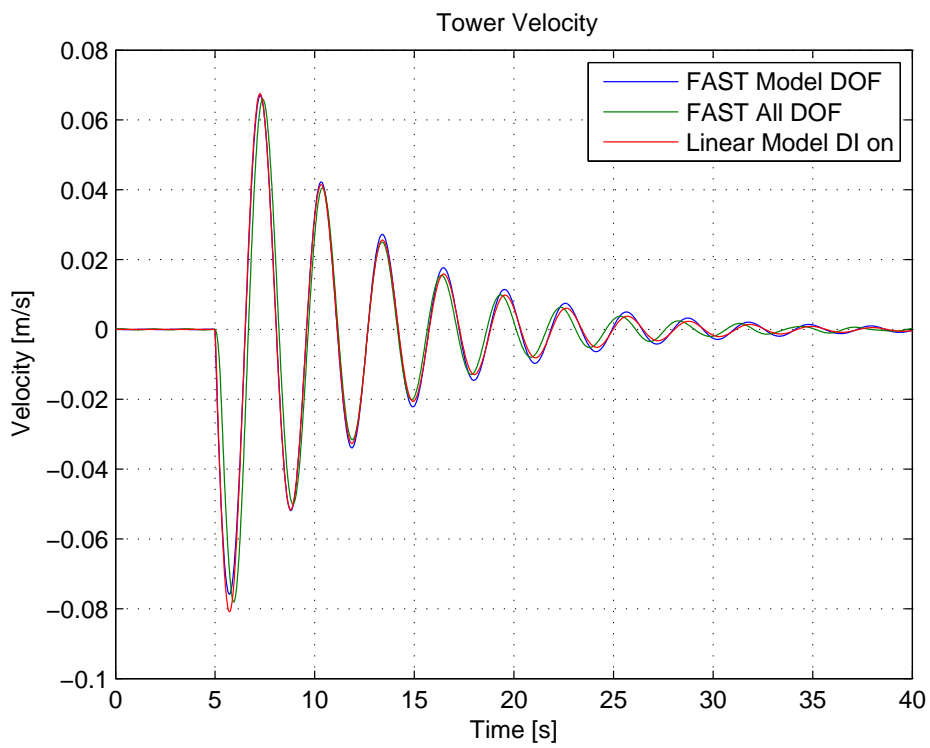

Figure 16.14. Wind and pitch step applied to FAST model with all DOF, with only the DOF used in the model and the linear model comparing tower velocity.

The error made by the simplified models in regard to tower velocity can be seen in Figure 16.14.

FAST with model DOF and the linear model is quite similar in frequency and phase. However, they differ a bit in frequency from FAST with all DOF. This minor error in tower velocity is also deemed small enough to support using the simplified model. Again if this turns out to be an incorrect assessment, the simplified model will be extended.

Estimation with All DOF Enabled

Another way to do the estimation process could be to have all DOF enabled in FAST while estimating parameters. To investigate how big a difference it makes for the result, the linear model with DI has been fitted to the data given by FAST with all DOF enabled. The estimation is done with the same input signal as seen in Figure 14.1 on page 62. The resulting parameters were:

Estimated Parameter	Model DOF	All DOF	Unit
Drive train inertia - J	41430600	51710000	$\left[\text{kgm}^2\right]$
Tower spring coefficient - K_t	1873530	1877000	$\left[\frac{\text{N}}{\text{m}}\right]$
Tower damper coefficient - B_t	65190.4	89600	$\left[\frac{\text{Ns}}{\text{m}}\right]$
Tower mass - M_t	447825	454000	$[\text{kg}]$

Table 16.4. Comparison of estimated parameters for nonlinear estimation process.

Generally the model based on FAST with all DOF is as good as the model based on model DOF. To illustrate this, a transient for a single pitch changes is plotted in Figure 16.15.
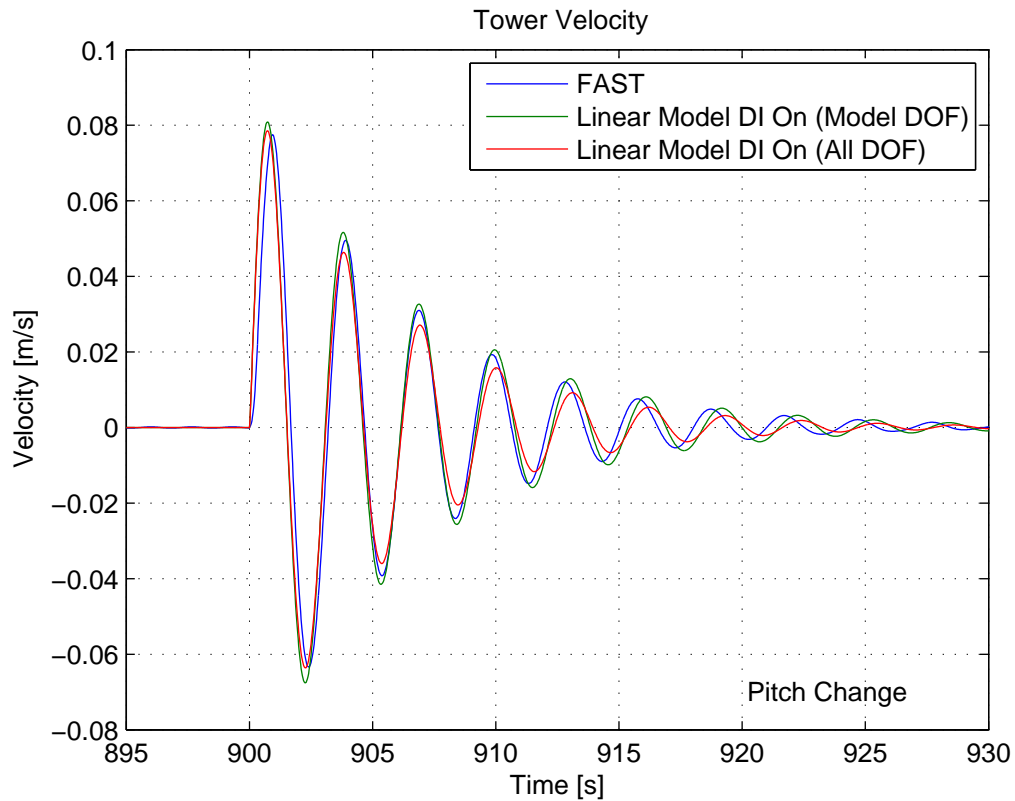

Figure 16.15. Comparison of tower velocity caused by a pitch change. The models have parameters as shown in Table 16.4.

In Figure 16.15 it can be seen that the model based on FAST with all DOF has a larger damping (as expected based on the parameters). This means it hits the first period better, than the model based on just model DOF, however on the rest of the periods it is worse. The frequency of the oscillations is also slower, than both FAST and the initial model. It is therefore decided to stick with the initial model, based on model DOF, as no decisive advantage is seen from the model based on ALL DOF.

16.6   Observability and Controllability

To see if the model developed can be used for control it is tested for observability and controllability.

There can be multiple reasons why a state cannot be measured e.g.:

- A sensor is not present at the needed state, either due to not being physically reachable or economically feasible.
- The state is a so called "dummy" state which does not describe anything real and measurable.

In this case the missing state information can be estimated through and observer, as described in the estimation chapter, by using a model that is observable. As mentioned in the estimation chapter full state measurements, except for the dynamic inflow state, are used in this project, since estimation is not the main focus of this work. The model is tested for observability to verify that the dynamic inflow state can be estimated by using input output data from the system.

A model with n states is observable, if the following holds true:

$$rank(\mathcal{Q}) = n \tag{16.2}$$

Where the $\mathcal{Q}$ matrix can be found as:

$$\mathcal{Q} = \begin{bmatrix} C & CA & \cdots & CA^{n-1} \end{bmatrix}^T \tag{16.3}$$

The model is found to be observable since $rank(\mathcal{Q}) = 6$.

To make sure the system model is controllable via the inputs, the model is tested for controllability.

A model with n states is controllable, if the following holds true:

$$rank(\mathcal{C}) = n \tag{16.4}$$

Where the $\mathcal{C}$ matrix can be found as:

$$\mathcal{C} = \begin{bmatrix} AB & A^2B & \cdots & A^{n-1}B \end{bmatrix} \tag{16.5}$$

The model is found controllable since $rank(\mathcal{C}) = 6$.

The model without DI is also both observable and controllable.

Throughout this chapter a validation and comparison of the developed models have been made. The models show to follow the wanted output from FAST. Inclusion of a simple dynamic inflow model showed to improve the model fit and there is therefore a strengthened basis for using this in an MPC. The following part will go through the basic MPC theory and the setup, before the results obtained using the developed model in an MPC is shown.

Part III
MPC Design

Introduction to MPC Design 17

In this part theory, implementation and tuning of an MPC is shown.

This project works on combining a simple dynamic inflow model with the already existing method of MPC. This means that the MPC theory is only described in a cursory manner, since the MPC format used is described in Appendix G and in even more detail in [Maciejowski, 2002].

With regard to implementation the important features of the tools used here are that they are well tested and used, such that only limited development time is used on errors using the tool. Computation time is often of great importance, when the algorithm is implemented on a real time system. This is not the case, now that the system is simulated and computation time therefore "only" is a matter of not having to wait too long for simulation results. The process of implementing MPC was done first using the same linear model as used in the controller for the system. The next step was implementing it with the nonlinear model as the plant and only after this worked sufficiently, then it was implemented on the full model in FAST. This was done to slowly increase the complexity of the controlled system, so potential errors in the implementation of MPC were easier to deduce a solution for.

A tuning of the implemented MPC is done, with regard to horizon lengths, estimation gain, and weights in the cost function. The goal of this project is not to find the optimal tuning of an MPC. It is to find good tuning parameters for the MPCs (with and without dynamic inflow) that operates well and then compare the two. As long as the tunings are comparable, e.g. using same input weights, the MPCs can be compared.

Theory 18

The theory used for the implementation of the MPC is here presented. The basic functionality and concept are described and the means of tuning the controller is clarified.

The motivation for using an MPC scheme is the ability to optimize the trajectories of a multi variable system, while staying within critical constraints. These features, especially the formal way of handling constraints, has made MPC one of the only control strategies, which is more advanced than PID, to be spread into the industry. Using an MPC for control of a wind turbine gives the advantage of controlling not only power generation, but also handling fatigue of the construction in an optimal way, while ensuring that no constraints are surpassed.

MPC is a family of predictive control methods, which all has the use of a model in common. These methods are often used in combination with a linear model and produces a linear control law. The explicit use of a model predicts future outputs of the plant given some input, within a certain horizon. An optimizer routine calculates the input, which gives the optimal predicted trajectory according to a described cost function and constraints. An illustration of an MPC scheme can be seen in Figure 18.1 [Camacho and Bordons, 1995].
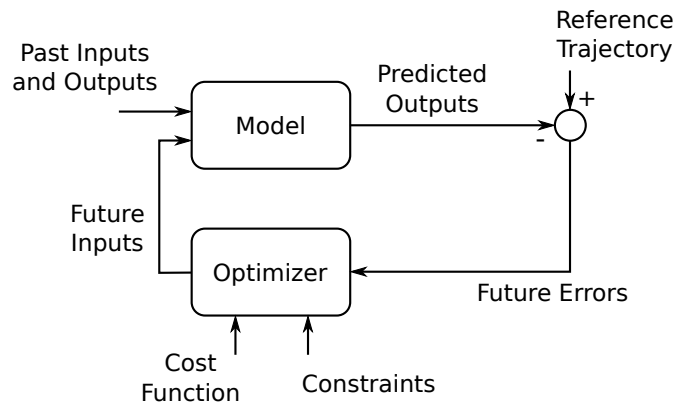

Figure 18.1. Concept of MPC [Camacho and Bordons, 1995]. The use of a model makes it possible to estimate the future outputs given future control inputs and past inputs and outputs.

The future of the plant trajectories are predicted within a prediction horizon of N_p time steps. This prediction is dependent of the assumed future control inputs in the prediction horizon. The future control inputs are applied in the control horizon of N_c time steps as seen in Figure 18.2 on the facing page and after that considered constant for the prediction.
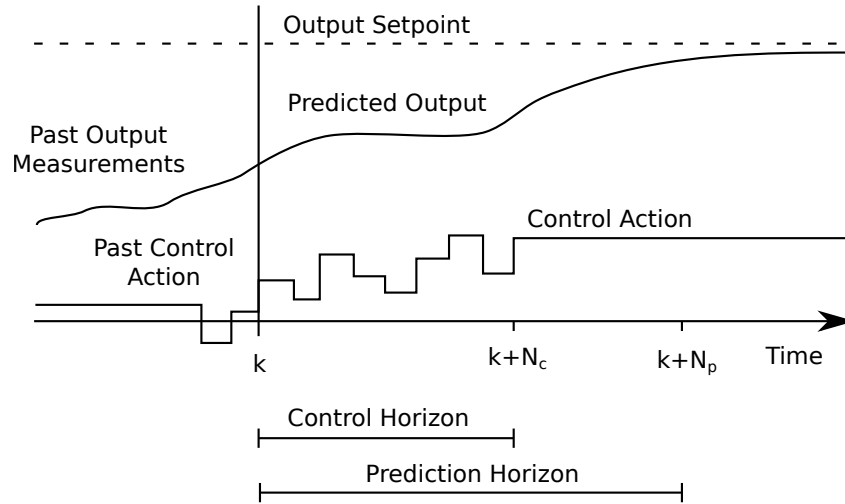
Figure 18.2. The future output of the plant is estimated, based on future control inputs and a model of the plant.

The objective is to reach the set point and by this the future control signals are calculated by optimizing some specific criteria given by an objective function, subject to constraints. The optimal control sequence, in the control horizon, giving the best predicted output trajectory, in the prediction horizon, is calculated in the optimizer. When the optimal trajectory is calculated only the first control input is applied to the plant. This is done every time step. This method of calculating forward a constant horizon every time step online is called receding horizon.

In the following description a linearized, discrete time, state space model is used:

$$x(k+1) = Ax(k) + Bu(k) \tag{18.1}$$

$$z(k) = C_z x(k) \tag{18.2}$$

Where: x are the states.

u are the control inputs.

z are the controlled outputs.

The notation and method for MPC used in this project is based on the works of [Maciejowski, 2002].

18.1 Objective Function

The optimization of the control input is done according to an objective function, which penalizes parameters of interest, e.g. the deviation from the desired trajectory and the control effort. A commonly used objective function is used [Maciejowski, 2002, P. 41]:

$$
V(k) = \sum_{i=N_w}^{N_p} ||\hat{z}(k+i|k) - r(k+i|k)||_{Q(i))}^2 + \sum_{i=0}^{N_u-1} ||\Delta \hat{u}(k+i|k)||_{R^\Delta(i)}^2
$$

$$
+ \sum_{i=0}^{N_u-1} ||\hat{u}(k+i|k)||_{R(i)}^2 \tag{18.3}
$$

Where: $\hat{z}$ denotes the predicted output.
r denotes the reference trajectory.
$\hat{u}$ denotes the control input.
$\Delta \hat{u}$ denotes the changes in the control input.
N_p is the prediction horizon.
N_w is the start of the prediction window.
N_u is the control horizon.

The weights Q, R^Δ and R are here respectively weights on the trajectory error, the input rate of change and the input size. By adjusting these weights the controller can be tuned towards a desired performance. N_w is often set to 1, meaning that the penalizing of the trajectory from the reference starts immediately. Alterations from this are seen if e.g. the effect of the control input is delayed, such that it only affects the trajectory later in the horizon.

Variations in MPC are often introduced, as the system might be time varying, varying with a parameter or convergence to non-zero states is desired. This way the controller can have different behaviour at a different operation point.

This was a cursory description of the form of the MPC used in this project, for more information about how subjects such as handling constraints or disturbances read Appendix G on page 142.

18.2 Estimation

Even though full state information was said to be used in Chapter 7, this is not true for the MPC with dynamic inflow, where the dynamic inflow state a_f is estimated. Apart from this integrated white noise disturbances are used on the outputs which results in integral action. These output disturbances also needs to be estimated. A Kalman filter is used for this, read Appendix F for further information on this. The setup including the Kalman filter is as seen in Figure 18.3.
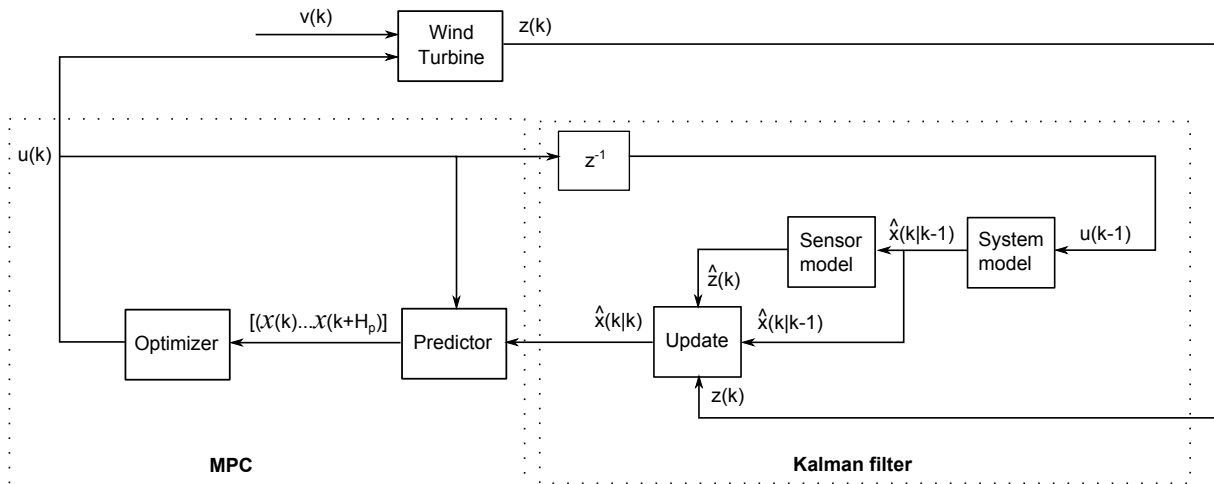

Figure 18.3. Location of the estimation in regard to the control structure.

The general form of how estimation, prediction and optimization is coupled into the complete control scheme was here described. Each of these three subjects were described in a very cursory form with pointers to where more information can be found.

Implementation 19

This chapter will go through the specific MPC implementation used throughout this project. The Simulink setup and quadratic programming solver used will be explained.

Different tools such as "quadproc", "CVX" and "Model Predictive Control Toolbox" are available for when implementing MPC in MATLAB. Having experience with the three mentioned tools "Model Predictive Control Toolbox" was chosen since it fulfils the needs of this project while being a well tested and documented tool. Since FAST runs in the Simulink environment the MPC related code is collected into what is called a MATLAB interpreted function as seen in Figure 19.1.

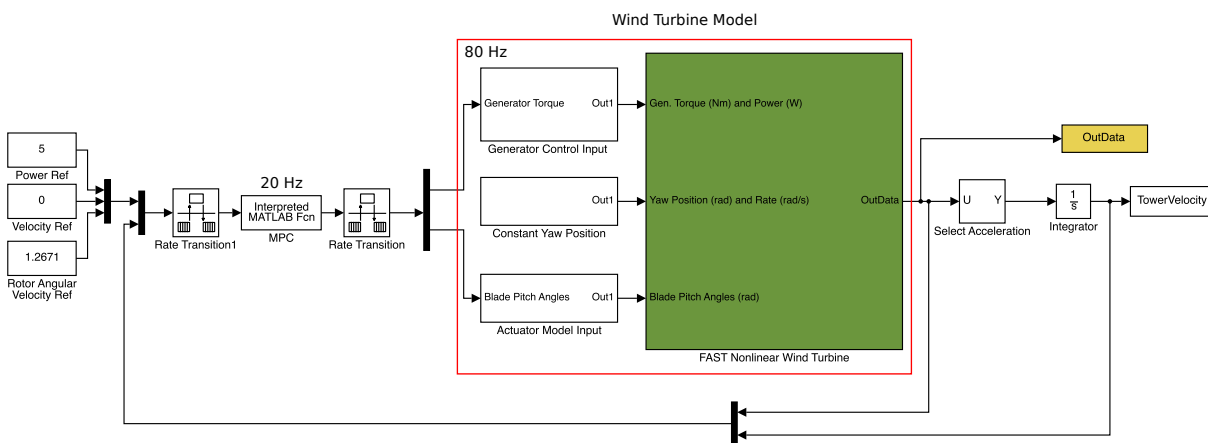An overview of the Simulink file can be seen in Figure 19.1.

Figure 19.1. The Simulink implementation of the MPC.

The red box indicates where the limits of the wind turbine model is. The model is used as a replica of a real world wind turbine. Inside the pitch actuator block is the defined model for the actuator, which includes a first order model, slew rates and actuator movement constraint. The green block is the model supplied by FAST, where the high-fidelity wind turbine model is being run.

The MATLAB interpreted function is where all MPC related code is running. The block takes the reference values for power generation and tower velocity and the wind turbine measured outputs as input. It then outputs a control signal. The reference is made in MW, in order to get MPC weights that are closer to unity. If it had been in W, a similar output power weight would have to be scaled by a factor 10^{-6} in order to create the same level of cost. This is done on all the forthcoming results.

The sampling time of the simulation is set to fixed time - 0.0125 s. The Runge-Kutta solver method is the used ODE solver. This is the ODE solver that NREL advises since FAST is build around this. The sampling time of the MPC is set equal to 0.05 s. The highest frequency looked described in the model used in fast is the tower frequency, at 0.324 Hz. Setting the sampling frequency to 20 Hz, should be more than enough to allow for good control performance.

To recapitulate the input, states and output of the model used for MPC are:

$$u = \begin{bmatrix} T_{g,ref} \\ \beta_{ref} \\ v_w \end{bmatrix} \qquad x = \begin{bmatrix} \omega_r \\ d_t \\ v_t \\ \beta \\ T_g \end{bmatrix} \qquad y = \begin{bmatrix} P \\ v_t \\ \omega_r \end{bmatrix} \qquad (19.1)$$

In the input only $T_{g,ref}$ and β_{ref} are manipulated variables, since the system have no control over the wind. In the cost function a rate constraint is applied to β_{ref} and on the size of $T_{g,ref}$. Using the actuators has a cost e.g. power for the actuators and increased wear and tear. The size of the real cost of using these inputs compared to the output costs are unknown. The size of the chosen pitch rate and generator torque weights are discussed further in the tuning of these.

Weights are added to the errors between the references and the outputs for all the outputs. Power and tower velocity references are respectively set to the rated power and zero tower velocity. If only weights were added to these two outputs, the system would be able to find an equilibrium, where the rotor speed and generator torque are not at their rated values, e.g. generator torque being lower and rotor speed faster. This is solved by adding the rotor rotational velocity as an output and applying a reference on the rated velocity. Something similar could be done by applying soft constraints around rated generator torque. From trying both of these methods in simulations the former was chosen.

19.1 Solver

The QP solver used is the "QPKWIK" described in [Schmid and Biegler, 1994]. This algorithm requires the Hessian to be positive definite. The karush kuhn tucker conditions are used as described in (G.76) (see Appendix G on page 142) as the necessary and sufficient conditions for the found solution being a global minimum. KWIK uses the cholesky factorisation for faster calculations of the inverse of a matrix which is used in the optimization. For calculating the first control input, the KWIK algorithm uses a cold start, where the initial guess is the solution to the unconstrained problem. From there on the initial guess at each control step is made using a warm start, where the set of active constraints are the one used in the solution of the previous control step.

It has here been described how MPC is interfaced with FAST in MATLAB using the MPC Toolbox and Simulink. FAST is sampling at 80 Hz, where the MPC is sampling with 20 Hz. The general form of the MPC, in regard to input, states and output was shown with and explanation of which are weighed in the cost function. The tuning of the MPC will now be addressed.

MPC Tuning 20

The MPC is now implemented with FAST and needs to be tuned to provide satisfactory control. This chapter describes methods used in the process of tuning the MPC. As explained the objective is not to ensure that the controller controls some parameter to some given standard. The objective is to tune a controller such that it has an overall control performance that can be assessed to be a good basis for comparison.

It is chosen to tune with only the DOF enabled in FAST which are present in the model used in the MPC. In this way it is easier to decipher cause and effect in the tuning process. Here another option could have been to tune on FAST with all DOF, since this is what the final results will be made on, such that a controller with general better performance on that system maybe could be found. As long as the controllers are tuned alike some relative small improvement in performance would not improve the final results which is the comparison, not the individual controllers performance.

The tuning is chosen to be done on realistic wind turbulence with the Kaimal spectrum. Since the tuning is done on time limited wind data, different seeding of the generated wind data gives small variations in spectrum. So if tuning is only done on one wind data file with generated from one seeding then it might not be optimal for other seeding. This is deemed a negligible as long as the wind files generated and tuned on are over a long enough time period. Another option could have been to do the tuning on step responses, but this means tuning for higher bandwidths than the control system experiences.

There are several parameters in the MPC, which can be tuned in order to change performance of the controller - constraints, horizons and weights. The implementation of these are here presented. The color coding of the plots is kept the same between different plots, when tuning a specific weight. This means that the transient plot of a controller has the same color as the corresponding controller in Pareto front plots.

The results during the tuning process is here only shown for the MPC with DI to make the plots simpler. The tuning of the MPC without DI is tuned following the same process and the results is shown in the end of the chapter.

20.1   Disturbance Signal

The disturbance signal will be the incoming wind with turbulence. The disturbance signal is generated with TurbSim and is set to have a mean wind speed of 12 m/s. The wind transient is inspected to make sure that it stays within the operating area. The disturbance input can be seen in Figure 20.1. During the first 60 s, the pitch is controlled by a PI-controller in the effort of driving the system to steady state before enabling the MPC. MCrunch is used for fatigue calculations (see Chapter 5 on page 14) and is started at 130 s to allow the MPC some settling time.
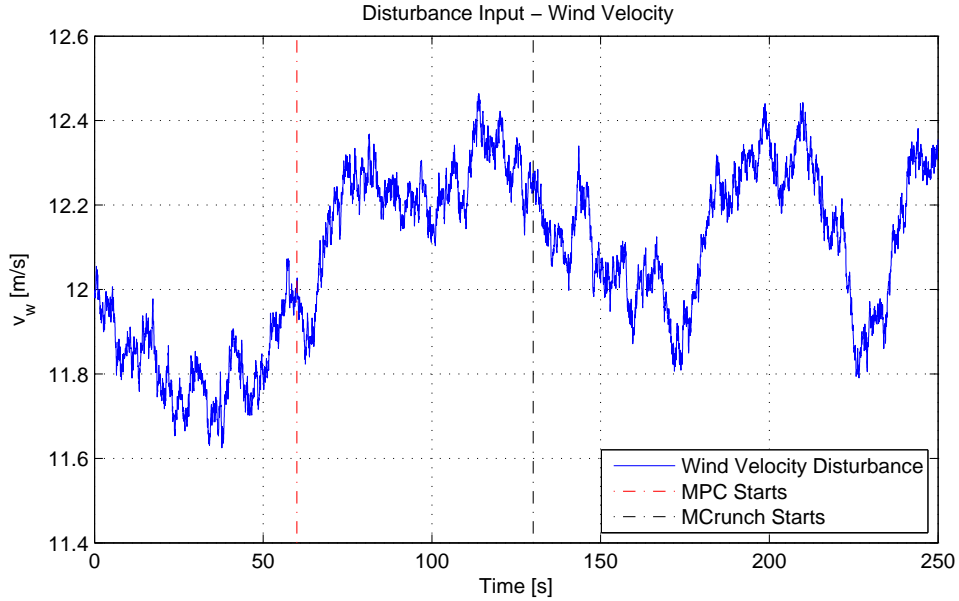
Figure 20.1. The disturbance input - wind velocity with kaimal turbulence spectrum. The start up is done using a PI-controller, which is active the first 60 s. The MPC is then activated. The fatigue is calculated with MCrunch from 130 s.

20.2 Constraints

Constraints are used in order to specify acceptable inputs and outputs to the controller. Constraints on the input are here determined from the physical specifications of the system, whereas the output constraints have been determined from a mix of physical limits and design goals. The generator power constraint should be determined by a damage analysis of generator over-power. This is however out of scope of this project, which is why a soft constraints is applied at 5.1 MW. The implementation of the MPC is done with the MATLAB MPC toolbox, which require constraints specified for all inputs, input rates and outputs. Constraints are shown in Table 20.1.

Parameter	Upper	Lower	Unit	Type
Generator torque	47403	0	$[Nm]$	Hard
Generator torque rate	-	-	$[Nm/s]$	Hard
Pitch	90	0	$[°]$	Hard
Pitch rate	10	-10	$[°/s]$	Hard
Generator power	5.1	0	$[MW]$	Soft
Tower velocity	-	-	$[m/s]$	Soft
Rotor angular velocity	0.207	0	$[Hz]$	Soft

Table 20.1. Constraints used for the MPC tuning.

All the constraints related to inputs are hard constraints, as this is physical limits of the actuators. The upper constraint on the torque is set 10% higher than rated torque, as done in [Jonkman et al., 2009]. The output constraints are all set as soft constraints by the MPC toolbox. A constraint is added to the rotor angular velocity, as it is important the rotor is not spinning too fast, because this will cause extra stress on the blades and if extreme enough possibly destroying them.

20.3   Integral Action

In order to ensure that there are no steady state errors on the power reference, integral action is added to the MPC setup. An output disturbance model is added to the setup, extending the model with two extra states - one on power and one on rotor speed. The output disturbance model is integrated white noise, meaning white noise on the changes of the output. This is done to give offset free tracking [Maciejowski, 2002, P. 202]. Due to the nonlinearities of the wind turbine, e.g. the DC gain of the linear model will never be exactly like the one at the plant giving rise to a disturbance which is the error between model and plant. The added disturbance states on the output will help remove this difference between model and plant.

The difference between an MPC with and without integral action with a step in wind can be seen in Figure 20.2.
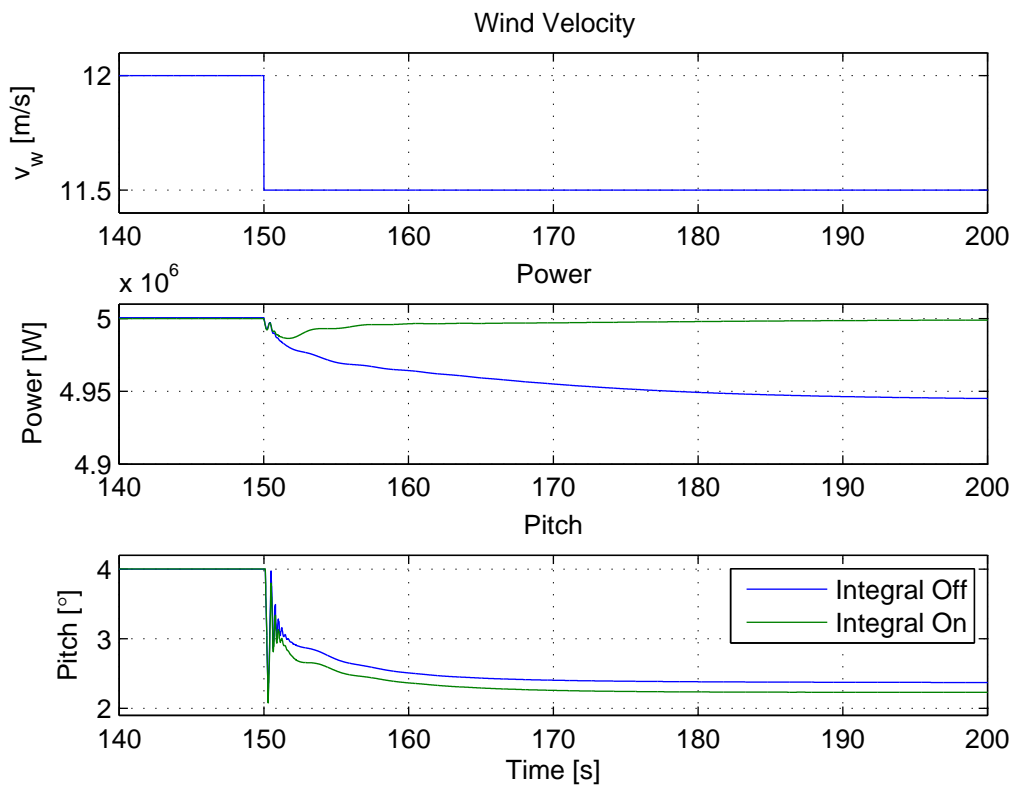
Figure 20.2. Comparison of MPC with and without integral action. When integral actions is enabled, steady state errors are rejected.

As can be seen from Figure 20.2, the green power trajectory converges to the 5 MW as wanted, whereas the blue trajectory is stuck around 4.95 MW having a steady state error. The tuning of the covariance matrix Q and R in the Kalman filter is done, such that the filter treats the disturbances more as system disturbances and than measurements noise.

20.4 Horizons

The prediction horizon for the MPC is normally a very specific implementation issue, depending on the hardware chosen, since each MPC move needs to be computed within the sampling time. Simulation does not have such problems, as the time it takes for each iteration will just be increased. If the horizons are extended towards infinity the controller converges towards the control of an LQR (considering no active constraint) which can be shown to be stable. If the prediction horizon becomes too low instability can occur. In general the horizons are choices based on the sampling time and the time period of the dynamics, which are to be addressed.

The natural frequency of the tower is of most interest, as the aim of the control is to minimize fatigue on the tower, while keeping power production performance. The highest frequency, which should be taken into account in the MPC, is assumed to be around 1st tower fore-aft natural frequency at 0.324 Hz. To ensure that the system is able to react on these oscillations, the sampling rate of the controller should be much larger (at least twice the frequency to avoid aliasing), than the highest frequency of interest. Based on this a sampling rate of 20 Hz was chosen. The control horizon should at least cover a period of the 1st tower fore-aft oscillations, which is $\frac{20}{0.3240} \approx 62$ samples. This ensures that the MPC is able to predict a control move for the entire period and thereby capable of suppressing these oscillations. The prediction horizon should be larger than the control horizon. The prediction horizon is used to see if any constraints are violated, which makes it interesting having it long. The prediction horizon is chosen to 10 s, which is 200 samples.
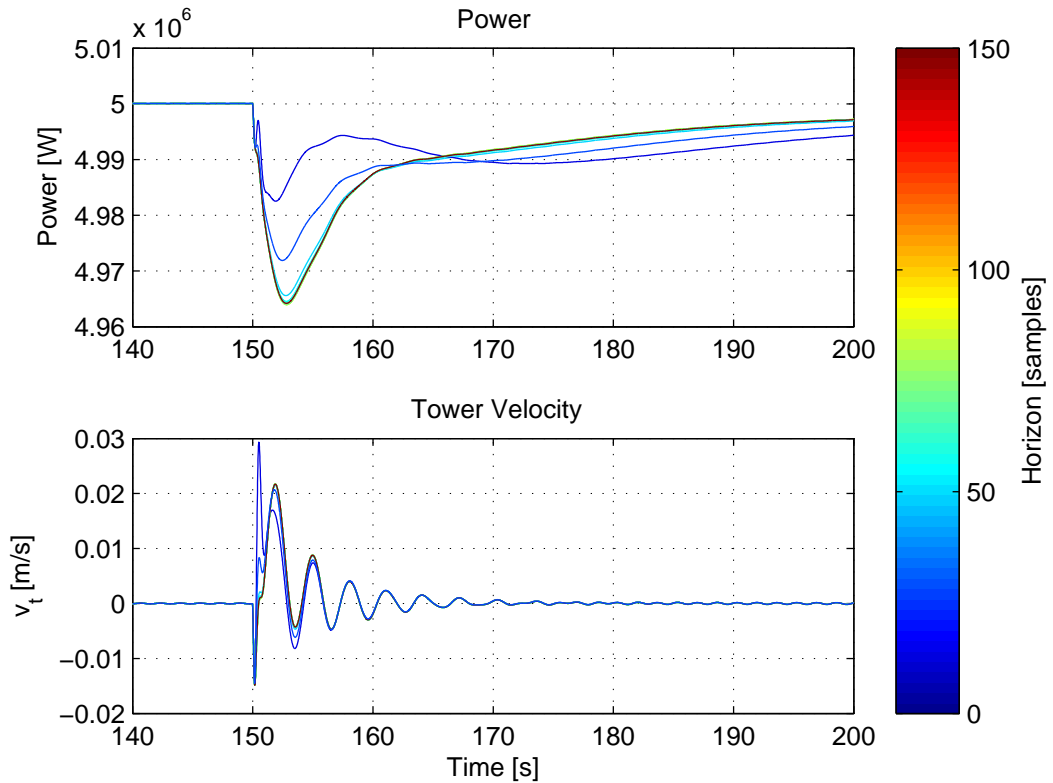

Figure 20.3. Transients of generator power and tower velocity, when changing the control horizon. The test is done applying a step as wind disturbance from 12 to 11.5 $^m/_s$.
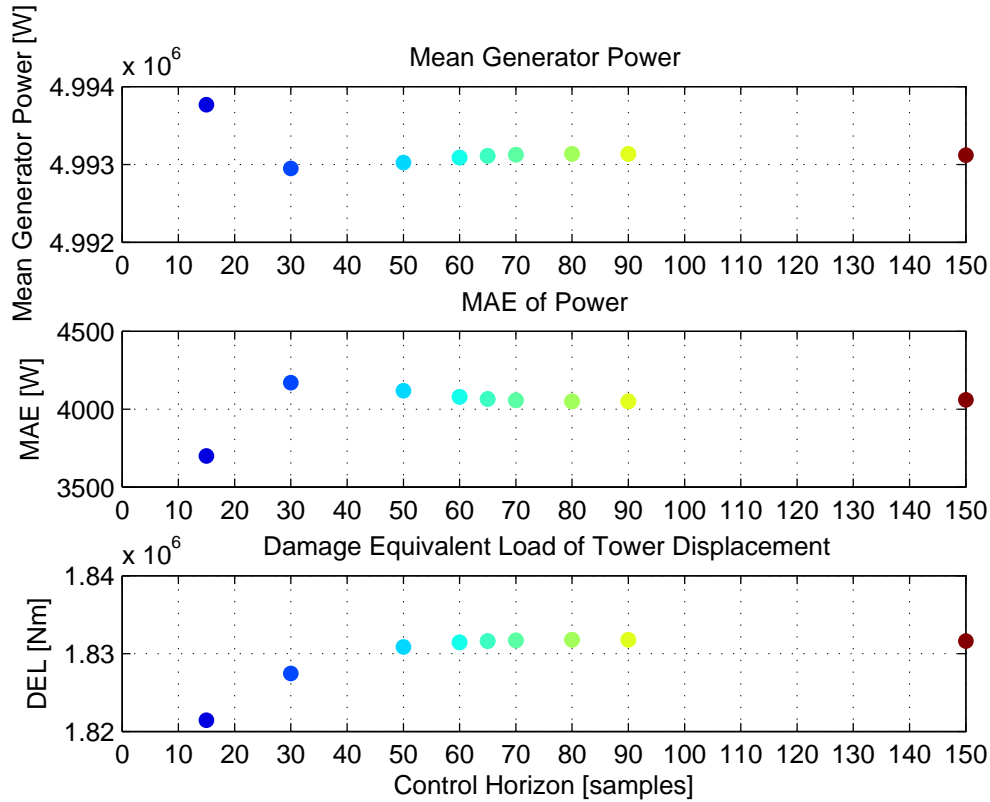
Figure 20.4. Variations in performance measures, when changing the control horizon. The test is done applying a step as wind disturbance from 12 to 11.5 $^m/_s$, equal to that shown in Figure 20.2.

In order to find a suitable control horizon, a simple test has been made. The test is done applying a step as wind disturbance from 12 to 11.5 $^m/_s$. The test is run several times with different control horizons, but the same prediction horizon of 200 samples. The results are plotted in Figure 20.3 and 20.4, where it can be seen that when approaching the 62 samples as calculated, the transients starts to show same performance. Furthermore, the performance measures (mean generator power, MAE of power and tower fatigue) starts converging.

Based on the test, the horizons are set as following:

Horizon	Samples	Time [s]
Prediction	200	10
Control	65	3.25

Table 20.2. Horizons used for the MPC Tuning. The sample rate is 20 Hz.

20.5 Weights

Weights can be used on the two control variables, pitch β_{ref} and generator torque $T_{g,ref}$ and each of their rate. Furthermore, the outputs, generator power P_g, tower velocity v_t and rotor speed ω_r can be weighted. In order to simplify the tuning process, the generator torque weight is set to 0.01, as this input generally is considered free to use. The pitch position is weighted to zero, as it is the movement - pitch rate that is causing wear and tear on the pitch actuator. The pitch rate weight is therefore initially set to 1. The rotor speed weight is in the beginning also set to 1. Further tuning of these are then addressed later on.

In the beginning the interesting weights are for the output variables, P_g and v_t. The velocity is assumed to have direct influence on fatigue (see Chapter 5 on page 14). It is further assumed that there is a trade off between power generation and tower velocity, thus the choice of weights on P_g and v_t will introduce a trade-off between the tracking of the power reference and minimisation of fatigue. The weights used in this initial setup are:

Parameter	Weight
Generator torque	0.01
Generator torque rate	0
Pitch	0
Pitch rate	1
Generator power	Variable
Tower velocity	1
Rotor Speed	1

Table 20.3. Weights used for the initial MPC.

20.6 Tuning

It is the weights times the states that determines the influence of a state in the cost function, which is to be minimised. Thus it is the weights, normalized with regard to state size, relative to each other that matters. That is why the weight on the tower velocity is kept constant, when the weight on the generator power is variable. The before mentioned trade-off can be seen in Figure 20.5, where the transient of two controllers (with DI) with different weight on power is plotted. The system is applied the disturbance seen in Figure 20.1 on page 89 and the weights given in Table 20.3 are used. As seen on the figure, the dark red favours the tracking of the power reference, but has larger oscillations on the velocity, which leads to a higher fatigue (measured by damage equivalent load): 2844100 Nm for dark red and 2393800 Nm for the blue.
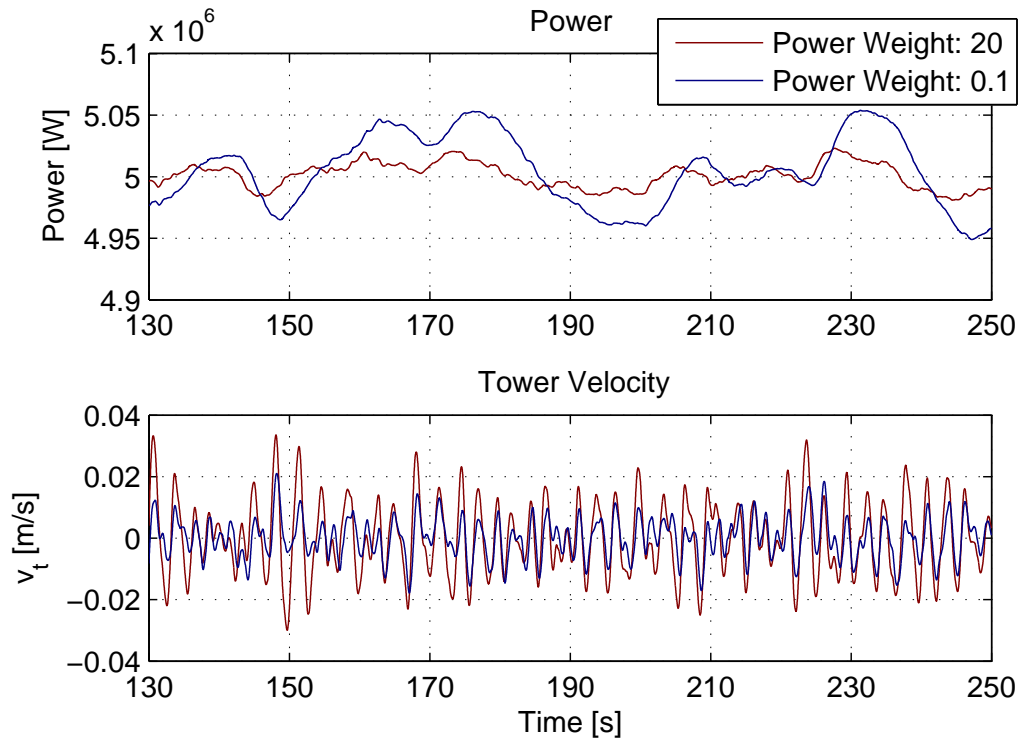
Figure 20.5. The trade-off between tracking of the power reference and minimisation of fatigue. The fatigue is calculated with MCrunch to 2844100 Nm for dark red and 2393800 Nm for the blue.

20.6.1 Generator Power

In order to show the performance changes, when tuning the weights, a Pareto front is made showing mean power and fatigue. Figure 20.6 shows results from controllers with weights on the power output in the interval [0.1; 20]. The value of the weight is represented by the colorbar. The magenta square will throughout this chapter indicate, which controller is chosen to continue with further tuning.
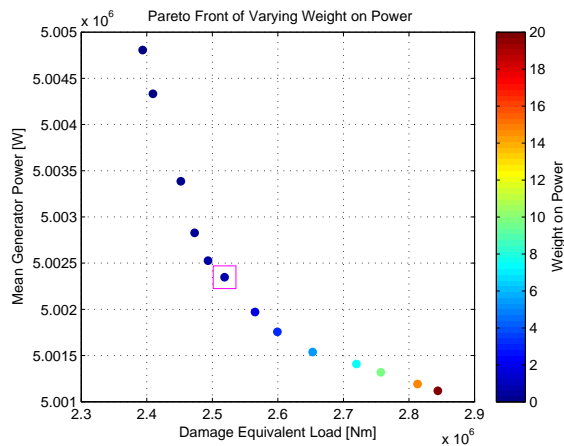
Figure 20.6. Pareto front showing the trade-off between mean power production and fatigue calculations. It is desired to have a mean power of 5 MW and smallest possible fatigue. The weights are represented by the colorbar.
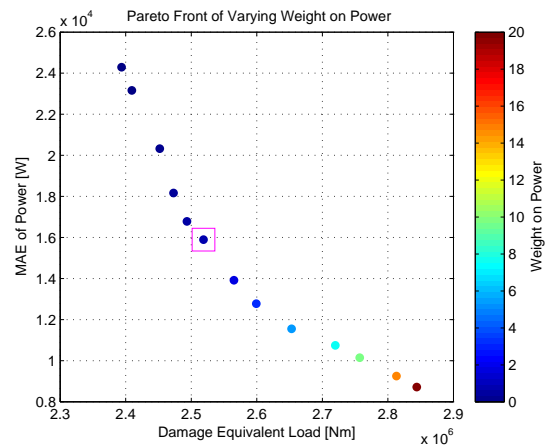
Figure 20.7. Pareto front showing the trade-off between MAE on generator power and fatigue calculations. It is desired to minimise both MAE and fatigue. The weights are represented by the colorbar.

The mean power on the generator is an important design driver, but is not enough for choosing a good controller. The mean power does not contain any information about how big an error is made, since a positive and a negative error can cancel each other. To address this issue another Pareto is shown in Figure 20.7 with the mean absolute error (MAE) vs. fatigue. In both Pareto fronts it can be seen that the assumption of a trade-off between power performance and fatigue is indeed correct.

In Figure 20.6 it is desired to find a controller with mean power as close to 5 MW and smallest fatigue, whereas in Figure 20.7 it is desired to minimise both parameters. The mean power is however the most important design driver. It is chosen to continue further work with the controller marked with the magenta square in Figure 20.6. This controller is also the magenta square marked controller in Figure 20.7, which is one of the best here as well. The transient of a run with this controller is shown in Figure 20.8 on the next page.
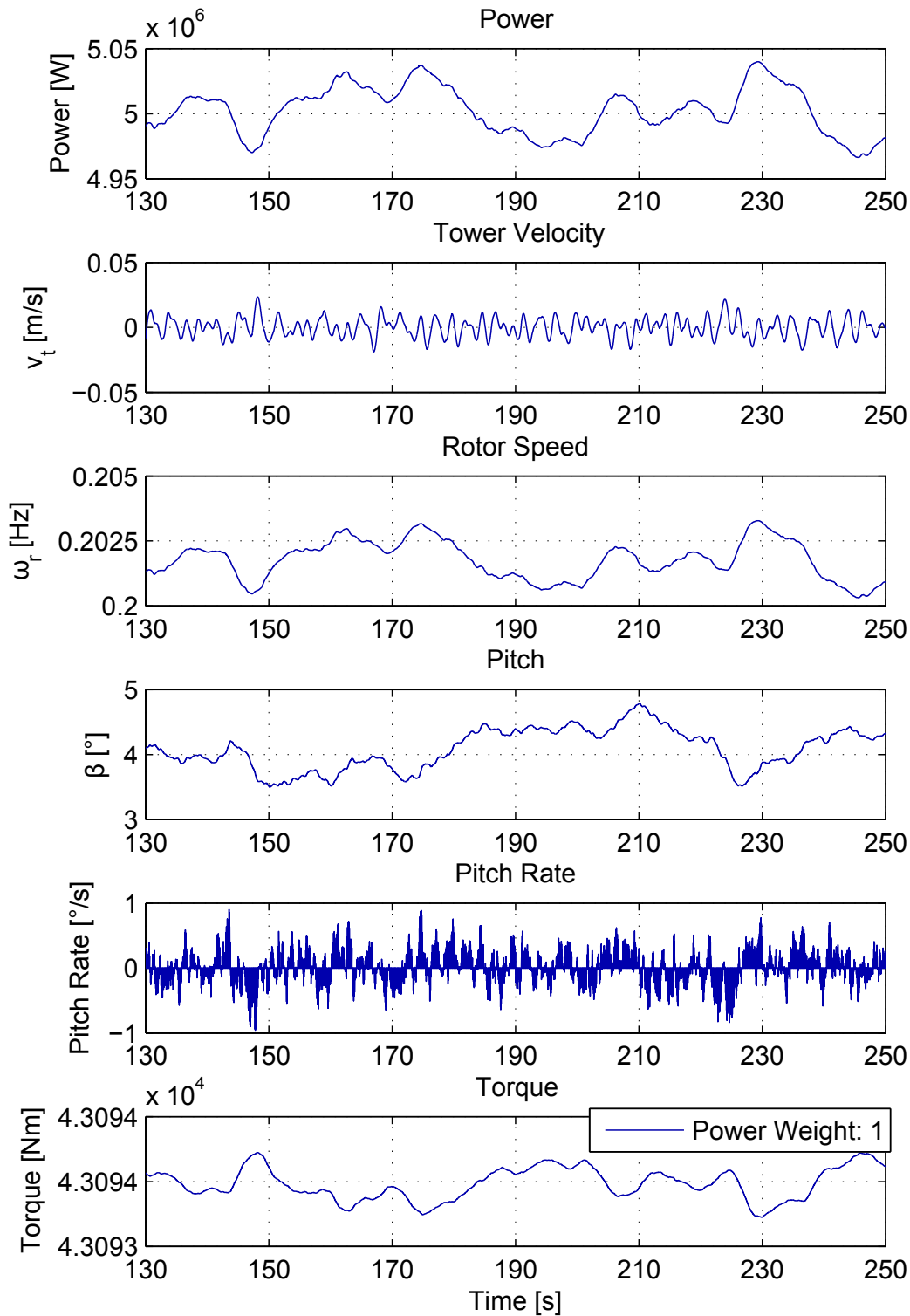
Figure 20.8. Transient plot of the chosen controller.

In Figure 20.8 it is seen that the generator power is oscillating around the desired 5 MW. The pitch is generally following the slow trends of the wind, while also having smaller oscillations to minimize the tower velocity. The generator torque is generally used very little in this transient response.

The next step in the tuning process is to look at the weight on rotor speed, to see how it affects the results in the Pareto front.

20.6.2 Rotor Speed

A weight on the rotor speed is needed, such that the rated rotational velocity and generator torque are the equilibrium at 5MW. Integral action was also added to this output. However having a weight on the rotor speed is indirectly punishing deviations in power, as the rotor speed is the foundation for the power generation. It is therefore kept low, while keeping an integrator effect, such that the power weight still is the main cost for power in the cost function. It is investigated what happens with the MPC, when the rotor weight is changed. The weights used in this initial setup are:

Parameter	Weight
Generator torque	0.01
Generator torque rate	0
Pitch	0
Pitch rate	1
Generator power	1
Tower velocity	1
Rotor Speed	Variable

Table 20.4. Weights used for tuning of rotor speed weight.

Weights in the interval $[10^{-3}; 10]$ are investigated. The results can be seen in Figure 20.9 and 20.10. A black square indicates the previous chosen tuning that is the basis of this variable tuning on rotor weight.
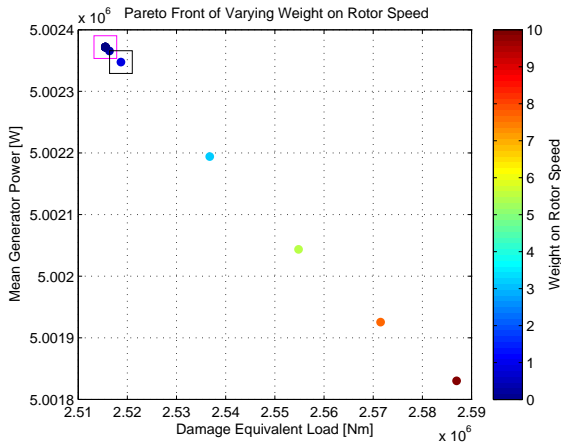

Figure 20.9. Pareto front showing the trade-off between mean power production and fatigue calculations. It is desired to have a mean power of 5 MW and smallest possible fatigue. The weights are represented by the colorbar.
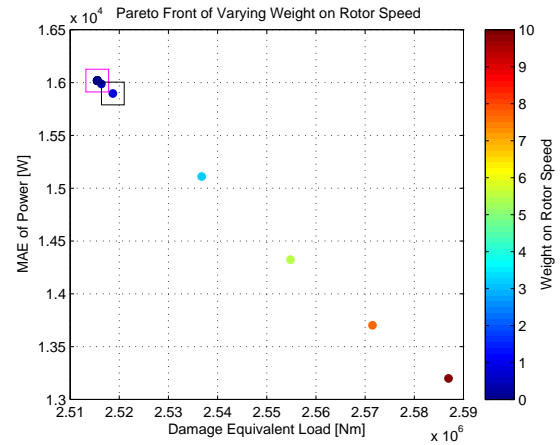
Figure 20.10. Pareto front showing the trade-off between MAE on generator power and fatigue calculations. It is desired to minimise both MAE and fatigue. The weights are represented by the colorbar.

As seen in the figures, the behaviour is like that of the power weight, which was to be expected. As the weight is increased, so is the fatigue level, because the rotor speed starts to matter more and tower velocity less. A weight for the rotor speed of 10^{-3} is chosen, because it gives the lowest fatigue level, while sacrificing a negligible drop in mean power and increase in MAE of power.

20.6.3 Input Weights

As explained in the introduction pitch rate and generator torque are weighed, as the use of these actuators demands power and causes wear and tear to the actuators. The real cost of using the inputs compared to cost of the outputs are not known, so this becomes a tuning parameter. However, the cost of the input is the same whether DI is considered or not.

Pitch rate is tuned first. By applying a high cost to pitch rate, the pitch is used less, which causes the control bandwidth to be smaller. In the extreme case the pitch rate cost becomes so large that the control system is slower than the critical frequency at where dynamic inflow does not have an effect.

The weights used while tuning the pitch rate is:

Parameter	Weight
Generator torque	0.01
Generator torque rate	0
Pitch	0
Pitch rate	Variable
Generator power	1
Tower velocity	1
Rotor Speed	10^{-3}

Table 20.5. Weights used for tuning of the pitch rate weight.

Use of the pitch actuator at different weights of pitch rate can be seen in Figure 20.11.
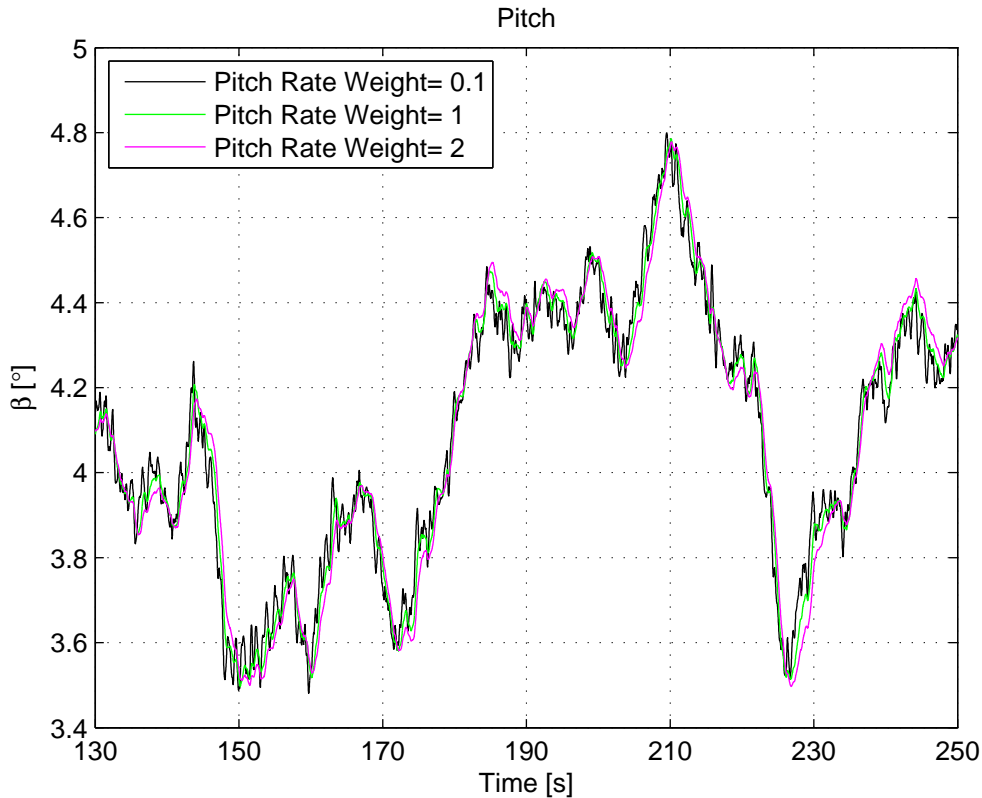

Figure 20.11. Transients of the pitch for different weights on the pitch rate.

The tuning of the pitch rate was done in a manner, where a cost high enough to have an influence, but small enough to still be able to respond to the dynamic inflow properties of the tower. A pitch rate weight of 2 was chosen.

Generator torque was tuned in the same fashion. Using the generator torque is deemed less "costly" and the weight was therefore through tuning found to be $6.15 \cdot 10^{-5}$. Remember the input rate weight on pitch and generator torque cannot be directly compared in regard to influence in cost function, as the states they act on are not the same numerical size.

20.6.4   Pareto with Final Tuning

The weights for the controllers have now been found. They turned out to be very similar, which is why the tuning of the MPC with DI is used for both. The weights used, when creating results in Part IV, are as seen in Table 20.6.

Parameter	Weight
Generator torque	$6.15 \cdot 10^{-5}$
Generator torque rate	0
Pitch	0
Pitch rate	2
Generator power	Variable
Tower velocity	1
Rotor Speed	10^{-3}

Table 20.6. Weights used for the final MPC tuning.

Using the chosen wieght and running both MPCs again creates the results that can be seen in Figure 20.12 and 20.13.
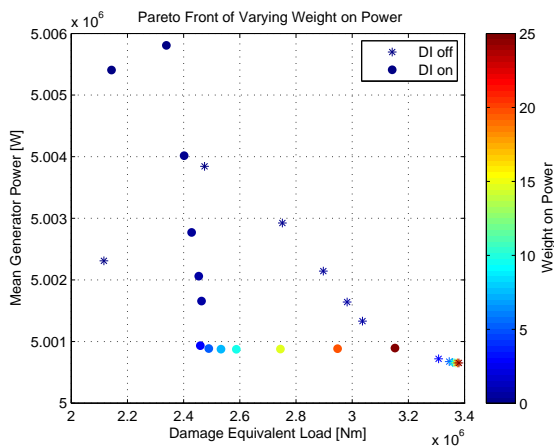

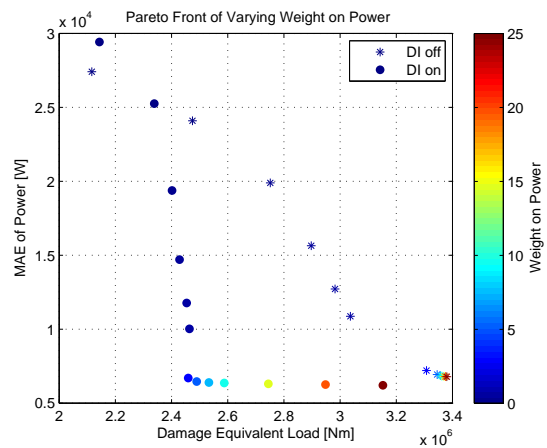**Figure 20.12.** Pareto front showing a comparison between the MPC with the two linear models.

Figure 20.13. Pareto front showing a MAE comparison between the MPC with the two linear models.

These Pareto plots shows the initial results of the comparison between including and not including dynamic inflow in an MPC. It can be seen that there is an improvement to be gained by including dynamic inflow. The system tested on is, as explained earlier, FAST with only

the DOF used in the model turned on, and therefore not a final result. Further analysis of the results will be done in Part IV.

A tuning used for both the MPC with and without dynamic inflow was found. This tuning will be used in the further work, where the controllers are tested and compared on the 5 MW NREL wind turbine in FAST with all modes enabled.

Part IV
Results

Results 21

In this chapter it will be tested how well the two MPC setups perform in comparison to eachother. The plant the controllers are tested on is the 5 MW NREL wind turbine simulated in FAST with all DOF enabled. The input wind will contain realistic turbulence using the IEC 1400-1 Kaimal spectrum running for 600 seconds. Besides comparing how the actuators perform on the key values, power generation and tower fatigue, it will also be investigated how the two setups differ in the use of pitch actuation.

So far the MPC has been tested on a simplified wind turbine, where only the modelled DOF have been enabled. It will now be investigated what happens, when the full set of DOF are enabled, emulating a wind turbine in the fullest degree FAST can deliver. Furthermore the controller will be running for longer time, than in the tuning process. This is done to get more data and thereby to better see the difference between the MPCs (with and without DI in the linear model).

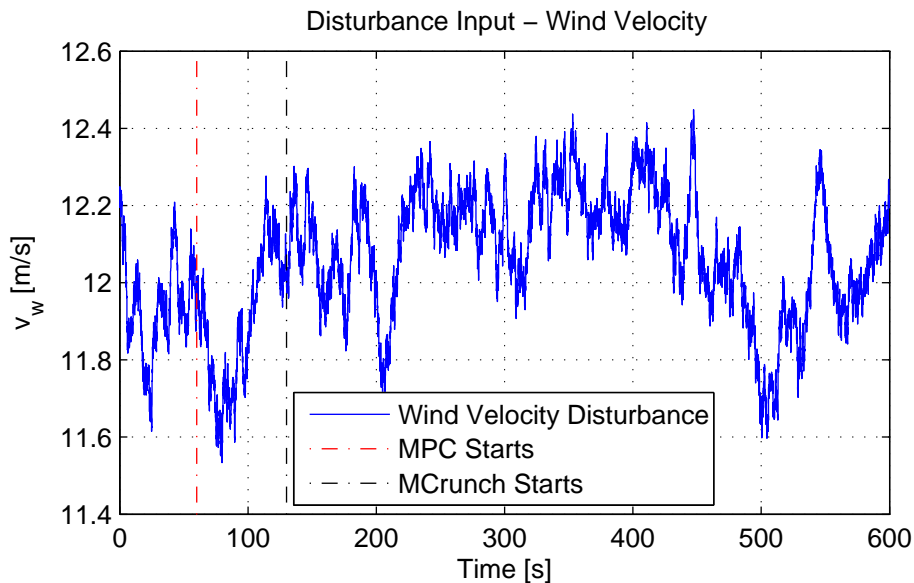The wind signal for this comparison can be seen in Figure 21.1.

Figure 21.1. Wind input this comparison of controller performance. The magenta line indicates where the MPC starts. The black line indicates where the evaluation of data and MCrunch starts.

21.1 Comparison

Running the MPCs with weights, as shown in Table 20.6 on page 99, the Pareto front for the input disturbance wind gives the following results:
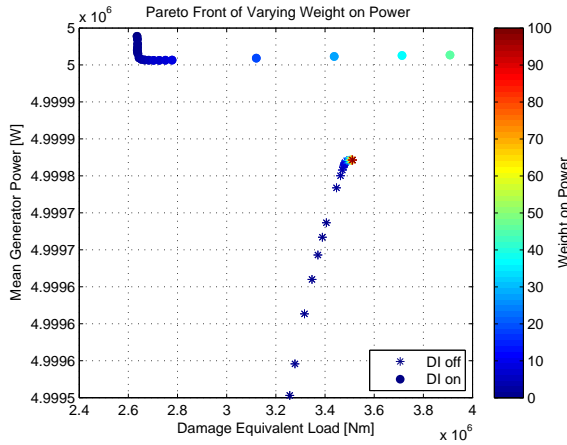

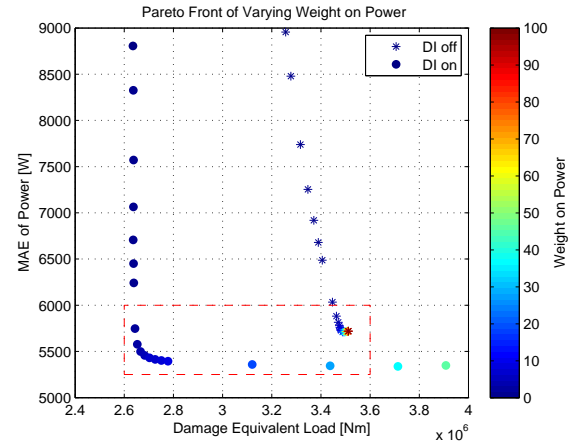***Figure 21.2.*** Pareto front showing a comparison between the MPCs.

Figure 21.3. Pareto front showing the MAE comparison between the MPCs.

In Figure 21.2 it can be seen that both controllers converge to a mean power of 5 MW as the power weight increases. The error in mean generator power at the worst controller with the worst weight regarding power, is 0.1‰, which is so small that results regarding mean generator power is deemed uninteresting. Instead the focus is on the MAE of the generator power compared with tower fatigue, which is seen in Figure 21.3.

By looking at the dots, in Figure 21.3, which correspond to a weight with a specific controller a tendency can be seen for both controllers, with and without dynamic inflow. An area representing a curve (if interpolation is imagined between the dots for each controller) is present at both controllers. This curve goes from low to high in power weight. In the lower and higher (with regard to power weight) end of this curve it becomes respectively vertical and horizontal. When the trend is horizontal the tower fatigue becomes worse, without gaining a lower MAE in power generation. When the trend is vertical the MAE in power generation becomes higher without gaining less fatigue on the tower. This is true, apart from the lower part of the curve representing no dynamic inflow controller, where the trend is not completely vertical, such that there is still some improvement to gain in tower fatigue on the cost of MAE on generator power. The interesting area of Figure 21.3 is therefore in the area marked with a red dashed line, which is depicted in Figure 21.4 on the next page.
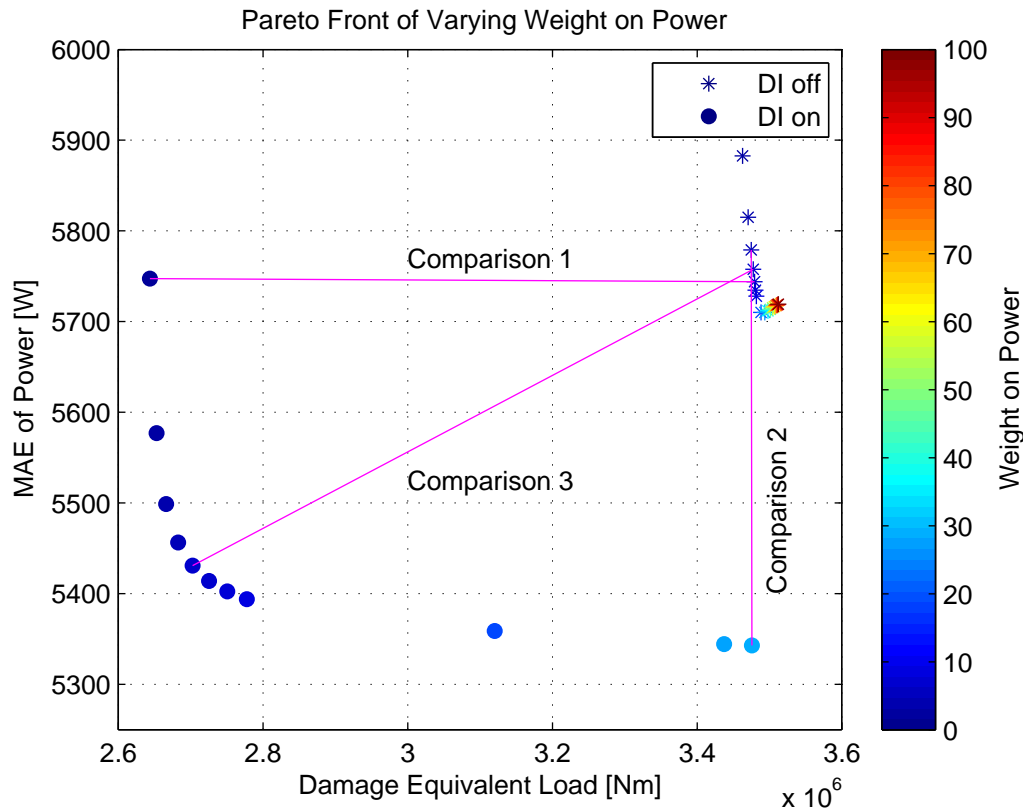
Figure 21.4. A close-up of Figure 21.3, where lines between controllers have been made.   The performance of these "connected" controllers will be compared.

As seen in Figure 21.4 an improvement from using dynamic inflow is seen, both on the MAE of the power and tower fatigue. To put numbers on these improvements specific controllers are chosen for comparison. The controllers which are connected with a magenta line will be compared. A comparison can be made in made many different ways, but is chosen to be done with the following equalities of the controllers:

First two controllers with an equal MAE of power will be compared. Secondly two controllers with equal level of fatigue of the tower will be compared. Finally controllers with equal power weights are compared. For comparison 2 an extra controller point has been calculated for DI on, such that the comparison is more equal in fatigue.

The comparison is done on the following data:

- Mean absolute error (MAE) of generator power - To see how well the power reference is followed.
- Damage equivalent load (DEL) of tower - To see how well the tower fatigue is diminished.
- Standard deviation (σ) of rotor speed - To see how well the rated value for rotor speed is followed.
- Standard deviation (σ) of the torque - To see how much generator torque is used.
- Mean absolute (MA) pitch rate - To see how fast pitch is changed.

Figure 21.5. Comparison 1 represented in a spider chart.
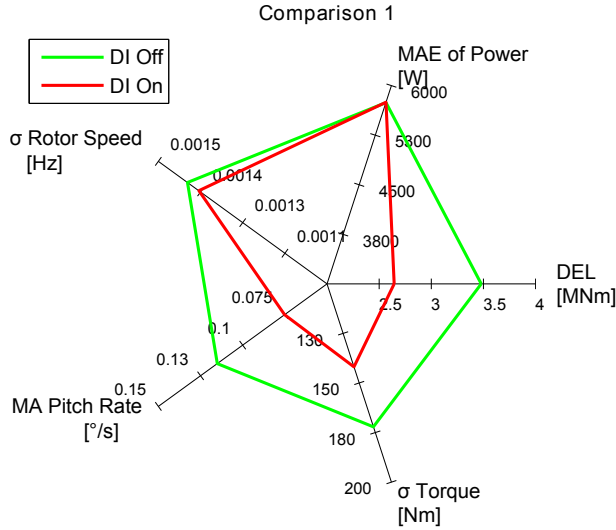
Comparison 1	Improvement [%]
DEL	24.02
MAE of Power	0
σ Rotor Speed	2.38
MA Pitch Rate	34.66
σ Torque	17.56

Table 21.1. Percentwise improvement between DI On and DI Off for comparison 1.

In comparison 1 controllers with equal MAE of the generator power was compared. Since the Pareto fronts of the two MPCs with different power weights, span over different areas and are of different sizes, it is an interesting comparison. Here the controllers perform equal in regard of following the power reference, but the DEL of the tower is 24% lower for the controller using dynamic inflow. This is a clear result showing that in this setup dynamic inflow is important to have. Emphasis must be put on the part "in this setup", since another MPC using a different model form (maybe a higher fidelity model) or another tuning of the locked weights might give different results.

Another point is that the MPC with dynamic inflow is able to maintain the same MAE of the power and improving the fatigue of the tower, while using 34% less in MA pitch rate and less changes in generator torque with a 17% lower standard deviation. Besides this σ of the rotor speed is improved slightly, such that it lies closer to the rated speed.
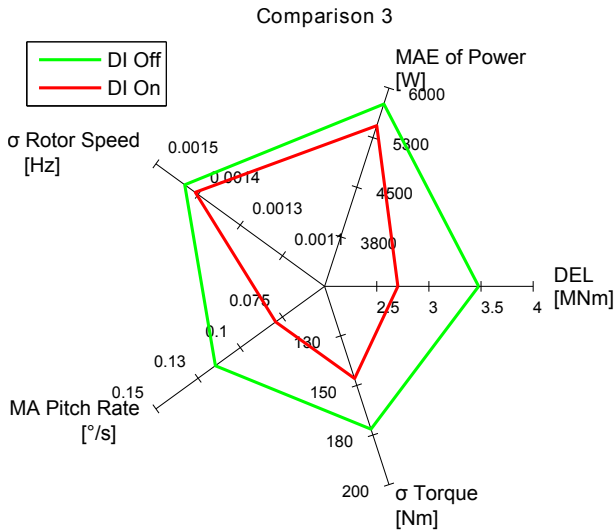
Figure 21.6. Comparison 2 represented in a spider chart.
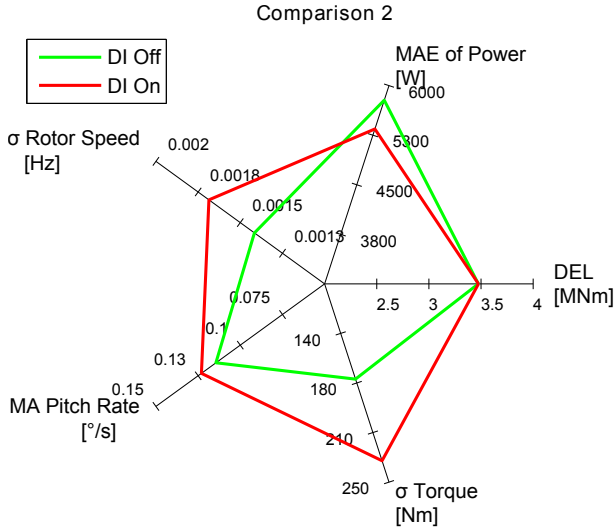
Comparison 2	Improvement [%]
DEL	0
MAE of Power	7.55
σ Rotor Speed	-19.09
MA Pitch Rate	-7.47
σ Torque	-35.94

Table 21.2. Percentwise improvement between DI On and DI Off for comparison 2.

In this comparison the controller with dynamic inflow offers the same level of fatigue as the controller without, but performs 7.5% better on the MAE of the generator power. This comes at the expense of using more pitch and torque. Using the torque more also leads to a higher standard deviation of the rotor speed. The weight used to find controllers with equal DEL is for the controller using dynamic inflow in an area, where only low performance increases on the MAE of the generator power is traded for a high impact on the fatigue on the tower.

Figure 21.7. Comparison 3 represented in a spider chart.

Comparison 3	Improvement [%]
DEL	22.28
MAE of Power	5.68
σ Rotor Speed	2.19
MA Pitch Rate	33.18
σ Torque	14.87

Table 21.3. Percentwise improvement between DI On and DI Off for comparison 3.

For comparison 3 the power weight is set to 7 for both controllers, such that the controllers have identical cost functions. In this comparison the controller using dynamic inflow is an improvement across the board. To visualise this further the transients for comparison 3 is shown in Figure 21.8.
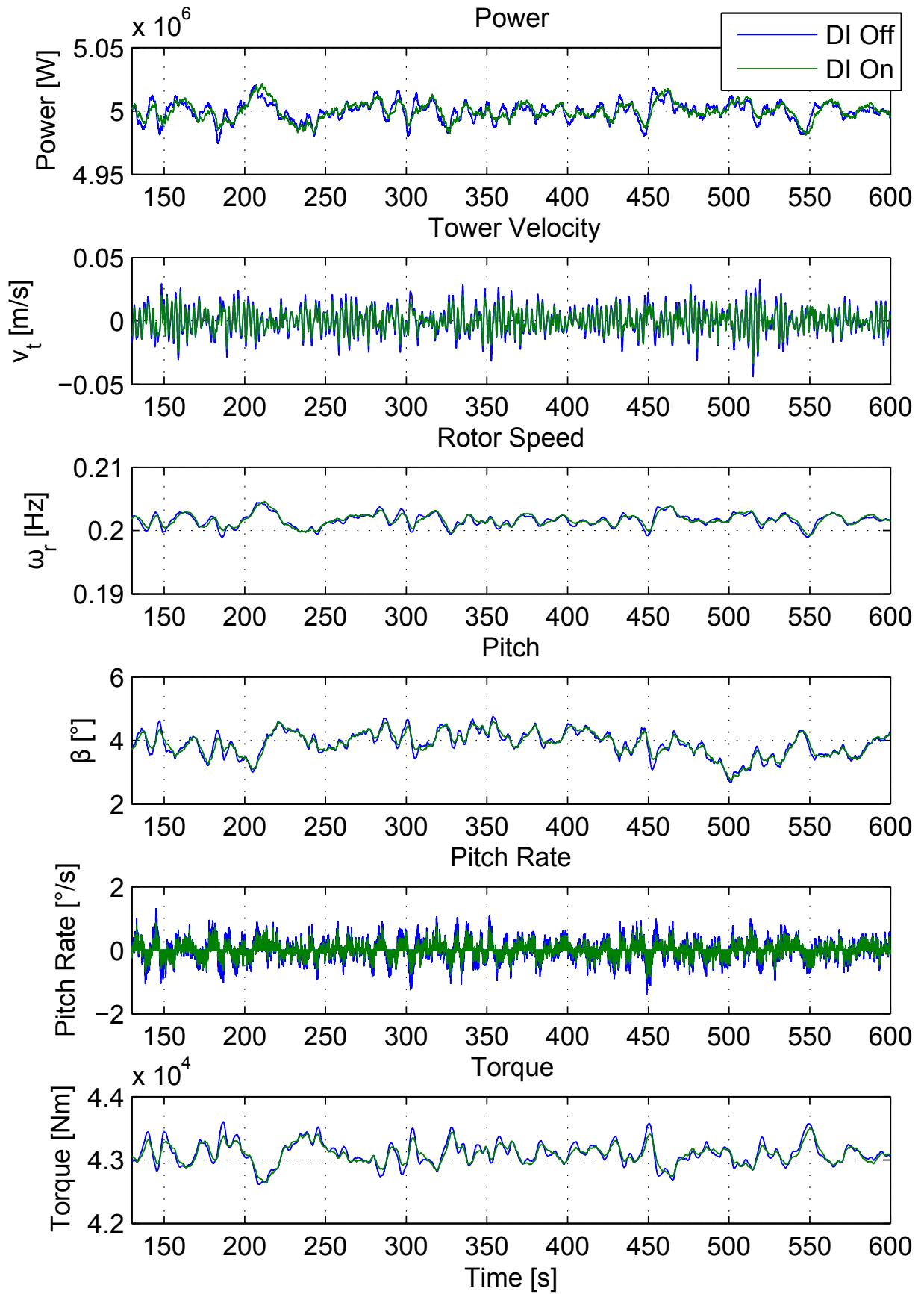
Figure 21.8. The transient response for comparison 3, where both controllers have a power weight of 7.

From Figure 21.8 it can be seen that the power output from the two controllers follows the same pattern. By inspection it can be seen that both controllers behave as expected, e.g. where power errors lead to large, but slow in frequency, changes in pitch and tower velocity errors leads to small, but faster in frequency, pitch changes. The main difference between the controllers is that the MPC, which does not contain DI seem to "overshoot" by applying too much torque and pitch. Going back to the modelling chapter, remembering the difference between the models with and without dynamic inflow in regard to tower velocity, this makes sense. In the comparison of the models the model without dynamic inflow estimated the amplitude of the oscillations lower than they were. In the controller this would lead to a prediction, where more input can be used in controlling to power since lower cost in tower velocity is predicted.

21.2   Use of Pitch

The mean absolute (MA) pitch rate is investigated for both controllers for all the weights as seen in Figure 21.2 and 21.3. The result can be seen in Figure 21.9.
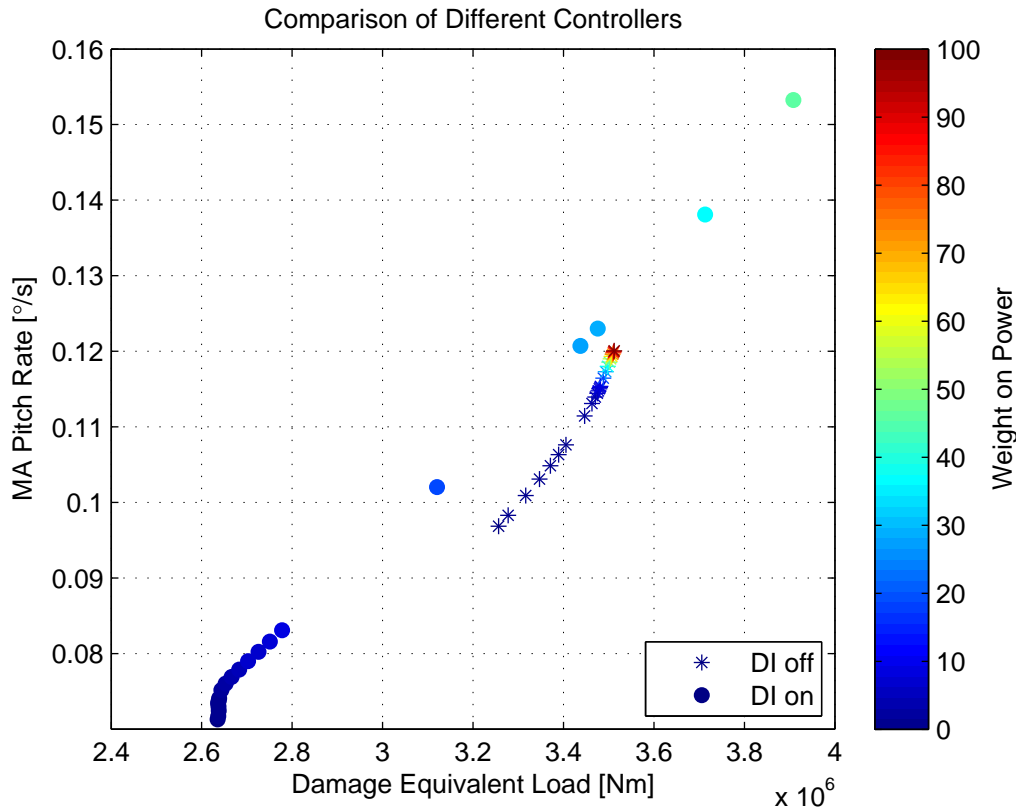

Figure 21.9. A comparison of the mean absolute pitch rate for the tested controllers (both with and without DI).

In Figure 21.9 it can be seen that the MPC setup with DI generally has a lower pitch rate than the counterpart (without DI, but same power weight). It is not until the power weight goes beyond 30 that the MPC with DI overtakes the MPC without DI and one would normally never take such a controller, as the reduction in MAE for high power weights are so small. This result can be due to the fact that the MPC with DI has more information, when predicting the effects of an input, which means that it does a better job in the prediction. When the MPC without

DI has less information to predict the effects, it will produce a less optimal control input than the MPC with DI. In the next iteration it will be fighting the error it has made.

21.3 Wind Seeding

To check that the MPC results are consistent, it will be tested how the MPC is performing with a larger set of wind inputs. The wind inputs will be similar, in the sense that they have the same mean wind, 12 $^m/_s$ and stays within the operating area. When a wind signal is generated in TurbSim, a seeding has to be specified (an initial number for the random number generator). This number is changed to create different wind signals, which can be applied to the wind turbine.

The result of four different wind signals with different seeding applied to the MPC setup can be seen in Figure 21.10 and 21.11. The red line (and associated points) is the data found from the wind signal shown in Figure 21.1.
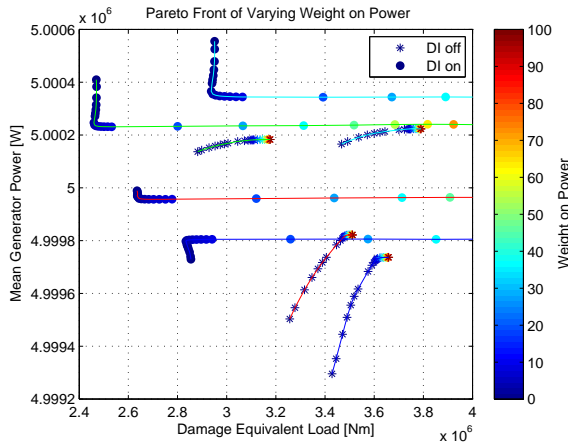

Figure 21.10. Pareto front showing a comparison between the MPCs. The coloured lines between the dots are indicated a similar wind. So e.g. a red line for DI On and DI Off have been subject to the same wind.
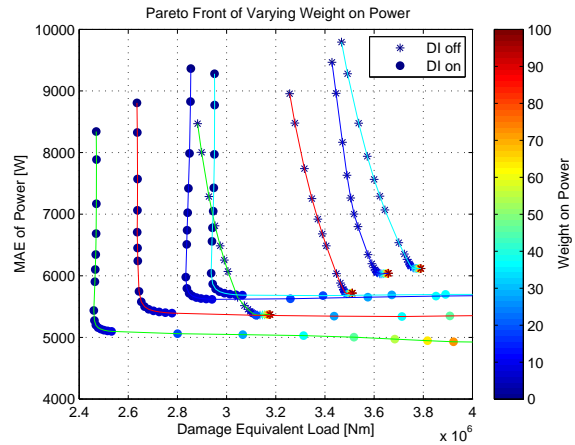
Figure 21.11. Pareto front showing the MAE comparison between the MPCs. The coloured lines between the dots are indicated a similar wind. So e.g. a red line for DI On and DI Off have been subject to the same wind.

In Figure 21.10 and 21.11 it can be seen that MPC where DI is included in all cases is better than its counter part. As earlier the DI On MPC is better both in fatigue and MAE.

21.4 Fatigue Sideways on Tower and on Blades

Since only fatigue on the fore-aft movement on the tower has been investigated and included in the MPC scheme, it is interesting to see if other relevant deflections have increased or decreased at the cost of adding dynamic inflow. To check that the MPC with DI is not introducing any extra fatigue in the system, the fatigue sideways on the tower and on the blades is investigated.

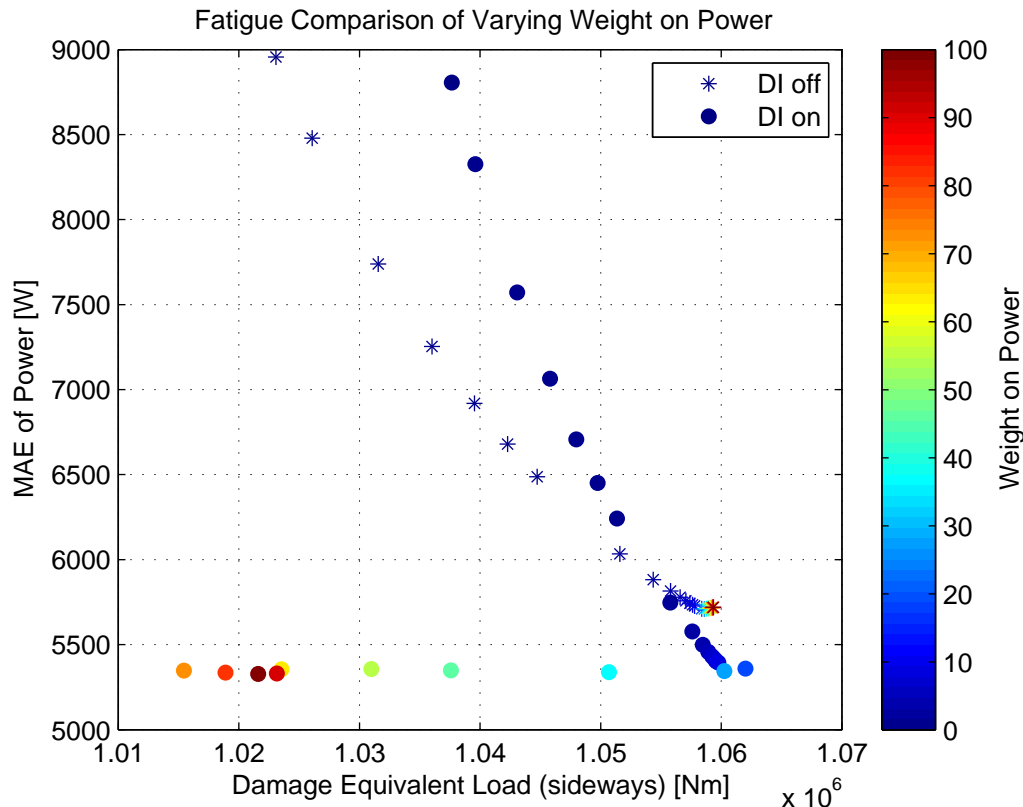The sideways fatigue on the tower plotted with MAE can be seen in Figure 21.12.

Figure 21.12. Pareto front showing the MAE comparison with respect to fatigue in the sideways tower direction.

In Figure 21.12 it can be seen that at lower power weights the DI off MPC is marginally better, than the MPC with DI. When the power weight on the MPC with DI goes above 30, its evaluated fatigue load stops to follow the increasing trend and starts to drop. This is an unexpected phenomenon and no explanation for the behaviour can directly be given. However, as the load is not increasing, further investigation will not be done. Since the change to the DEL is so small it is concluded that the sideways tower fatigue level is not changing significantly between the two controller setups.

To investigate the fatigue levels of the blades, the torque load at the bottom of a blade is analysed. The blades for wind turbines are normally made of a combination of fiberglass and other materials. This makes it hard to get a general Wöhler constant for a blade, as it is very blade specific. A Wöhler constant for fiberglass is therefore used. In [Burton et al., 2001, P. 386] a Wöhler constant of 10.25 is found for fiberglass. It is therefore decided to use 10 as the Wöhler constant, when analysing the fatigue on a blade.

The following numbers are used when analysing the blade:

Blade Direction	L^{Ult} [Nm]	L^{MF} [Nm]	m [-]
Edgewise	7750000	775000	10
Flapwise	83750000	8375000	10

Table 21.4. Constants used in MCrunch blade fatigue analysis.

The mean load and ultimate load is found by looking at the mean load for a simulated run in FAST and then multiplying that with a factor 10 to get the ultimate load, as explained in Chapter 5 on page 14.

The blade fatigue in flapwise and edgewise direction can be seen in Figure 21.13 and 21.14.
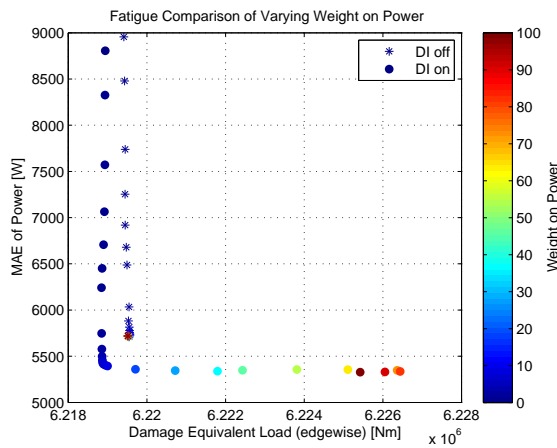

Figure 21.13. Pareto front showing the MAE comparison with respect to fatigue in the blade edgewise direction.
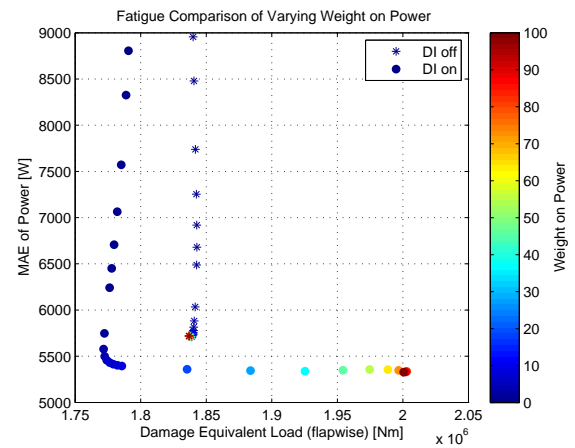
Figure 21.14. Pareto front showing the MAE comparison with respect to fatigue in the blade flapwise direction.

From Figure 21.13 and 21.14 it can be seen that MPC with DI has a lower fatigue level than the MPC without DI both in the edgewise and flapwise direction. The flapwise relative fatigue decrease between the two controllers match that of the tower fatigue, which makes sense since it is mainly the power in the flapwise direction of the blades that leads to the rotor thrust.

21.5 Assessment

The results showed remarkable improvements on the tower fatigue, with relative decrease of the DEL in the 20% range, while still maintaining the same power performance. With such a result, it is very important to highlight the following disclaimers:

- The results were achieved by using one general form of model for the MPC and then adding a simple dynamic inflow model. Another model in the MPC containing more or less DOF, or more advanced physics, may lead to a different result.
- The results were achieved using tuned weights and Kalman filter gain values, which apart from power weights were kept constant. Another tuning may lead to another result.
- The specific wind turbine NREL 5 MW wind turbine with added pitch actuator with dynamics and rate constraint was used in the FAST environment, which uses a General Dynamic Wake model for the inflow. Changing any of these may also lead to a change in the results.

To asses if the results differ by changing some of these items the results gain from the work done in the article [Henriksen et al., 2012b]. In this article another model for the MPC is used derived from Lagrangian mechanics and the added simple model for dynamic inflow is based of local axial induced velocities. Two tunings are made in this work named "MPC1" and "MPC2", for further information about these tunings read [Henriksen et al., 2012b]. Both "MPC1" and "MPC2" are made with and without using dynamic inflow. The wind turbine used is also the NREL 5 MW, but is simulated in HAWC2 instead.

By inspecting the results from this work, especially around wind speed used in this thesis of $12\ ^m/s$, the conclusion is the same as the results from this thesis conclude: By adding dynamic inflow to the MPC scheme tower fatigue can be decreased, while maintaining the same power performance. Furthermore, in these results the blade pitch is also used less in the controller using dynamic inflow.

The size of the relative decrease in tower fatigue, by using dynamic inflow, varies between "MPC1" and "MPC2". The relative improvement in "MPC1" is greater, than seen in this work, while the relative improvement in "MPC2" is less, than in this work.

This leads to the assessment that results found in this project is reasonable for the type of MPC and tuning that is used.

In this chapter a comparison of the two MPC were made. The results show that at the chosen operating area around $12\ ^m/s$, the difference between the controllers are significant. The MPC with dynamic inflow information is able to improve the fatigue by more than 20%, while also improving the MAE of the power about 5%. The following part will go through the results obtained throughout the entire project and what work that is natural to continue with, considering the results that were obtained.

Part V
Epilogue

Conclusion 22

Throughout this thesis the goal has been to answer if, the inclusion of dynamic, is able to improve power generation and/or decrease fatigue of the tower.

In the analysis part the difference between a quasi-static and dynamic inflow model was investigated. It was shown that the dynamic inflow model has an increased gain from pitch to torque and thrust at higher frequencies, while also having a phase change around the critical frequency, see Figure 10.6 on page 47 and 10.8 on page 49. Furthermore, it was shown that this difference had an impact, especially on the tower displacement, see Figure 10.9 on page 50. These findings gave further incentive to investigate, if especially fatigue of the tower could be minimized, by taking dynamic inflow into consideration in a linear model, which can be implemented into an MPC setup.

A nonlinear model, incorporating a simple dynamic inflow model, of the wind turbine was created. Unknown parameters for the model was estimated using PEM in MATLAB. This model was then linearised and compared to a similar model without the dynamic inflow information. The comparison showed a minor improvement in fitting for the linear model with dynamic inflow.

The two developed models were then incorporated into the MPC setup, where first horizons and then weights were tuned. The MPCs were tested on a realistic wind in order to make a comparison. Pareto fronts were made for different power weights, see Figure 21.2 and 21.3 on page 103, where it was shown that the MPC with dynamic inflow can improve the fatigue levels more than 20%, while improving the mean absolute power tracking error with 5%. This was further backed up by running other wind seedings, where it was shown that in all case the fatigue was decreased. The fatigue for the sideways motion of the tower and edgewise and flapwise on the blades were also tested. Regarding sideways motion no deterioration was found, when including dynamic inflow in the MPC. Improvements were seen on both edgewise and flapwise motion.

The answer to the problem statement is that inclusion of the dynamic inflow effect is beneficial both for the power production and fatigue in the tower. The benefit of having knowledge of dynamic inflow in the controller increases the closer the operating area is to rated wind speed due to lower pitch angles, where dynamic inflow is more outspoken. Furthermore, the results obtained indicated that it is possible to decrease the MA pitch rate, while still having the improvement in performance. It is assessed that this improvement is possible, as the MPC with dynamic inflow has a better model to describe the tower movement. This enables the MPC to give a better prediction of the final cost in tower movement by using the pitch actuator, and thereby minimizing any later correction movements.

Perspective 23

As always, there are things that could be improved or tried with a different approach. The things, which the authors would have continued with are here given in a prioritised list and explained following.

- More detailed model of wind turbine dynamics
    - 2nd tower fore-aft deflection mode
    - Blade deflections
- Test using other platforms.
- Broader operating area.

23.1 Wind Turbine Dynamics

As is now, the mass of the rotor and tower is modelled as a lumped mass, which gives rise to an error, when deflecting from the operating point. This can be addressed in several ways.
One way is to add the 2nd tower fore-aft deflection mode to the model. This could be done by dividing the tower into two mass-spring-damper systems. This would distribute the mass of the tower more evenly, which should reduce the error. Another approach could be to model the tower as a multiple hinge model, dividing the tower into even smaller parts.
Furthermore, this could be addressed by modelling the rotor or even each blade as an individual system connected to the tower by a spring and damper. This also opens up for modelling each blade as a flexing system e.g. as a multiple of mass-spring-damper systems. This will take blade deflections into account and should reduce the error caused by the lumped mass.

23.2 Test on Other Platforms

One of the big concerns in this thesis is the accuracy of the simulation tool FAST using GDW for inflow calculations. If this aerodynamics model does not represent the real phenomenon then the results are invalid. A lot of the aerodynamic models used in other works are validated against data from the Tjæreborg 2 MW wind turbine which was published in 1995. Creating new measurement data from a real wind turbine, to have more data to create models from would increase the validity of the used models.

Without new data from a real wind turbine another approach to validate the results could be to test against other simulation tools using other inflow models than GDW and see if the results correspond.

23.3   Broader Operating Area

Now that the inclusion of DI shows significant improvement in performance in the specified operating area, it would off course be interesting to investigate if this has potential in a wider operating area as well. This could entail minimising fatigue in region 2, at higher wind velocities in region 3 or at the switching point between region 2 and 3. When region 2 are in play, the theory from Appendix B on page 126 about calculating a set point with optimal TSR can used for the reference to the MPC.

Widening the operating area also gives rise to a more complex model or several simpler linear models. The latter has the advantage that they all are simpler and linear models often describe the system very well in a narrow operating area. These can be used in MMPC, which uses a bank of several models describing a wide operating area. It then switches between these, as the operating point changes.

Bibliography

Aeolus, **2014**. Aeolus. *About Aeolus*. URL: `http://www.ict-aeolus.eu/about.html` Copy on the cd 💿 Sources/Aeolus.pdf , 2014. Downloaded 03-03-2014.

Ariduru, **December 2004**. S. Ariduru. *Fatigue Life Calculation by Rainflow Cycle Counting Method*, 2004.

ASTM International, **2011**. ASTM International. *Standard Practices for Cycle Counting in Fatigue Analysis*, 2011.

Bayne and Giesselmann, **2000**. S. B. Bayne and M. G. Giesselmann. *Effect of Blade Passing on a Wind Turbine Output*. 2000.

Beddoes, **1983**. T. Beddoes. *Representation of airfoil behaviour*. Vertica, 1983.

Bianchi, Battista, and Mantz, **2007**. F. D. Bianchi, H. D. Battista, and R. J. Mantz. *Wind Turbine Control Systems: Principles, Modelling and Gain Scheduling Design*. ISBN: 1-84628-492-9. Springer, 2007.

Bir and Jonkman, **2007**. G. Bir and J. Jonkman. *Aeroelastic Instabilities of Large Offshore and Onshore Wind Turbines*. 2007.

Bossanyi and Hassan, **2003**. E. A. Bossanyi and G. Hassan. *Individual Blade Pitch Control for Load Reduction*. Wind Energy, 2003.

Burton, Sharpe, Jenkis, and Bossanyi, **2001**. T. Burton, D. Sharpe, N. Jenkis, and E. Bossanyi. *Wind Energy Handbook*. ISBN: 0-471-48997-2. John Wiley & Sons, 2001.

Camacho and Bordons, **1995**. E.F. Camacho and C. Bordons. *Model Predictive Control in the Process Industry*. ISBN: 3-540-19924-1. Springer, 1995.

Danish Standards, **02 2007**. Danish Standards. *Eurocode 3: Stålkonstruktioner – Del 1-9: Udmattelse*, 2. edition, 2007.

Friis, Nielsen, and Bønding, **2010**. J. Friis, E. Nielsen, and J. Bønding. *Repetitive Individual Pitch Model Predictive Control for Horizontal Axis Wind Turbine*, 2010.

GWEC, **2012**. GWEC. *Global Wind Report Annual Market Update 2012*. URL: `http://www.gwec.net/wp-content/uploads/2012/06/Annual_report_2012_LowRes.pdf` Copy on the cd 💿 Sources/Annual_report_2012_LowRes.pdf , 2012. Downloaded 19-02-2014.

Hammerum, **2006**. K. Hammerum. *A Fatigue Approach to Wind Turbine Control*, 2006.

Hayman, **June 2012a**. G. Hayman. *NWTC Design Codes*. URL: `https://wind.nrel.gov/designcodes/postprocessors/mcrunch/`, 2012.

Hayman, **October 2012b**. G. J. Hayman. *MLife Theory Manual for Version 1.00*. NREL, URL: `http://wind.nrel.gov/designcodes/postprocessors/MLife/MLife_Theory.pdf` Copy on the cd 💿 Sources/MLife_Theory.pdf , 2012.

Henriksen, Hansen, and Poulsen, **2012a**. L. C. Henriksen, M. H. Hansen, and N. K. Poulsen. *A simplified dynamic inflow model and its effect on the performance of free mean wind speed estimation*. Wind Energy, 2012.

Henriksen, Hansen, and Poulsen, **2012b**. L. C. Henriksen, M. H. Hansen, and N. K. Poulsen. *Beyond the CP-curve in Model-based Control of Wind Turbines*. 2012.

Holierhoek, Vaal, Zuijlen, and Bijl, **2013**. J.G. Holierhoek, J.B. de Vaal, A.H. van Zuijlen, and H. Bijl. *Comparing different dynamic stall models*. Wind Energy, 2013.

Hwas and Katebi, **2012**. A. Hwas and R. Katebi. *Wind Turbine Control Using PI Pitch Angle Controller*. 2012.

Jafarnejadsani, Pieper, and Ehlers, **2013**. H. Jafarnejadsani, J. Pieper, and J. Ehlers. *Adaptive Control of a Variable-Speed, Variable-Pitch Wind Turbine Using Radial-Basis Function Neural Network*. IEEE TRANSACTIONS ON CONTROL SYSTEMS TECHNOLOGY, 2013.

Johnson, Pao, Balas, and Fingersh, **2006**. K. E. Johnson, L. Y. Pao, M. J. Balas, and L. J. Fingersh. *Control of Variable-Speed Wind Turbines*. 2006.

Jonkman and Buhl Jr., **2005**. J. M. Jonkman and M. L. Buhl Jr. *FAST User's Guide*, 2005.

Jonkman, Butterfield, Musial, and Scott, **2009**. J. M. Jonkman, S. Butterfield, W. Musial, and G. Scott. *Definition of a 5-MW Reference Wind Turbine for Offshore System Development*, National Renewable Energy Laboratory, 2009.

Knudsen and Bak, **2013**. T. Knudsen and T. Bak. *Simple Model for Describing and Estimating Wind Turbine Dynamic Inflow*. pages 640–646, 2013.

Kumar and Stol, **2009**. A. Kumar and K. Stol. *Simulating feedback linearization control of wind turbines using high-order models*. WIND ENERGY, 2009.

Laino and Hansen, **2002**. D. J. Laino and A. C. Hansen. *User's guide Aerodyn*. URL: `http://wind.nrel.gov/designcodes/simulators/aerodyn/AeroDyn.pdf` Copy on the cd 💿 Sources/AeroDyn.pdf , 2002.

Larsen, **2013a**. J. A. Larsen. *Linear Kalman filtering*. Copy on the cd 💿 Sources/JesperLarsenNonlinearControlMM11.pdf , 2013.

Larsen, **2013b**. J. A. Larsen. *Linear Kalman filtering*. Copy on the cd 💿 Sources/JesperLarsenNonlinearControlMM12.pdf , 2013.

Maciejowski, **2002**. J.M. Maciejowski. *Predictive Control with Constraints*. ISBN: 0-201-39823-0. Prentice Hall, 2002.

Mathworks, **2014**. Mathworks. *PEM*. URL: `http://www.mathworks.se/help/ident/ref/pem.html` Copy on the cd 💿 Sources/PEM.pdf , 2014. Downloaded 09-03-2014.

Moriarty and Hansen, **2005**. P.J. Moriarty and A.C. Hansen. *AeroDyn Theory Manual*. URL: `http://www.nrel.gov/docs/fy05osti/36881.pdf` Copy on the cd 💿 Sources/AeroDyn Theory Manual.pdf , 2005.

Odgaard and Larsen, **2014**. P. F. Odgaard and L.F.S Larsen. *Inclusion of Dynamic Inflow in Model Predictive Control of Wind Turbines*. Copy on the cd 💿 Sources/Vestas - MPC Dynamic Inflow.pdf , 2014.

Østergaard, Brath, and J, **2007**. K. Z. Østergaard, P. Brath, and Stoustrup. J. *Estimation of Effective WindSpeed*. 2007.

Øye, **1986**. S. Øye. *Unsteady wake effects caused by pitch-angle changes*. IEA R&D WECS Joint Action on Aerodynamics of Wind Turbines, 1986.

Ragan and Manuel, **2007**. P. Ragan and L. Manuel. *Comparing Estimates of Wind Turbine Fatigue Loads using Time-Domain and Spectral Methods*. WIND ENGINEERING, 2007.

Ragheb and Ragheb, **2011**. M. Ragheb and A. M. Ragheb. *Wind Turbines Theory - The Betz Equation and Optimal Rotor Tip Speed Ratio*. 2011.

RISØ and Miljødata, **1999**. RISØ and Energi og Miljødata. *Average Wind speed in Denmark*. URL: `http://www.emd.dk/files/windres/images/Resmap_100m-5.jpg` Copy on the cd 💿 Sources/Resmap_100m-5.jpg , 1999.

Schmid and Biegler, **1994**. C. Schmid and L. T. Biegler. *Quadratic programming methods for reduced Hessian SQP*. 1994.

Smith, Link, Randall, and McCoy, **2002**. B. Smith, H. Link, G. Randall, and T. McCoy. *Applicability of Nacelle Anemometer Measurements for Use in Turbine Power Performance Tests*. URL: `http://www.nrel.gov/docs/fy02osti/32494.pdf` Copy on the cd 💿 Sources/Applicability of Nacelle Anemometer Measurements for Use in Turbine Power Performance Tests.pdf , 2002. Downloaded 13-03-2014.

Suzuki, **2000**. A. Suzuki. *APPLICATION OF DYNAMIC INFLOW THEORY TO WIND TURBINE ROTORS*, 2000.

The Faculty of Engineering and Science Aalborg University, **2011**. The Faculty of Engineering and Science Aalborg University. *Curriculum for the Master of Science (MSc) in Engineering (Control and Automation)*. URL: `http://www.sict.aau.dk/digitalAssets/36/36175_control_automation_godkendt.pdf` Copy on the cd 💿 Sources/curriculum-control-automation.pdf , 2011.

Engelen and Hooft, **2004**. T.G. van Engelen and E.L. van der Hooft. *Dynamic Inflow Compensation for Pitch Controlled Wind Turbines*. European Wind Energy Conference, 2004.

WeatherQuestions, **2010**. WeatherQuestions. *What is wind shear?* URL: `http://www.weatherquestions.com/What_is_wind_shear.htm` Copy on the cd 💿 Sources/What is wind shear.pdf , 2010. Downloaded 16-02-2014.

Welch and Bishop, **2001**. G. Welch and G. Bishop. *An Introduction to the Kalman Filter*. URL: `http://www.cs.unc.edu/~tracker/media/pdf/SIGGRAPH2001_CoursePack_08.pdf` Copy on the cd 💿 Sources/KalmanIntro.pdf , 2001.

Part VI

Appendix

Table of Contents - Appendix

FAST A

FAST (Fatigue, Aerodynamics, Structures, and Turbulence) is a wind turbine simulator developed by "National Renewable Energy Laboratory" under the "U.S. Department of Energy". FAST is here summarized, for more information read [Jonkman and Buhl Jr., 2005]. FAST consists of three different modules: FAST, AeroDyn and ADAMS. Shortly described FAST contains all the structural models and the tools to runs simulations, AeroDyn does the aerodynamical calculations and ADAMS can be used to extract linearized models and create ADAMS datasets. Figure A.1 visualizes how these elements come together.
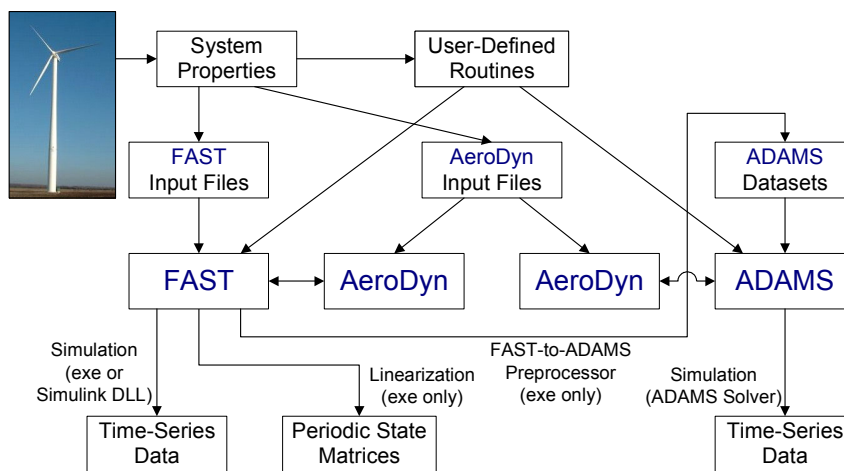

Figure A.1. Illustration of how modules works together in FAST [Jonkman and Buhl Jr., 2005].

The Adams module will not be used in this project. When a simulation is run data is distributed as seen in Figure A.2:
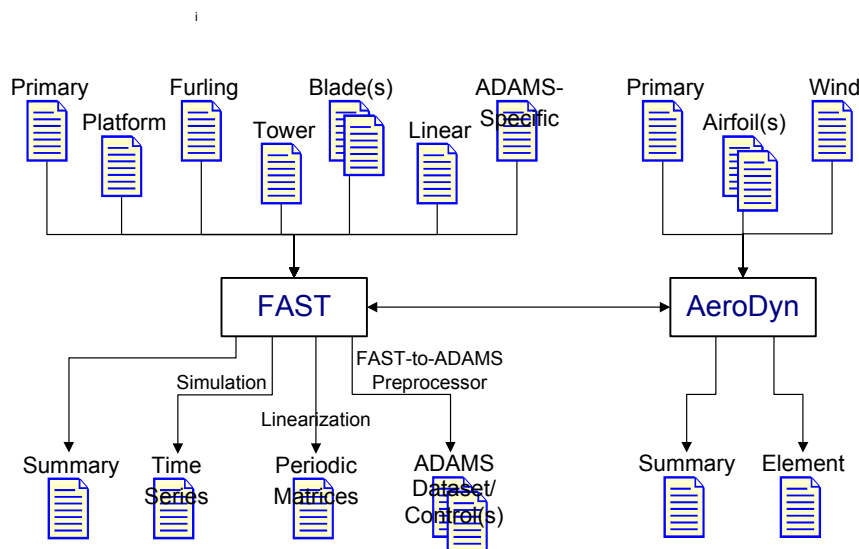
Figure A.2. Illustration of input output relations while a simulation is run [Jonkman and Buhl Jr., 2005].

A.1 FAST

As mentioned FAST does all the structural computations. The FAST model for a 3 bladed HAWT contains nine rigid bodies (earth, support platform, base plate, nacelle, armature, gears, hub, tail, and structure furling with the rotor) and four flexible bodies (tower, two blades, and drive shaft).

An illustration of a standard upwind 3 bladed wind turbine structure and the support platform can be seen on Figure A.3:
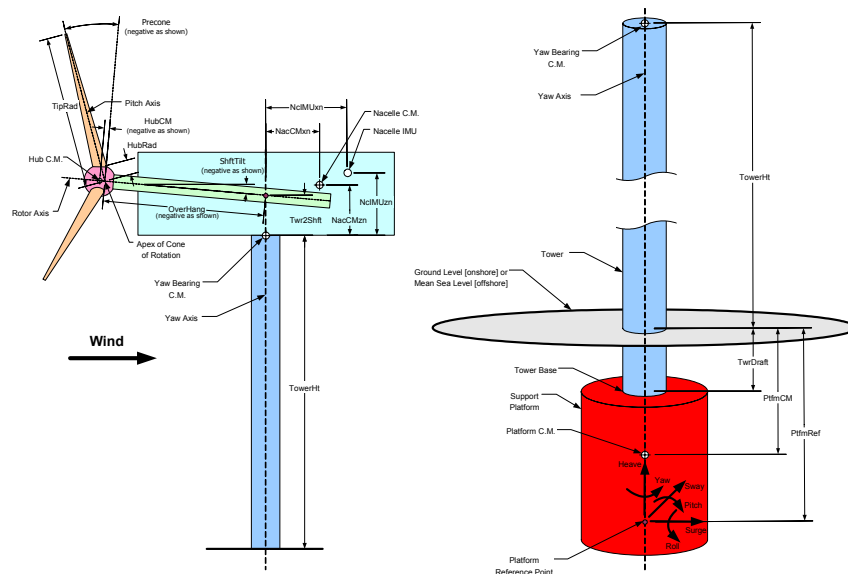
Figure A.3. Wind turbine and the support platform structure [Jonkman and Buhl Jr., 2005].

The model contains 24 DOF:

1-6 The translational (surge, sway and heave) and the rotational (roll, pitch and yaw) motions of the support platform.

6-8 Tower motions, longitudinal and lateral for first mode.

8-10 Tower motions, longitudinal and lateral for second mode.

11 Yawing motion of nacelle.

12 Generator azimuth angle.

13 Compliance in the drivetrain between the rotor and the generator.

13-16 Blade flapwise tip motion for the first mode.

16-19 Blade flapwise tip motion for the second mode.

19-22 Blade edgewise tip displacement.

22-24 Rotor- and tail-furl.

The flexible elements consist of multiple nodes, how these nodes deflect are called modes. As an example two modes for tower motions can be chosen. An illustration of the difference in deflection between two nodes in one plane can be seen in Figure A.4:

Figure A.4. Two different deflection modes [Jonkman and Buhl Jr., 2005].

The DOF can be enabled or disabled depending on need and desired complexity.

A.2   AeroDyn

As seen in Figure A.2 AeroDyn takes in different files to compute the aerodynamics. Each of the files are described here.

The primary file describes alot of the setup parameters such as which inflow model to use, sampling time of the aerodynamical computations, what wind and aerofoil files to use, the density of the air or how much tower shadow effect that is present.
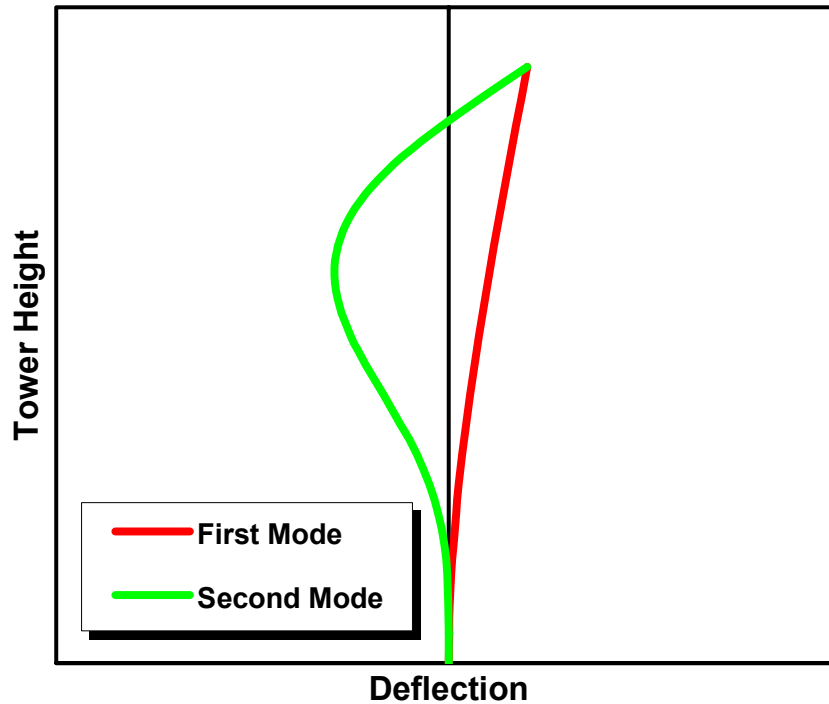
A wind input file describing the wind is used by AeroDyn. This wind file can as an example be a full-field turbulence wind data file. In this file velocities in all three directions for all wind points (fidelity can be adjusted) is contained varying in space and time. A full-field turbulence wind data file can be made with the program TurbSim. A hub-height wind file can also be used as input. The difference between these two wind methods are that in the hub-height-formatted files the wind is stored uniformly across the rotor disk (perhaps with shear), whereas the full-field-formatted files store wind that varies spatially across the rotor disk. In both methods one of the key points is that shear is taken into account and is therefore present in the wind-file. If other phenomenons such as wake from another wind turbine is to be included it is also put into the wind-file. An example of full-field turbulence wind data can be seen in Figure A.5 and A.6.

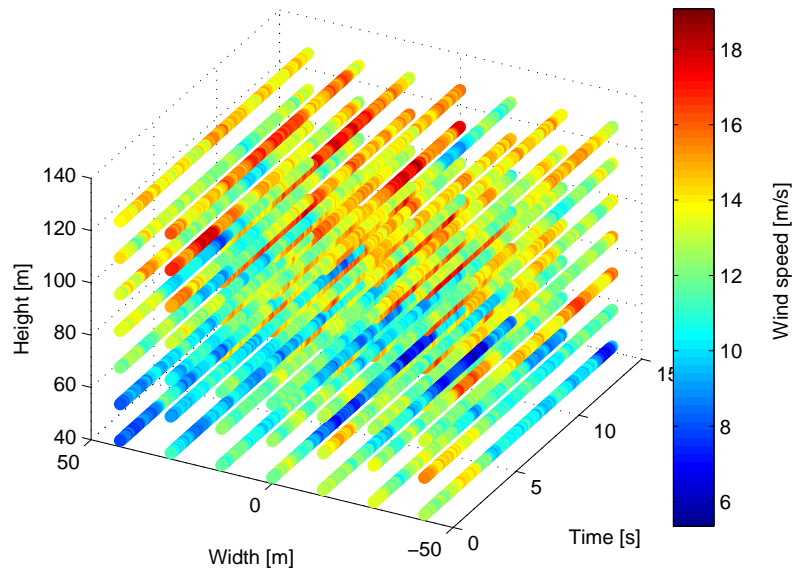**Figure A.5.** Wind data where color represents the resulting speed. Wind shear can be detected since the velocity generally gets faster higher up.
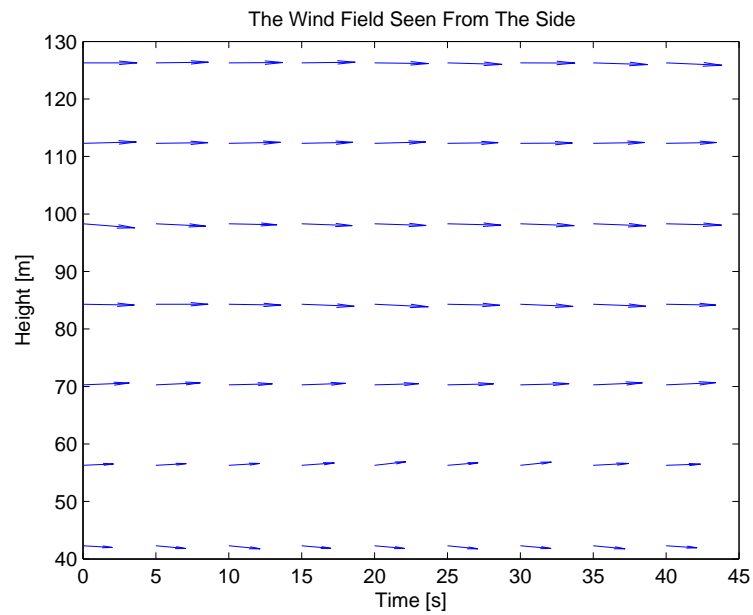

Figure A.6. Velocity of the wind seen from the side. It is noticed that only a little turbulence was added when making this windfile.

The airfoil files describes the aerodynamical properties of the blades.

For more information about AeroDyn read [Laino and Hansen, 2002].

Classic Region 2 Control B

A common way of optimizing energy extraction is addressed in [Johnson et al., 2006] and is here summarized. In this region variable speed is used to ensure optimal power extraction from the wind.

Since region 2 is about optimizing the energy extraction, the pitch of the blades are kept constant at a low pitch angle. The torque on the generator is then controlled to achieve the TSR that optimizes the C_p. This is usually done by using the following control law to calculate the set point for the generator torque:

$$T_g(t) \;=\; K\omega_r^2(t) \tag{B.1}$$

Where: $T_g(t)$ is the torque applied by the generator [Nm].
K denotes the optimal gain $\left[\text{Nms}^2\right]$.

The optimal gain is determined from the optimal TSR:

$$K \;=\; \frac{1}{2}\rho A R^3 \frac{C_{p,max}}{\lambda_{opt}^3} \tag{B.2}$$

Where: A is the area the rotor sweeps $\left[\text{m}^2\right]$.
ρ is the density of the air $\left[\frac{\text{kg}}{\text{m}^3}\right]$.
$C_{p,max}$ is the maximum power coefficient at a given pitch angle [-].
λ_{opt} is the TSR that gives the maximum power coefficient [-].

Next it is shown that this optimal gain indeed controls the rotor speed to the optimal TSR. Using a simple model of a rigid rotor, the change in the angular acceleration can be described, as the difference between aerodynamic and generator torque acting on the combined inertia (omitting gearing):

$$\dot{\omega}_r(t) \;=\; \frac{1}{J}\left(T_a(t) - T_g(t)\right) \tag{B.3}$$

Where: J is the combined inertia of the mechanical system, such as rotor, gears, shaft and the generator $\left[\text{kgm}^2\right]$.
$T_a(t)$ is the aerodynamic torque [Nm].

Now $T_a(t)$ is deduced starting with the expression for rotor power:

$$P_r(t) \;=\; T_a(t)\omega_r(t) \tag{B.4}$$

By inserting (4.2) into it and solving for T_a it becomes:

$$T_a(t) = \frac{C_p(\lambda(t), \beta(t)) P_w(t)}{\omega_r(t)} \tag{B.5}$$

The wind power can be calculated as:

$$P_w(t) = \frac{1}{2} \rho A v_w^3(t) \tag{B.6}$$

By inserting the expression for the wind power and (4.3) into (B.5):

$$T_a(t) = \frac{1}{2} \rho A R \frac{C_p(\lambda(t), \beta(t))}{\lambda(t)} v_w^2(t) \tag{B.7}$$

Now by inserting (B.7) and (B.1) with (B.2) into (B.3) the following can be obtained:

$$\dot{\omega}_r(t) = \frac{1}{2J} \rho A R^3 \omega_r^2(t) \left(\frac{C_p(\lambda(t), \beta(t))}{\lambda^3(t)} - \frac{C_{p,max}}{\lambda_{opt}^3} \right) \tag{B.8}$$

The last term is denoted F:

$$F = \frac{C_{p,max}}{\lambda_{opt}^3} \tag{B.9}$$

Since the other parameter are all positive, the sign of the acceleration is determined from the difference of the terms in the parentheses. When $\lambda(t) > \lambda_{opt}$ the acceleration will always be negative due to the following always being true $C_p(\lambda(t), \beta(t)) \leq C_{p,max}$. When $\lambda(t) < \lambda_{opt}$ the acceleration will be positive if the following holds true:

$$C_p(\lambda(t), \beta(t)) > F \lambda^3(t) \tag{B.10}$$

$$> \frac{C_{p,max}}{\lambda_{opt}^3} \lambda^3(t) \tag{B.11}$$

This means that $\lambda(t)$ will go towards λ_{opt} except for the situation where $\lambda(t) < \lambda_{opt}$ and the inequality (B.11) is false. This can be illustrated by plotting (B.11) as seen in Figure B.1.
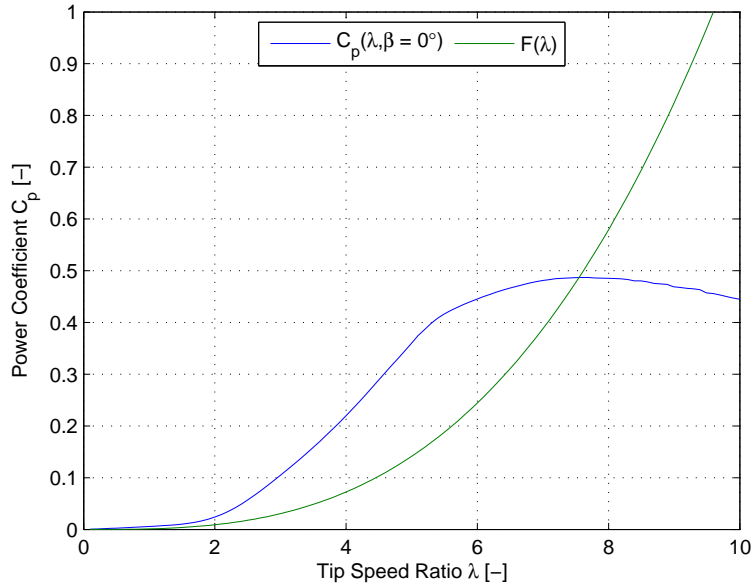
Figure B.1. $C_p(\lambda(t), \beta(t))$ as a function of TSR at a constant pitch retrieved from the NREL 5 MW plotted with (B.11).

The figure should be read in the way that whenever $\lambda(t) < \lambda_{opt}$ and the $C_p(\lambda(t), \beta(t))$ plot value is higher than $F(\lambda)$ then the rotor accelerates. Whenever $\lambda(t) > \lambda_{opt}$ and the C_p plot value is lower than $F(\lambda)$, then the rotor decelerates. In Figure B.1 this is always true, such that $\lambda(t)$ always converges to λ_{opt}. Having another $C_p(\lambda(t), \beta(t))$ characteristic could create an area where $\lambda(t)$ diverges as seen in Figure B.2.
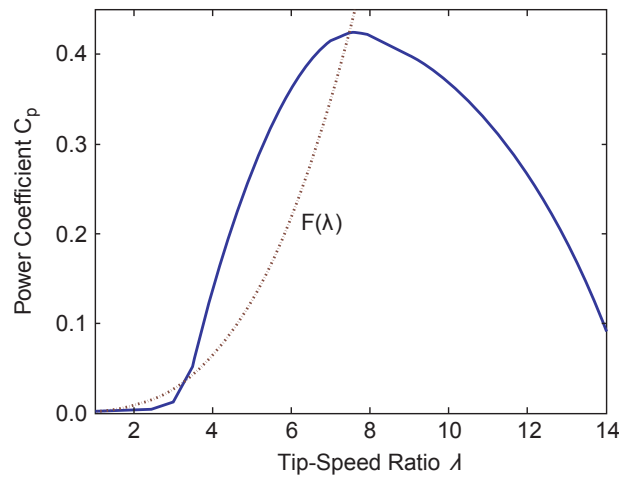
Figure B.2. $C_p(\lambda(t), \beta(t))$ as a function of TSR at a constant pitch plotted with [Johnson et al., 2006].

Here it can be seen that at a TSR below 3.3, the rotor would decelerate the rotor to a stop. Separate control mechanisms are put in place to prohibit this behaviour.

128

Rainflow Counting C

The algorithm for rainflow counting is described in [ASTM International, 2011] and is here described in the flow diagram in Figure C.1. The algorithm is started at the first point in the dataset. This point is at the start denoted S. X is defined as the present range. Y denotes the previous range.
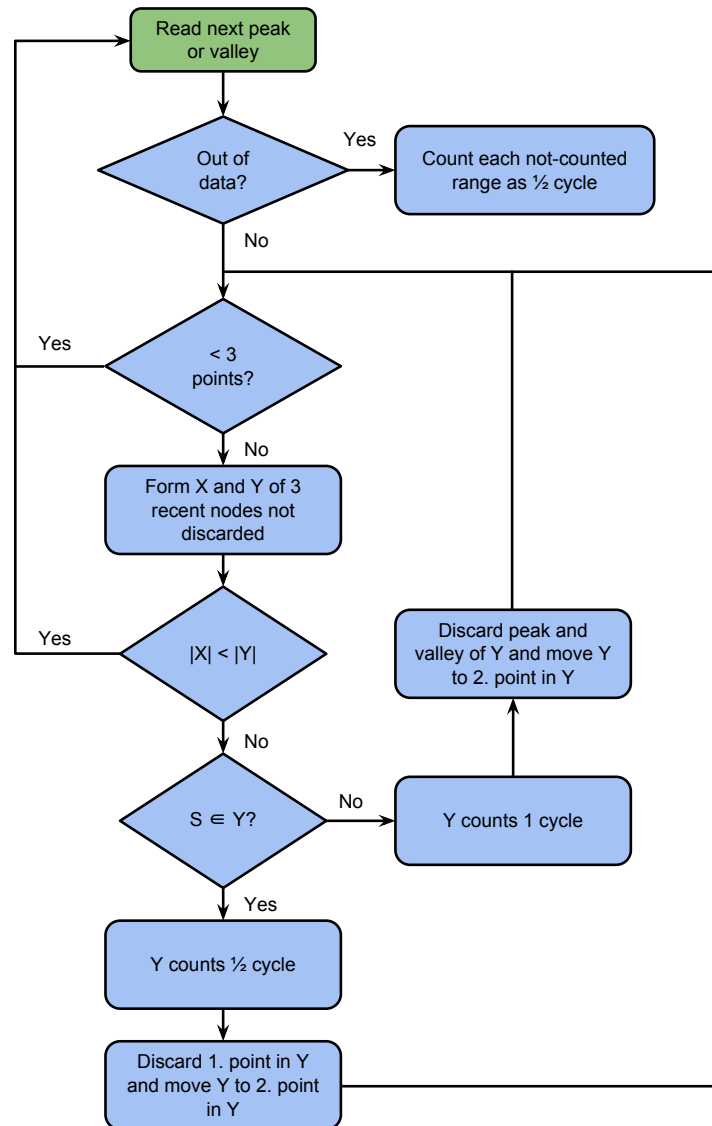
Figure C.1. The rainflow algorithm is here depicted in a flowchart. Start at the top node (green).
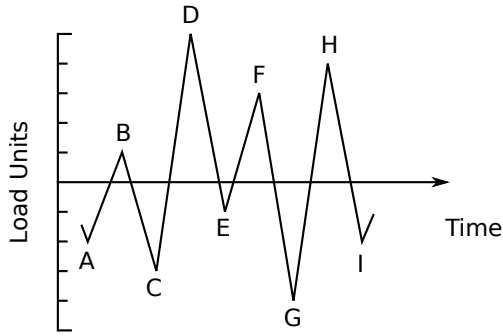
Figure C.2. Example of time series measurement of a load causing fatigue [ASTM International, 2011].

Range	Cycle Counts	Events
10	0	
9	0.5	D-G
8	1	C-D, G-H
7	0	
6	0.5	H-I
5	0	
4	1.5	B-C, E-F
3	0.5	A-B
2	0	
1	0	

Table C.1. Rainflow count results from the load time series in Figure C.2 [ASTM International, 2011].

The algorithm produces a cycle count at the different amplitude ranges. The result can be expressed by showing the counts in an amplitude-mean plot as seen in Figure C.3, where the mean is taken on the start- and end value of a cycle. Figure C.3 is generated with MCrunch [Hayman, 2012a], which is a widely recognised set of tools for fatigue analysis.
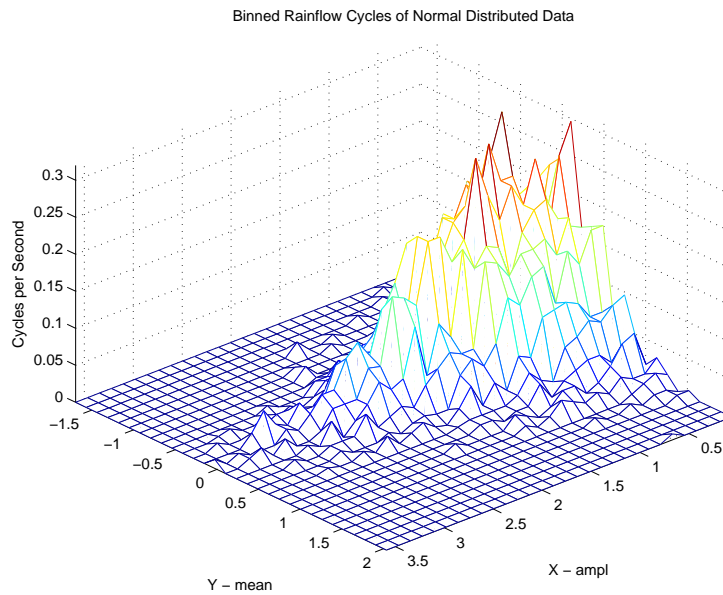
Figure C.3. Example of rainflow count produced by the implementation generated with MCrunch [Hayman, 2012a].

Fatigue Calculation D

Often a damage equivalent load (DEL) is used, when evaluating the damage. The DEL is a measure of a constant-amplitude fatigue load, which comes at fixed load-mean and frequency [Hayman, 2012b]. This results in an equivalent damage to a varying frequency and amplitude of the loads. This means that the varying cycles are converted into equivalents, where following is true:

$$\sum_i \frac{n_i}{N_i} = \frac{n^{\mathrm{STeq}}}{N^{\mathrm{eq}}} \tag{D.1}$$

Where: n_i is the damage count for cycle i.
N_i denotes the number of cycles until failure for the load range of cycle i.
n^{STeq} is the equivalent cycle counts.
N^{eq} denotes the number of equivalent cycles to failure.

N_i is given by:

$$N_i = \left(\frac{L^{\mathrm{Ult}} - |L^{\mathrm{MF}}|}{\frac{1}{2} L_i^{\mathrm{RF}}} \right)^m \tag{D.2}$$

Where: L^{Ult} is the ultimate load.
L^{MF} denotes the mean load.
m is the Wöhler constant.
L_i^{RF} denotes the Goodman-corrected load range about a fixed-mean for cycle i.

The Goodman-correction is given by (D.3) and ensures that the fatigue cycle load ranges are represented as if they occured around a fixed mean load.

$$L_i^{\mathrm{RF}} = L_i^{\mathrm{R}} \left(\frac{L^{\mathrm{Ult}} - |L^{\mathrm{MF}}|}{L^{\mathrm{Ult}} - |L_i^{\mathrm{M}}|} \right)^m \tag{D.3}$$

Where: L_i^{R} denotes the load range for cycle i.
L_i^{M} is the mean load of cycle i.

Now N^{eq} is calculated as:

$$N^{eq} = \left(\frac{L^{\mathrm{Ult}} - |L^{\mathrm{MF}}|}{\frac{1}{2} DEL^{\mathrm{STF}}} \right)^m \tag{D.4}$$

Where: DEL^{STF} denotes the Goodman-corrected short-term damage equivalent load.

Combining Equation (D.1), (D.2) and (D.4) and solving for DEL^{STF} gives:

$$DEL^{\mathrm{STF}} = \left(\frac{\sum_i \left(n_i \left(L_i^{\mathrm{RF}} \right)^m \right)}{n^{\mathrm{STeq}}} \right)^{1/m} \tag{D.5}$$

Again, this gives an equivalent damage to a varying frequency and amplitude of the loads. Now Equation (D.4) forms an S-N curve, which tells how many cycles with S_x amplitude at a certain mean load the system can tolerate before failure (Example in Figure D.1).
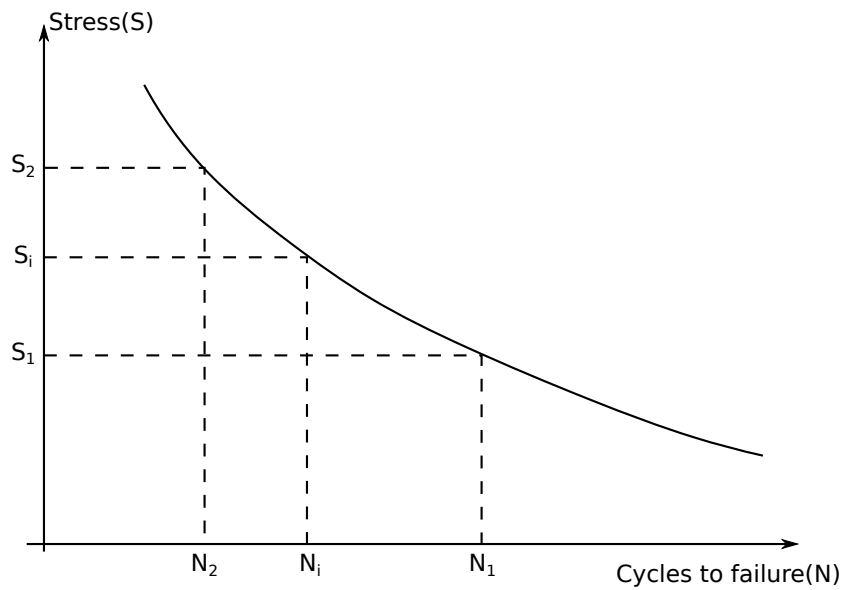
Figure D.1. The S-N curve shows the relation between a stress at a certain mean load and how many cycles before failure. These are usually based on constant amplitude tests [Ariduru, 2004].

Linearisation E

This appendix will show the partial derivatives found for the linearised wind turbine models from Chapter 15 on page 65.

E.1 Linearisation Procedure

The derivatives of the nonlinear model, can be described through a set of equations described in Chapter 13 on page 54, from here called f(x,u).
The nonlinear model can be described as:

$$\dot{x} = f(x,u) \tag{E.1}$$

$$y = h(x,u) \tag{E.2}$$

To make the linear model the partial derivatives the following procedure is done for $\dot{x}$:

$$\dot{x} \approx \frac{\partial f}{\partial x^T}(x - \bar{x}) + \frac{\partial f}{\partial u^T}(u - \bar{u}) + f(\bar{x}, \bar{u}) \tag{E.3}$$

The linearisation is done at a state state point, meaning $f(\bar{x}, \bar{u}) = 0$. When a variable is indicated with a bar on top, it means it is evaluated to the value at the steady state point.

The output of the linear model will be linearised as:

$$y \approx h(\bar{x}, \bar{u}) + \frac{\partial h}{\partial x^T}(x - \bar{x}) + \frac{\partial h}{\partial u^T}(u - \bar{u}) \tag{E.4}$$

To simplify the derivation process, it is initially assumed that the tower velocity is not substituted from the incoming wind, see explanation before (E.42a). When the partial derivatives have been found, the subtraction of the tower velocity is included again.

Only the derivatives that do not equal zero will be presented.

E.2 Linear Model With Dynamic Inflow

The derivatives are as follows:

$$f_1(x,u) = \dot{a}_f = \frac{1}{\tau_{DI}(v_w)}(a_s - a_f) \tag{E.5}$$

$$\frac{\partial \dot{a}_f}{\partial a_f} = -\frac{1}{\tau_{DI}(\bar{v}_w)} \tag{E.6}$$

$$\frac{\partial \dot{a}_f}{\partial \omega_r} = \frac{1}{\tau_{DI}(\bar{v}_w)}\frac{\partial a_s}{\partial \omega_r} \tag{E.7}$$

$$\frac{\partial a_s}{\partial \omega_r} = \frac{1}{4}\frac{1}{\sqrt{1 - C_t\left(\bar{\lambda}, \bar{\beta}\right)}}\frac{\partial C_t\left(\lambda, \bar{\beta}\right)}{\partial \omega_r} \tag{E.8}$$

$$\frac{\partial C_t\left(\lambda, \bar{\beta}\right)}{\partial \omega_r} = \frac{\partial C_t\left(\lambda, \bar{\beta}\right)}{\partial \lambda}\frac{\partial \lambda}{\partial \omega_r} \tag{E.9}$$

$$\frac{\partial \lambda}{\partial \omega_r} = \frac{R}{\bar{v}_a} \tag{E.10}$$

$$\frac{\partial \dot{a}_f}{\partial \beta} = \frac{1}{\tau_{DI}(\bar{v}_w)}\frac{\partial a_s}{\partial \beta} \tag{E.11}$$

$$\frac{\partial a_s}{\partial \beta} = \frac{1}{4}\frac{1}{\sqrt{1 - C_t\left(\bar{\lambda}, \bar{\beta}\right)}}\frac{\partial C_t(\bar{\lambda}, \beta)}{\partial \beta} \tag{E.12}$$

$$\frac{\partial \dot{a}_f}{\partial v_w} = \frac{2}{3D}\frac{\partial a_s}{\partial v_w} \tag{E.13}$$

$$\frac{\partial a_s}{\partial v_w} = \frac{1}{4}\frac{1}{\sqrt{1 - C_t\left(\bar{\lambda}, \bar{\beta}\right)}}\frac{\partial C_t\left(\lambda, \bar{\beta}\right)}{\partial v_w} \tag{E.14}$$

$$\frac{\partial C_t\left(\lambda, \bar{\beta}\right)}{\partial v_w} = \frac{\partial C_t\left(\lambda, \bar{\beta}\right)}{\partial \lambda}\frac{\partial \lambda}{\partial v_w} \tag{E.15}$$

$$\frac{\partial \lambda}{\partial v_w} = -\frac{\bar{\omega}_r R}{\bar{v}_w^2} \tag{E.16}$$

$$f_2(x,u) = \dot{\omega}_r = \frac{T_a - NT_g}{J}, \quad T_a = \frac{1}{2\omega_r}\rho v_f^3 A C_p\left(\lambda, \beta\right) \tag{E.17}$$

$$\frac{\partial T_a}{\partial a_f} = \frac{1}{2\bar{\omega}_r}\rho A 3\bar{v}_f^2 \frac{\partial v_f}{\partial a_f}C_p\left(\bar{\lambda}, \bar{\beta}\right) \tag{E.18}$$

$$\frac{\partial v_f}{\partial a_f} = -\frac{\bar{v}_w}{1 - \bar{a}_s} \tag{E.19}$$

$$\frac{\partial T_a}{\partial \omega_r} = -\frac{1}{2\bar{\omega}_r^2}\rho A \bar{v}_f^3 C_p\left(\bar{\lambda}, \bar{\beta}\right) + \frac{1}{2\bar{\omega}_r}\rho A 3\bar{v}_f^2 \frac{\partial v_f}{\partial \omega_r}C_p\left(\bar{\lambda}, \bar{\beta}\right)$$
$$+\frac{1}{2\bar{\omega}_r}\rho A \bar{v}_f^3 \frac{\partial C_p\left(\lambda, \bar{\beta}\right)}{\partial \lambda}\frac{\partial \lambda}{\partial \omega_r} \tag{E.20}$$

$$\frac{\partial T_a}{\partial \beta} = \frac{1}{2\bar{\omega}_r}\rho A 3\bar{v}_f^2 \frac{\partial v_f}{\partial \beta}C_p\left(\bar{\lambda}, \bar{\beta}\right) + \frac{1}{2\bar{\omega}_r}\rho A \bar{v}_f^3 \frac{\partial C_p\left(\bar{\lambda}, \beta\right)}{\partial \beta} \tag{E.21}$$

$$\frac{\partial v_f}{\partial \beta} = \bar{v}_w \frac{1 - \bar{a}_f}{(1 - \bar{a}_s)^2} \frac{\partial a_s}{\partial \beta} \tag{E.22}$$

$$\frac{\partial T_a}{\partial v_w} = \frac{1}{2\omega_r} \rho A 3 \frac{\partial v_f}{\partial v_w} v_f^2 C_p \left(\bar{\lambda}, \bar{\beta}\right) + \frac{1}{2\omega_r} \rho A v_f^3 \frac{\partial C_p \left(\lambda, \bar{\beta}\right)}{\partial \lambda} \frac{\partial \lambda}{\partial v_w} \tag{E.23}$$

$$\frac{\partial v_f}{\partial v_w} = \frac{1 - \bar{a}_f}{1 - \bar{a}_s} + v_w \frac{1 - \bar{a}_f}{(1 - \bar{a}_s)^2} \frac{\partial a_s}{\partial v_w} \tag{E.24}$$

$$f_3(x, u) = \dot{d}_t = v_t \tag{E.25}$$

$$f_4(x, u) = \dot{v}_t = \frac{F_t - K_t d_t - B_t v_t}{M_t}, \quad F_t = \frac{1}{2}\rho v_f^2 A C_t (\lambda, \beta) \tag{E.26}$$

$$\frac{\partial F_t}{\partial a_f} = \frac{1}{2}\rho A 2 \frac{\partial v_f}{\partial a_f} v_f C_t \left(\lambda, \bar{\beta}\right) \tag{E.27}$$

$$\frac{\partial F_t}{\partial \omega_r} = \frac{1}{2}\rho A 2 \frac{\partial v_f}{\partial \omega_r} \bar{v}_f C_t \left(\bar{\lambda}, \bar{\beta}\right) + \frac{1}{2}\rho A 2 \bar{v}_f^2 \frac{\partial C_t \left(\lambda, \bar{\beta}\right)}{\partial \lambda} \frac{\partial \lambda}{\partial \omega_r} \tag{E.28}$$

$$\frac{\partial F_t}{\partial \beta} = \frac{1}{2}\rho A 2 \frac{\partial v_f}{\partial \beta} \bar{v}_f C_t \left(\bar{\lambda}, \bar{\beta}\right) + \frac{1}{2}\rho A 2 \bar{v}_f^2 \frac{\partial C_t \left(\bar{\lambda}, \beta\right)}{\partial \beta} \tag{E.29}$$

$$\frac{\partial F_t}{\partial v_w} = \frac{1}{2}\rho A 2 \frac{\partial v_f}{\partial v_w} \bar{v}_f C_t \left(\bar{\lambda}, \bar{\beta}\right) + \frac{1}{2}\rho A 2 \bar{v}_f^2 \frac{\partial C_t \left(\lambda, \bar{\beta}\right)}{\partial \lambda} \frac{\partial \lambda}{\partial v_w} \tag{E.30}$$

$$f_5(x, u) = \dot{\beta} = \frac{1}{\tau_p}\beta_{ref} - \frac{1}{\tau_p}\beta \tag{E.31}$$

$$\frac{\partial \dot{\beta}}{\partial \beta_{ref}} = \frac{1}{\tau_p} \tag{E.32}$$

$$\frac{\partial \dot{\beta}}{\partial \beta} = -\frac{1}{\tau_p} \tag{E.33}$$

$$f_6(x, u) = \dot{T}_g = \frac{1}{\tau_g}T_{g,ref} - \frac{1}{\tau_g}T_g \tag{E.34}$$

$$\frac{\partial \dot{T}_g}{\partial T_{g,ref}} = \frac{1}{\tau_g} \tag{E.35}$$

$$\frac{\partial \dot{T}_g}{\partial T_g} = -\frac{1}{\tau_g} \tag{E.36}$$

$$h_1(x, u) = P_g = N\omega_r T_g \tag{E.37}$$

$$\frac{\partial P_g}{\partial \omega_r} = N\bar{T}_g \tag{E.38}$$

$$\frac{\partial P_g}{\partial T_g} = N\bar{\omega}_r \tag{E.39}$$

$$h_2(x, u) = v_t \tag{E.40}$$

$$h_3(x, u) = \omega_r \tag{E.41}$$

The wind speed hiting the rotors are $v_a = v_w - v_t$. To include the tower velocity into the state space model, the partial derivatives for the incoming wind speed v_w is used with a change in sign in the forth column in the A matrix.

The state space representation therefore becomes:

$$
\begin{bmatrix} \dot{a}_f^\Delta \\ \omega_r^\Delta \\ d_t^\Delta \\ v_t^\Delta \\ \beta^\Delta \\ T_g^\Delta \end{bmatrix} =
\begin{bmatrix}
-\frac{1}{\bar{\tau}_{DI}(v_w)} & \frac{\partial \dot{a}_f}{\partial \omega_r} & 0 & -\frac{\partial \dot{a}_f}{\partial v_w} & \frac{\partial \dot{a}_f}{\partial \beta} & 0 \\
\frac{1}{J}\frac{\partial T_a}{\partial a_f} & \frac{1}{J}\frac{\partial T_a}{\partial \omega_r} & 0 & -\frac{1}{J}\frac{\partial T_a}{\partial v_w} & \frac{1}{J}\frac{\partial T_a}{\partial \beta} & \frac{-N}{J} \\
0 & 0 & 1 & 0 & 0 & 0 \\
\frac{1}{M_t}\frac{\partial F_t}{\partial a_f} & \frac{1}{M_t}\frac{\partial F_t}{\partial \omega_r} & -\frac{K_t}{M_t} & \frac{1}{M_t}\left(-B_t - \frac{\partial F_t}{\partial v_w}\right) & \frac{1}{M_t}\frac{\partial F_t}{\partial \beta} & 0 \\
0 & 0 & 0 & 0 & -\frac{1}{\tau_p} & 0 \\
0 & 0 & 0 & 0 & 0 & -\frac{1}{\tau_g}
\end{bmatrix}
\begin{bmatrix} a_f^\Delta \\ \omega_r^\Delta \\ d_t^\Delta \\ v_t^\Delta \\ \beta^\Delta \\ T_g^\Delta \end{bmatrix}
$$

$$
+
\begin{bmatrix}
0 & 0 & \frac{\partial \dot{a}_f}{\partial v_w} \\
0 & 0 & \frac{1}{J}\frac{\partial T_a}{\partial v_w} \\
0 & 0 & 0 \\
0 & 0 & \frac{1}{M_t}\frac{\partial F_t}{\partial v_w} \\
0 & \frac{1}{\tau_p} & 0 \\
\frac{1}{\tau_g} & & 0
\end{bmatrix}
\begin{bmatrix} T_{g,ref}^\Delta \\ \beta_{ref}^\Delta \\ v_w^\Delta \end{bmatrix}
\tag{E.42a}
$$

$$
\begin{bmatrix} P \\ v_t \\ \omega_r \end{bmatrix} =
\begin{bmatrix} \bar{P} \\ \bar{v}_t \\ \bar{\omega}_r \end{bmatrix} +
\begin{bmatrix}
0 & \frac{\partial P_g}{\partial \omega_r} & 0 & 0 & 0 & \frac{\partial P_g}{\partial T_g} \\
0 & 0 & 0 & 1 & 0 & 0 \\
0 & 1 & 0 & 0 & 0 & 0
\end{bmatrix}
\begin{bmatrix} a_f^\Delta \\ \omega_r^\Delta \\ d_t^\Delta \\ v_t^\Delta \\ \beta^\Delta \\ T_g^\Delta \end{bmatrix} + 0
\begin{bmatrix} T_{g,ref}^\Delta \\ \beta_{ref}^\Delta \\ v_w^\Delta \end{bmatrix}
\tag{E.42b}
$$

E.3 Linear Model Without Dynamic Inflow

The same procedure is applied to this linearisation.

$$f_1(x, u) = \dot{\omega}_r = \frac{T_a - NT_g}{J}, \quad T_a = \frac{1}{2\omega_r}\rho v_w^3 A C_p\left(\lambda, \beta\right) \tag{E.43}$$

$$\frac{\partial T_a}{\partial \omega_r} = -\frac{1}{2\bar{\omega}_r^2}\rho\bar{v}_w^3 A C_p\left(\bar{\lambda}, \bar{\beta}\right) + \frac{1}{2\bar{\omega}_r}\rho\bar{v}_w^3 A\frac{\partial C_p\left(\lambda, \bar{\beta}\right)}{\partial\lambda}\frac{\partial\lambda}{\partial\omega_r} \tag{E.44}$$

$$\frac{\partial T_a}{\partial \beta} = \frac{1}{2\bar{\omega}_r}\rho\bar{v}_w^3 A\frac{\partial C_p\left(\bar{\lambda}, \beta\right)}{\partial\beta} \tag{E.45}$$

$$\frac{\partial T_a}{\partial v_w} = \frac{1}{2\bar{\omega}_r}\rho 3\bar{v}_w^2 A C_p\left(\lambda, \beta\right) - \frac{1}{2\bar{\omega}_r}\rho\bar{v}_w^3 A\frac{\partial C_p\left(\lambda, \bar{\beta}\right)}{\partial\lambda}\frac{\partial\lambda}{\partial v_w} \tag{E.46}$$

$$f_2(x, u) = \dot{d}_t = v_t \tag{E.47}$$

$$f_3(x, u) = \dot{v}_t = \frac{F_t - K_t d_t - B_t v_t}{M_t}, \quad F_t = \frac{1}{2}\rho v_w^2 A C_t\left(\lambda, \beta\right) \tag{E.48}$$

$$\frac{\partial F_t}{\partial \omega_r} = \frac{1}{2}\rho\bar{v}_w^2 A\frac{\partial C_t\left(\lambda, \bar{\beta}\right)}{\partial\lambda}\frac{\partial\lambda}{\partial\omega_r} \tag{E.49}$$

$$\frac{\partial F_t}{\partial \beta} = \frac{1}{2}\rho\bar{v}_w^2 A\frac{\partial C_t\left(\bar{\lambda}, \beta\right)}{\partial\beta} \tag{E.50}$$

$$\frac{\partial F_t}{\partial v_w} = \frac{1}{2}\rho 2\bar{v}_w A C_t\left(\lambda, \bar{\beta}\right) - \frac{1}{2}\rho\bar{v}_w^2 A\frac{\partial C_t\left(\lambda, \bar{\beta}\right)}{\partial\lambda}\frac{\partial\lambda}{\partial v_w} \tag{E.51}$$

$$f_4(x, u) = \dot{\beta} = \frac{1}{\tau_p}\beta_{ref} - \frac{1}{\tau_p}\beta \tag{E.52}$$

$$\frac{\partial\dot{\beta}}{\partial\beta_{ref}} = \frac{1}{\tau_p} \tag{E.53}$$

$$\frac{\partial\dot{\beta}}{\partial\beta} = -\frac{1}{\tau_p} \tag{E.54}$$

$$f_5(x, u) = \dot{T}_g = \frac{1}{\tau_g}T_{g,ref} - \frac{1}{\tau_g}T_g \tag{E.55}$$

$$\frac{\partial\dot{T}_g}{\partial T_{g,ref}} = \frac{1}{\tau_g} \tag{E.56}$$

$$\frac{\partial\dot{T}_g}{\partial T_g} = -\frac{1}{\tau_g} \tag{E.57}$$

$$h_1(x, u) = P_g = N\omega_r T_g \tag{E.58}$$

$$\frac{\partial P_g}{\partial \omega_r} = N\bar{T}_g \tag{E.59}$$

$$\frac{\partial P_g}{\partial T_g} = N\bar{\omega}_r \tag{E.60}$$

$$h_2(x, u) = v_t \tag{E.61}$$

$$h_3(x, u) = \omega_r \tag{E.62}$$

The state space representation for the model is (including the tower velocity subtraction, as explained earlier):

$$
\begin{bmatrix} \dot{\omega}_r^\Delta \\ d_t^\Delta \\ v_t^\Delta \\ \beta^\Delta \\ T_g^\Delta \end{bmatrix} =
\begin{bmatrix}
\frac{1}{J}\frac{\partial T_a}{\partial \omega_r} & 0 & -\frac{1}{J}\frac{\partial T_a}{\partial v_w} & \frac{1}{J}\frac{\partial T_a}{\partial \beta} & \frac{-N}{J} \\
0 & 1 & 0 & 0 & 0 \\
\frac{1}{M_t}\frac{\partial F_t}{\partial \omega_r} & -\frac{K_t}{M_t} & \frac{1}{M_t}\left(-B_t - \frac{\partial F_t}{\partial v_w}\right) & \frac{1}{M_t}\frac{\partial F_t}{\partial \beta} & 0 \\
0 & 0 & 0 & -\frac{1}{\tau_p} & 0 \\
0 & 0 & 0 & 0 & -\frac{1}{\tau_g}
\end{bmatrix}
\begin{bmatrix} \omega_r^\Delta \\ d_t^\Delta \\ v_t^\Delta \\ \beta^\Delta \\ T_g^\Delta \end{bmatrix}
$$
$$
+ \begin{bmatrix}
0 & 0 & \frac{1}{J}\frac{\partial T_a}{\partial v_w} \\
0 & 0 & 0 \\
0 & 0 & \frac{1}{M_t}\frac{\partial F_t}{\partial v_w} \\
0 & \frac{1}{\tau_p} & 0 \\
\frac{1}{\tau_g} & & 0
\end{bmatrix}
\begin{bmatrix} T_{g,ref}^\Delta \\ \beta_{ref}^\Delta \\ v_w^\Delta \end{bmatrix} \tag{E.63a}
$$

$$
\begin{bmatrix} P \\ v_t \\ \omega_r \end{bmatrix} =
\begin{bmatrix} \bar{P} \\ \bar{v}_t \\ \bar{\omega}_r \end{bmatrix} +
\begin{bmatrix}
\frac{\partial P_g}{\partial \omega_r} & 0 & 0 & 0 & \frac{\partial P_g}{\partial T_g} \\
0 & 0 & 1 & 0 & 0 \\
1 & 0 & 0 & 0 & 0
\end{bmatrix}
\begin{bmatrix} \omega_r^\Delta \\ d_t^\Delta \\ v_t^\Delta \\ \beta^\Delta \\ T_g^\Delta \end{bmatrix} + 0
\begin{bmatrix} T_{g,ref}^\Delta \\ \beta_{ref}^\Delta \\ v_w^\Delta \end{bmatrix} \tag{E.63b}
$$

Kalman Filtering F

This appendix will introduce the concept of Kalman filtering. The linear and extended Kalman filter will be explained.

Whenever a sensor is sampled and used in a control system, noise will be present. If the signal to noise ratio is low, the noise will affect the performance of the control loop. To minimize the effect this noise, a Kalman filter can be used to estimate internal states, for better control performance. Besides this the desired state information may not be directly measurable, but is still observable through knowledge of the of the system using a Kalman filter. The Kalman filter uses knowledge of the system and the sensor to generate the desired state information.

Assuming that a model of the control process is available and that Gaussian white noise is affecting the states and sampled output signal, it can predict the current state in an optimal fashion. This is done through the linear minimum mean square error, between the predicted state and the actual state. The Kalman filter combines model estimations with noisy sensor measurements, to make a stochastic estimation [Welch and Bishop, 2001].

The equations for the discrete state space system is:

$$x_k = \Phi_{k-1}\hat{x}_{k-1} + \Gamma_k u_{k-1} + G_{k-1}W_{k-1} \tag{F.1}$$

$$z_k = H_k x_k + D_k u_k + V_k \tag{F.2}$$

Where: x is the state vector.

        Φ is the system matrix.

        Γ is the input matrix.

        u is the control signal.

        Z is the measured output(s).

        H is the output matrix.

        D is the feedthrough matrix.

        W and V are white noise affecting states and measured output.

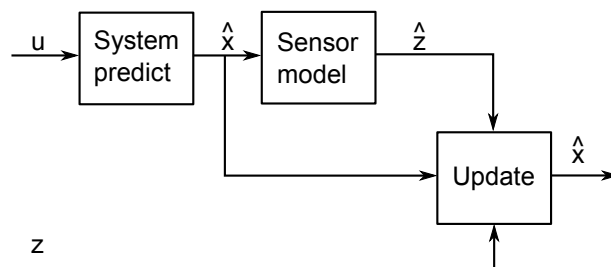A block diagram of the linear Kalman filter (LKF) is as follows:

Figure F.1. A block diagram overview of the LKF. A prediction of the current state and measurement values are made. These values are compared to the actual measurement and an update process is made, to correct the prediction.

The equations used in the LKF is (the superscript - and + indicates before and after the update process):

Predict - A priori knowledge

$$\hat{x}_k^- = \Phi_{k-1}\hat{x}_{k-1}^- + \Gamma_{k-1}u_{k-1} \tag{F.3}$$

$$\hat{z}_k = H_k\hat{x}_k^- \tag{F.4}$$

$$P_k^- = \Phi_k P_{k-1}^+ \Phi_k^T + Q_{k-1} \tag{F.5}$$

$$\tag{F.6}$$

Update - A posteriori knowledge

$$K_k = P_k^- H_k^T (H_k P_k^- H_k^T + R_k)^{-1} \tag{F.7}$$

$$\hat{x}_k^+ = \hat{x}_k^- + K_k(z_k - \hat{z}_k) \tag{F.8}$$

$$P_k^+ = (I - K_k H_k)P_k^- \tag{F.9}$$

Where: $\hat{x}$ is the estimate of the state(s).

$\hat{z}$ is the estimate of the output(s).

P is the covariance matrix.

Q is the covariance matrix of the state noise.

R is the covariance matrix of the output noise.

The Q and R matrix is used for tuning purposes. The entries in R can be found by sampling data from a constant output, to see how big the variance is. The Q matrix can be tuned by hand or computationally based on simulations.

If e.g. the sampled outputs are very noise, the Kalman filter can be tuned to trust mainly on the given system model, by having low values in the Q matrix. On the other hand, if only a bad model is available it is possible to trust the measurement more, by having low values in the R matrix.

The covariance propagation, in Equation F.5 is done through a linear map, as illustrated in Figure F.2.
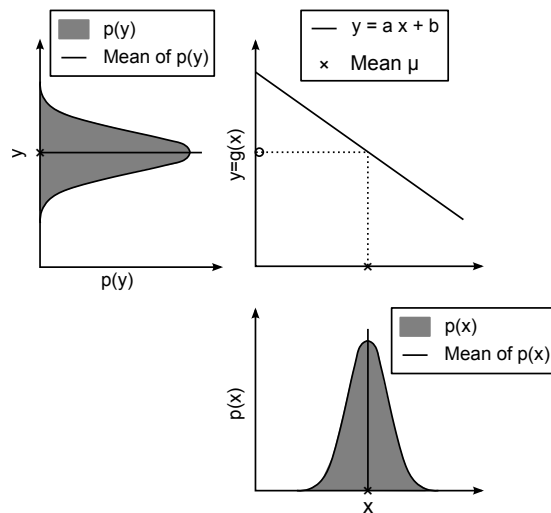

Figure F.2. Covariance propagation in the LKF. A linear map is mapping the probability distribution of the previous states to the current states [Larsen, 2013a].

F.1 The Extended Kalman Filter

If the system model is not linear another type of Kalman filter is utilised. The extended Kalman filter (EKF) predicts the states through the nonlinear model. However when the covariance is propagated it makes a local linearisation around the current operating point. The Jacobian is evaluated at each sample, given the current states. This of course requires that the nonlinear model is differentiable. The principle is illustrated in Figure F.3.
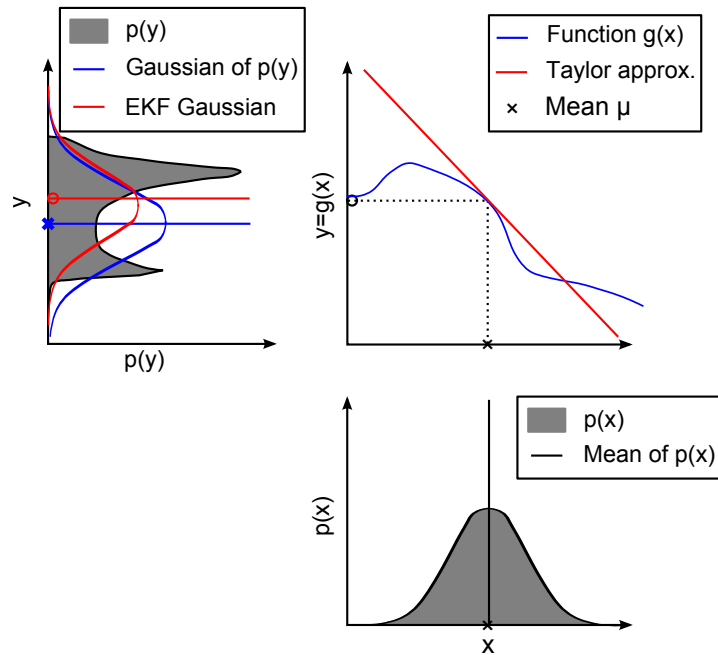
Figure F.3. Covariance propagation in the EKF. A linear approximation of the nonlinear map is mapping the probability distribution of the previous states to the current states [Larsen, 2013b].

The biggest issue with the EKF, is that stability is not guaranteed. This means that it can become unstable, and thereby needs to be reinitialised. One way of keeping track of stability is to compare the output, to another simpler but stable way of computing the state vector. If it differ more than allowed (in percentage) the filter is reinitialised.

MPC Theory G

G.1 Prediction Model

The prediction model that will be used is based on a state space model of the system with full state measurements. Without full state measurement, full state knowledge could be obtained through estimates as described in Chapter 7 on page 25. The model uses the present states and the future control [Maciejowski, 2002, P. 54]:

$$\hat{x}(k+1|k) = Ax(k) + B\hat{u}(k|k) \tag{G.1}$$

$$\hat{x}(k+2|k) = A\hat{x}(k+1|k) + B\hat{u}(k+1|k) \tag{G.2}$$

$$= A^2x(k) + AB\hat{u}(k|k) + B\hat{u}(k+1|k) \tag{G.3}$$

$$\vdots$$

$$\hat{x}(k+N_p|k) = A^{N_p}x(k) + A^{N_p-1}B\hat{u}(k|k) + \ \ldots \ + B\hat{u}(k+N_p-1|k) \tag{G.4}$$

Where: $\hat{x}$ are the predicted states.

$\hat{u}$ denotes the future control inputs.

A and B are the model matrices.

The method that is going be used to solve the optimization problem splits the model up into future and past, such that the optimization problem only is a function of the future. How this is done will be shown later. For this reason the model will be put in a suitable form. First step is to divide the control action into two terms:

The control moves can be expressed by:

$$\Delta u(k) = u(k) - u(k-1) \tag{G.5}$$

Combining the prediction equations with (G.5), the predictions can be written as:

$$\hat{x}(k+1|k) = Ax(k) + B(\Delta\hat{u}(k|k) + u(k-1)) \tag{G.6}$$

$$\hat{x}(k+2|k) = A^2x(k) + (AB+B)u(k-1) + AB\Delta\hat{u}(k|k)$$
$$+ B\left(\Delta\hat{u}(k+1|k) + \Delta\hat{u}(k|k)\right) \tag{G.7}$$

$$\vdots$$

$$\hat{x}(k+N_p|k) = A^{N_p}\hat{x}(k) + \sum_{i=1}^{N_p-1} A^i B\hat{u}(k-1)$$

$$+ \sum_{i=0}^{N_p-1} A^i B\Delta\hat{u}(k) + \ \ldots \ + \sum_{i=0}^{N_p-N_u} A^i B\Delta\hat{u}(k+N_u-1|k) \tag{G.8}$$

If the states and control signals are stacked into vectors the prediction can be reduced to the form:

$$
\mathcal{X}(k) = \begin{bmatrix} \hat{x}(k+1|k) \\ \vdots \\ \hat{x}(k+N_u|k) \\ \hat{x}(k+N_u+1|k) \\ \vdots \\ \hat{x}(k+N_p|k) \end{bmatrix} , \quad \Delta\mathcal{U}(k) = \begin{bmatrix} \Delta\hat{u}(k|k) \\ \vdots \\ \Delta\hat{u}(k+N_u-1|k) \end{bmatrix} \tag{G.9}
$$

$$
\mathcal{A} = \begin{bmatrix} A \\ \vdots \\ A^{N_u} \\ A^{N_u+1} \\ \vdots \\ A^{N_p} \end{bmatrix} \tag{G.10}
$$

$$
\mathcal{B}_u = \begin{bmatrix} B \\ \vdots \\ \sum_{i=0}^{N_u-1} A^i B \\ \sum_{i=0}^{N_u} A^i B \\ \vdots \\ \sum_{i=0}^{N_p-1} A^i B \end{bmatrix} , \quad
\mathcal{B}_{\Delta u} = \begin{bmatrix}
B & 0 & \cdots & 0 \\
AB+B & B & \cdots & 0 \\
\vdots & AB+B & \cdots & 0 \\
\vdots & \vdots & \ddots & \vdots \\
\sum_{i=0}^{N_u-1} A^i B & \sum_{i=0}^{N_u-2} A^i B & \cdots & B \\
\sum_{i=0}^{N_u} A^i B & \sum_{i=0}^{N_u-1} A^i B & \cdots & AB+B \\
\vdots & \vdots & \ddots & \vdots \\
\sum_{i=0}^{N_p-1} A^i B & \sum_{i=0}^{N_p-2} A^i B & \cdots & \sum_{i=0}^{N_p-N_u} A^i B
\end{bmatrix} \tag{G.11}
$$

$$
\mathcal{X}(k) = \mathcal{A}\hat{x}(k|k) + \mathcal{B}_u u(k-1) + \mathcal{B}_{\Delta u}\Delta\mathcal{U}(k) \tag{G.12}
$$

Now the future outputs can be described as:

$$
\mathcal{Z}(k) = \begin{bmatrix} \hat{z}(k+N_w|k) \\ \vdots \\ \hat{z}(k+N_p|k) \end{bmatrix} , \quad \mathcal{X}(k) = \begin{bmatrix} \hat{x}(k+1|k) \\ \vdots \\ \hat{x}(k+N_p|k) \end{bmatrix} \tag{G.13}
$$

$$
\mathcal{C} = \begin{bmatrix} C & 0 & \cdots & 0 \\ 0 & C & \cdots & 0 \\ \vdots & \vdots & \ddots & \vdots \\ 0 & 0 & \cdots & C \end{bmatrix} \tag{G.14}
$$

$$
\mathcal{Z}(k) = \mathcal{C}\mathcal{X}(k) \tag{G.15}
$$

Now a measurable input disturbance is added.

G.2 Disturbances

In the controller used for the wind turbine the wind is a measured disturbance. Measured disturbances can be used for compensation in the controller as feedforward and can be implemented as shown in Figure G.1. As the disturbance is in the prediction model, its size can be determined as constant in the prediction horizon.
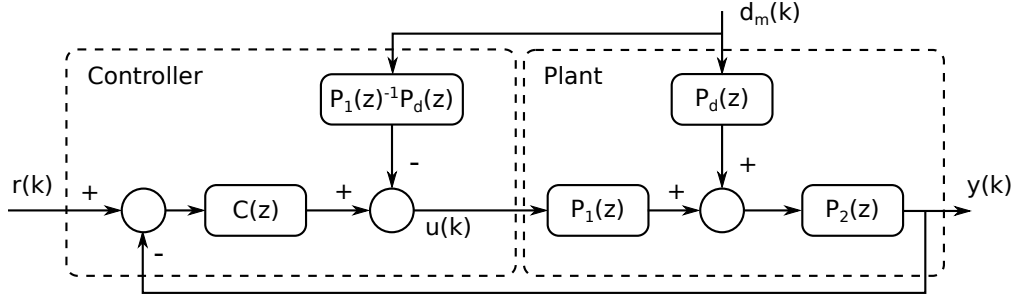

Figure G.1. Feedforward from measured disturbance [Maciejowski, 2002, P. 146].

The states of the plant can then be expressed as in (G.16), where the measured disturbance d_m affect the states through the B_d matrix.

$$\hat{x}(k+1|k) = A\hat{x}(k|k) + Bu(k) + B_d d_m(k) \tag{G.16}$$

By using the same stacking method as in the prediction model this becomes [Maciejowski, 2002, P. 147]:

$$\mathcal{D}_m(k) = \begin{bmatrix} d_m(k) \\ \hat{d}_m(k+1|k) \\ \vdots \\ \hat{d}_m(k+N_p-1|k) \end{bmatrix} \tag{G.17}$$

$$\mathcal{B}_d = \begin{bmatrix} B & 0 & \cdots & 0 \\ AB & B & \cdots & 0 \\ \vdots & \vdots & \ddots & \vdots \\ A^{N_p-1}B & A^{N_p-2}B & \cdots & B \end{bmatrix} \tag{G.18}$$

$$\mathcal{X}(k) = \mathcal{A}\hat{x}(k|k) + \mathcal{B}_u u(k-1) + \mathcal{B}_{\Delta u}\Delta\mathcal{U}(k) + \mathcal{B}_d\mathcal{D}_m(k) \tag{G.19}$$

As no additional information about the future wind is available it is considered constant having the value that was last measured over the prediction horizon.

By defining $\Psi = \mathcal{C}\mathcal{A}$, $\Upsilon = \mathcal{C}\mathcal{B}_u$, $\Theta = \mathcal{C}\mathcal{B}_{\Delta u}$, $\Lambda = \mathcal{C}\mathcal{B}_d$
$\mathcal{Z}(k)$ can now be written as:

$$\mathcal{Z}(k) = \Psi\hat{x}(k|k) + \Upsilon u(k-1) + \Theta\Delta\mathcal{U}(k) + \Lambda\mathcal{D}_m(k) \tag{G.20}$$

G.2.1 Disturbance Dynamics

With the form:

$$x(k+1) = Ax(k) + Bu(k) + \Gamma d(k) \tag{G.21}$$
$$y(k) = Cx(k) \tag{G.22}$$

No dynamics of the disturbance is shown. If the disturbance has dynamics and is on the form:

$$x_w(k+1) = A_w x_w(k) + \Gamma_w w(k) \tag{G.23}$$
$$d(k) = C_w x_w(k) + w(k) \tag{G.24}$$

This can be extended to the system like:

$$\begin{bmatrix} x(k+1) \\ x_w(k+1) \end{bmatrix} = \begin{bmatrix} A & \Gamma C_w \\ 0 & A_w \end{bmatrix} \begin{bmatrix} x(k) \\ x_w(k) \end{bmatrix} + \begin{bmatrix} B \\ 0 \end{bmatrix} u(k) + \begin{bmatrix} \Gamma \\ \Gamma_w \end{bmatrix} w(k) \tag{G.25}$$

$$y(k) = \begin{bmatrix} C & 0 \end{bmatrix} \begin{bmatrix} x(k) \\ x_w(k) \end{bmatrix} \tag{G.26}$$

If white noise is added to the changes in input the controller through the estimation of this integrated white noise leads to integral action.

G.3 Constraints

The optimization can be subject to constraints, which comes from the physical system e.g. actuator range or slew rate or constraints that the designer wish to impose on the system. Constraint are here given for control effort, control rate and output size. When expanded into either the control or prediction horizon the matrix representations are respectively F, E and G. F and E are control effort and rate and therefore needs to be expanded into the control horizon N_u. G is the output constraints and therefore needs to be expanded into the prediction horizon N_p. The constraint can then be described as [Maciejowski, 2002, P. 81]:

$$E \begin{bmatrix} \Delta \mathcal{U}(k) \\ 1 \end{bmatrix} \leq \mathbf{0} \tag{G.27}$$

$$F \begin{bmatrix} \mathcal{U}(k) \\ 1 \end{bmatrix} \leq \mathbf{0} \tag{G.28}$$

$$G \begin{bmatrix} \mathcal{Z}(k) \\ 1 \end{bmatrix} \leq \mathbf{0} \tag{G.29}$$

Where: E denotes a matrix containing the constraints for change in control input.
F denotes a matrix containing the constraints of the values of control input.
G denotes a matrix containing the constraints of the values of the system output.
$\mathcal{U}(k) = [\hat{u}(k|k)^T, \ldots, \hat{u}(k+N_u-1|k)^T]^T$.
$\mathbf{0}$ is the null vector.

The notation are alike for the representation of F, E and G so only F will be shown:

$$
F = \begin{bmatrix}
\dfrac{1}{u_{min,1}} & & & & & & -1 \\
\dfrac{1}{u_{max,1}} & & & \mathbf{0} & & & \\
& \dfrac{1}{u_{min,2}} & & & & & \vdots \\
& \dfrac{1}{u_{max,2}} & & & & & \\
& & \ddots & & & & \vdots \\
\mathbf{0} & & & & \dfrac{1}{u_{min,N_u}} & & \\
& & & & \dfrac{1}{u_{max,N_u}} & & -1
\end{bmatrix}
\tag{G.30}
$$

As explained in the prediction section the control problem is solved for only the change in control action, so all of the constraint needs to be rewritten as dependent of $\Delta\mathcal{U}(k)$.

The constraint for control input needs to be changed since it is now dependent of $\mathcal{U}$. This is done by first writing (G.28) as:

$$
0 \geq \sum_{i=1}^{N_u} F_i \hat{u}(k+i-1|k) + f
\tag{G.31}
$$

The future control input is a combination of an older input plus the changes done since that:

$$
\hat{u}(k+i-1|k) = u(k-1) + \sum_{j=0}^{i-1} \Delta\hat{u}(k+j|k)
\tag{G.32}
$$

By inserting this into (G.31) it becomes:

$$
\begin{aligned}
0 \geq{} & \sum_{j=1}^{N_u} F_j \Delta\hat{u}(k|k) + \sum_{j=2}^{N_u} F_j \Delta\hat{u}(k+1|k) + ... + F_{N_u}\Delta\hat{u}(k+N_u-1|k) \\
& + \sum_{j=1}^{N_u} F_j \hat{u}(k-1) + f
\end{aligned}
\tag{G.33}
$$

Now the following is defined $\mathcal{F}_i = \sum_{j=i}^{N_u}$ and $\mathcal{F} = [\mathcal{F}_1, \ldots, \mathcal{F}_{N_u}]$ and it turns into:

$$
\mathcal{F}\Delta\mathcal{U}(k) \leq -\mathcal{F}_1 u(k-1) - f
\tag{G.34}
$$

The right hand side of the inequality is a known vector at time k, which makes the constraint now dependent of $\Delta\mathcal{U}$. Now the same has to be done for G. By inserting the expression for $\mathcal{Z}(k)$ from (G.20) into the equation describing the output constraints, (G.29), it becomes:

$$
\mathbf{0} \geq G \begin{bmatrix} \Psi\hat{x}(k|k) + \Upsilon u(k-1) + \Theta\Delta\mathcal{U}(k) + \Lambda\mathcal{D}_m(k) \\ 1 \end{bmatrix}
\tag{G.35}
$$

By writing $G = [\Gamma, g]$, g is the last column of G it turns into:

$$0 \geq \Gamma[\Psi\hat{x}(k|k) + \Upsilon u(k-1) + \Gamma\Lambda\mathcal{D}_m(k)] + \Gamma\Theta\Delta\mathcal{U}(k) + g \tag{G.36}$$

$$\Updownarrow$$

$$\Gamma\Theta\Delta\mathcal{U}(k) \leq -\Gamma[\Psi\hat{x}(k|k) + \Upsilon u(k-1) + \Gamma\Lambda\mathcal{D}_m(k)] - g \tag{G.37}$$

Now the output constraints are also described as dependent on $\Delta\mathcal{U}(k)$. The constraints on the input rate is obviously already dependent on $\Delta\mathcal{U}(k)$, which only leaves to the rearranging by defining $E = [W, w]$ where w is the last column of E and inserting this into the equation for input rate constraints, (G.28):

$$\mathcal{W}\Delta\mathcal{U} \leq -w \tag{G.38}$$

By assembling the newly constructed inequalities into a single results in:

$$\begin{bmatrix} \mathcal{F} \\ \Gamma\Theta \\ \mathcal{W} \end{bmatrix} \Delta\mathcal{U}(k) \leq \begin{bmatrix} -\mathcal{F}_1 u(k-1) - f \\ -\Gamma[\Psi\hat{x}(k|k) + \Upsilon u(k-1) + \Gamma\Lambda\mathcal{D}_m(k)] - g \\ -w \end{bmatrix} \tag{G.39}$$

These constraints are now on the form that will be used when solving the optimization problem.

G.4   Softening Constraints

As the constraints are formulated now a problem can occur, where a large disturbance or mismatch between the internal model and the plant makes the controller unable to keep the plant within the constraints The optimization problem therefore becomes infeasible. In such a situation no solution would be found from a standard quadratic programming controller, which would leave the system without any control input. A way of handling this is simply to input the old control input until the problem becomes feasible again or even the second horizon input from last iteration. A different solution is to soften the constraints. When softening the constraint the formulation moves from never being able to cross the constraints to in a strictly necessary situation being able to cross the constraint at high cost penalty. Softening constraints is usually only done on the output constraints, since input constraints are often determined by actuator limitations. An easy way of adding soft constraints is adding so called slack variables to the cost function. The slack variable increases, when the constraint is crossed and penalized in the objective function so the controller has strong incentive to minimize the slack variable. With added slack variables to the optimization problem it becomes:

$$\min_{\theta, \epsilon} \quad \frac{1}{2}\theta^T\Phi\theta + \phi^T\theta + \rho||\epsilon||^2 \tag{G.40}$$

$$\text{subject to} \quad \Omega\theta \leq \omega + \epsilon$$

$$\text{and} \quad \epsilon \geq 0$$

Where ρ is the weight on the slack variable determining how "soft" the constraint is. Is $\rho = 0$ the constraints are hard.

G.5 Optimization

As in the case with the constraint the optimization problem is solved in regard to $\Delta\mathcal{U}$, so the problem needs to be reformulated before it can be solved [Maciejowski, 2002, P. 81].

The objective function was chosen to be:

$$V(k) = \sum_{i=N_w}^{N_p} ||\hat{z}\,(k+i|k) - r\,(k+i|k)\,||^2_{Q(i))} + \sum_{i=0}^{N_u-1} ||\Delta\hat{u}\,(k+i|k)\,||^2_{R(i)} \qquad \text{(G.41)}$$

By adding the horizon stacked matrices for the weights ($\mathcal{Q}$ and $\mathcal{R}$) and the stacked vector for the reference ($\mathcal{T}(k)$) as:

$$\mathcal{Q} = \begin{bmatrix} Q(N_w) & 0 & \cdots & 0 \\ 0 & Q(N_w+1) & \cdots & 0 \\ \vdots & \vdots & \ddots & \vdots \\ 0 & 0 & \vdots & Q(N_p) \end{bmatrix}, \quad \mathcal{R} = \begin{bmatrix} R(0) & 0 & \cdots & 0 \\ 0 & R(1) & \cdots & 0 \\ \vdots & \vdots & \ddots & \vdots \\ 0 & 0 & \vdots & R(N_u-1) \end{bmatrix}$$

$$\mathcal{T}(k) = \begin{bmatrix} \hat{r}(k+N_w|k) \\ \vdots \\ \hat{r}(k+N_p|k) \end{bmatrix} \qquad \text{(G.42)}$$

The objective function can be rewritten as:

$$V(k) = ||\mathcal{Z}(||) - \mathcal{T}(k)||^2_{\mathcal{Q}} + ||\Delta\mathcal{U}(k)||^2_{\mathcal{R}} \qquad \text{(G.43)}$$

Remember that the predicted outputs can be written as:

$$\mathcal{Z}(k) = \Psi x(k) + \Upsilon u(k-1) + \Theta\Delta\mathcal{U}(k) + \Lambda\mathcal{D}_m(k) \qquad \text{(G.44)}$$

and the following is defined:

$$\mathcal{E}(k) = \mathcal{T}(k) - \Psi x(k) - \Upsilon u(k-1) - \Lambda\mathcal{D}_m(k) \qquad \text{(G.45)}$$

Where $\mathcal{E}(k)$ is the tracking error over the prediction horizon, if no input changes are made.

From this the objective function can now be written as:

$$V(k) = ||\Theta\Delta\mathcal{U}(k) - \mathcal{E}(k)||^2_{\mathcal{Q}} + ||\Delta\mathcal{U}(k)||^2_{\mathcal{R}} \qquad \text{(G.46)}$$

$$= [\Delta\mathcal{U}(k)^T\Theta^T - \mathcal{E}(k)^T]\mathcal{Q}[\Theta\Delta\mathcal{U}(k) - \mathcal{E}(k)] + \Delta\mathcal{U}(k)^T\mathcal{R}\Delta\mathcal{U}(k) \qquad \text{(G.47)}$$

$$= \mathcal{E}(k)^T\mathcal{Q}\mathcal{E}(k) - 2\Delta\mathcal{U}(k)^T\Theta^T\mathcal{Q}\mathcal{E}(k) + \Delta\mathcal{U}(k)^T[\Theta^T\mathcal{Q}\Theta + \mathcal{R}]\Delta\mathcal{U}(k) \qquad \text{(G.48)}$$

This can be formulated as:

$$V(k) = const - \Delta \mathcal{G}^T \mathcal{U}(k) + \Delta \mathcal{U}(k)^T \mathcal{H} \Delta \mathcal{U}(k) \tag{G.49}$$

Where:

$$\mathcal{G} = 2\Theta^T \mathcal{Q}\mathcal{E}(k) \tag{G.50}$$

$$\mathcal{H} = \Theta^T \mathcal{Q}\Theta + \mathcal{R} \tag{G.51}$$

Now neither the constant part, $\mathcal{H}$ nor $\mathcal{G}$ depends on $\Delta \mathcal{U}(k)$ and the quadratic programming (QP) problem with the constraints found before can be formulated as:

$$\min_{\Delta \mathcal{U}} \qquad \Delta \mathcal{U}(k)^T \mathcal{H} \Delta \mathcal{U}(k) - \mathcal{G}^T \Delta \mathcal{U}(k) \tag{G.52}$$

$$\text{subject to} \begin{bmatrix} \mathcal{F} \\ \Gamma\Theta \\ \mathcal{W} \end{bmatrix} \Delta \mathcal{U}(k) \leq \begin{bmatrix} -\mathcal{F}_1 u(k-1) - f \\ -\Gamma[\Psi\hat{x}(k|k) + \Upsilon u(k-1) + \Gamma\Lambda\mathcal{D}_m(k)] - g \\ -w \end{bmatrix} \tag{G.53}$$

This is a standard QP with constraints, which can be written on the standard form:

$$\min_{\theta} \qquad \frac{1}{2}\theta^T \Phi\theta + \phi^T \theta \tag{G.54}$$

$$\text{subject to} \quad \Omega\theta \leq \omega$$

G.6   Solving the QP

Had the problem been without constraints the optimal input change could have been found by letting the gradient equate to zero [Maciejowski, 2002, P. 88]:

$$\frac{\partial V(k)}{\partial \Delta \mathcal{U}(k)} = -\mathcal{G} + 2\mathcal{H}\Delta U(k) \tag{G.55}$$

$$\Downarrow$$

$$\Delta \mathcal{U}(k)_{opt} = \frac{1}{2}\mathcal{H}^{-1}\mathcal{G} \tag{G.56}$$

To establish if this minimum is indeed a global minimum the Hessian is examined:

$$\frac{\partial^2 V(k)}{\partial \Delta \mathcal{U}(k)^2} = 2\mathcal{H} = 2(\Theta^T \mathcal{Q}\Theta + \mathcal{R}) \tag{G.57}$$

The Hessian needs to be positive definite ($\mathcal{H} < 0$) for the problem to be solvable in this way and for it to be convex, meaning that the minimum is indeed a global minimum. Now usually the solution is not computed by using the inverse of the Hessian as here, since this can often be ill conditioned due to Θ being ill conditioned. As an example if two control variables in Θ behaves alike the rank of Θ would be less than full and $\Theta^T \mathcal{Q}\Theta$ becomes singular. Instead other methods such as least squares can be used to solve it.

Having an unconstrained problem is not the case in MPC, where constraints are in the very core of the control problem, so another solver is needed. As per equation G.55 the problem is on a standard QP formulation, which means it can be solved using a multitude of solvers using different methods such as active set or interior point methods. Here a short explanation of the active set method is done.

As long as no variable is hitting its constraint the solution is as in the unconstrained case. As soon as one or more of the variable hits their constraint this set of constraints becomes active, which means:

$$\Omega_a \theta = \omega_a \tag{G.58}$$

Where Ω_a are the active constraints from Ω and ω_a are the corresponding elements from ω. So if knowledge was available of which constraints would be active, in the optimal solution before solving, the problem the problem could be formulated as:

$$\min_{\theta} \quad \frac{1}{2}\theta^T \Phi \theta + \phi^T \theta \tag{G.59}$$

$$\text{subject to} \quad \Omega_a \theta = \omega_a$$

This problem could be solved by using Lagrange multipliers:

$$\min_{\theta, \lambda} \quad \frac{1}{2}\theta^T \Phi \theta + \phi^T \theta + \lambda(\Omega_a \theta - \omega_a) \tag{G.60}$$

Where the gradients are:

$$\frac{\partial L(\theta, \lambda)}{\partial \theta} = \Phi \theta + \phi + \Omega_a^T \lambda \tag{G.61}$$

$$\frac{\partial L(\theta, \lambda)}{\partial \lambda} = \Omega_a \theta - \omega_a \tag{G.62}$$

This can be put into matrix form:

$$\nabla L(\theta, \lambda) = \begin{bmatrix} \Phi & \Omega_a^T \\ \Omega_a & 0 \end{bmatrix} \begin{bmatrix} \theta \\ \lambda \end{bmatrix} - \begin{bmatrix} -\phi \\ \omega_a \end{bmatrix} \tag{G.63}$$

By equating this to zero the optimal solution is found as:

$$\begin{bmatrix} \theta \\ \lambda \end{bmatrix}_{opt} = \begin{bmatrix} \Phi & \Omega_a^T \\ \Omega_a & 0 \end{bmatrix}^{-1} \begin{bmatrix} -\phi \\ \omega_a \end{bmatrix} \tag{G.64}$$

Now by remembering that $\Omega = [\mathcal{F} \ \Gamma\Theta \ \mathcal{W}]$ and $\Phi = \mathcal{H}/2$ in the original problem, it can be seen that none of these elements depend on the signals at time k. This means that the matrix being inverted in the problem above is constant as long as the same constraints are active. Both ϕ and ω_a depends on the signal at time k. This results in the control problem being a linear time invariant problem as long as the active constraints are constant. This opens up for the opportunity of solving the inverse matrix for all combinations of active constraints in advance. There are a number of reason why this is not feasible, one being the sheer amount of solutions

as the number of constraints rise. This is were the active set method can be used.

For the further explanation the standard QP problem involving both equality and inequality constraints will be used on the form:

$$\min_{\theta} \quad \frac{1}{2}\theta^T \Phi\theta + \phi^T\theta \tag{G.65}$$

$$\text{subject to} \quad H\theta = h$$
$$\text{and} \quad \Omega\theta \leq \omega \tag{G.66}$$

The name active set stems from the use of an active set of constraints as in the formulation used earlier:

$$\Omega_a\theta = \omega_a \tag{G.67}$$

In the active set method it is assumed that a feasible solution is available, where a set of constraints are active and therefore hold with equality. This set can be empty, when none is active. Now this method is used and is at iteration r, where the feasible solution θ_r is found. The active set method then finds an improved solution $\theta_r + \Delta\theta$, which still complies with $\Omega_a\theta = \omega_a$ and $H\theta = h$, without caring about inactive constraints being violated. Then the improved solution is tested for feasibility against all the constraints $\Omega(\theta_r + \Delta\theta) \leq \omega$. If it is feasible, it is accepted as the next iteration, if not then a line-search is performed in the direction of $\Delta\theta$ to find the point, where feasibility is lost. The new iteration then becomes $\theta_{r+1} = \theta_r \alpha_r \Delta\theta$ with $0 < \alpha_r < 1$. Now the question is if the solution found θ_{r+1} is an global optimal solution or further iterations are needed.

Since the QP problem was convex, the necessary and sufficient conditions for a solution θ being a global minimum are given by the Karush–Kuhn–Tucker (KKT) conditions: There must exist vectors $\lambda \geq 0$, $\zeta \geq 0$ and $t \geq 0$, such that solutions can be found to:

$$\Phi\theta + H^T\zeta + \Omega^T\lambda = -\phi \tag{G.68}$$
$$-H\theta = -h \tag{G.69}$$
$$-\Omega\theta - t = -\omega \tag{G.70}$$
$$t^T\lambda = 0 \tag{G.71}$$

λ consist of elements for each constraint. The elements of the constraint that are inactive are zero, so those does not need to be solved. The rest are solved and if $\lambda \geq 0$ then a global solution has been found, else more iteration are needed. If an element of λ is negative, this indicates that the cost function can be improved by removing the corresponding constraint from the set. This is then done and a new active set is found and the process is repeated.

Now by taking into account that the problem is solved iteratively by finding the best new cost through a change the new cost function at iteration r would be:

$$V(\theta_r + \Delta\theta) = \frac{1}{2}(\theta_r\Delta\theta)^T\Phi(\theta + \Delta\theta) + \phi^T(\theta_r + \Delta\theta) \tag{G.72}$$
$$\Downarrow$$
$$= V(\theta_r) + \frac{1}{2}\Delta\theta^T\Phi\Delta\theta + (\phi^T + \theta_r^T)\Delta\theta \tag{G.73}$$

And since only the active set of constraints are used the minimization problem becomes:

$$\min_{\Delta\theta} \quad \frac{1}{2}\Delta\theta^T\Phi\Delta\theta+(\phi^T + \Phi\theta_r)\Delta\theta \tag{G.74}$$

subject to $\quad H\theta = h$

and $\quad \Omega_a\theta = \omega_a \tag{G.75}$

Since only equality constraints are present now due to the active set only the following equations from the KKT conditions are needed:

$$\begin{bmatrix} \Phi & H^T & \Omega_a^T \\ H & 0 & 0 \\ \Omega_a & 0 & 0 \end{bmatrix} \begin{bmatrix} \Delta\theta \\ \Delta\zeta \\ \Delta\lambda \end{bmatrix} = \begin{bmatrix} -\phi_r \\ h \\ \omega_a \end{bmatrix} \tag{G.76}$$

This can now be solved. How this problem is solved varies between the different active set methods. For documentation on the specific active set algorithm used for MPC see the implementation chapter.